npj | nanophotonics

Review

https://doi.org/10.1038/s44310-025-00081-6

From performance to structure: a comprehensive survey of advanced metasurface design for next-generation imaging

Yunhui Zeng[1,2], Haopeng Zhong[1], Zhenwei Long[1], Hongkun Cao[2] & Xin Jin[1] ✉

This review introduces a 'from performance to structure' imaging metasurface design paradigm, which starts with essential imaging specifications and translates them into corresponding electromagnetic requirements. These requirements are then mapped onto specialized metasurface microstructures, ensuring precise electromagnetic response control. Artificial intelligence (AI) serves as a unifying thread by accelerating inverse design through efficient navigation of high-dimensional parameter spaces and by enhancing imaging performance via AI-driven computational reconstruction algorithms. We synthesize the remarkable performance of metasurfaces across six electromagnetic response control methods in nine imaging domains and categorize three main design approaches—physically-driven, meta-heuristic, and AI-driven methods—while providing a detailed analysis of six primary encoding and decoding strategies and eight common AI techniques. Additionally, nine prospective research directions are highlighted. The review emphasizes that future metasurface imaging systems will leverage electromagnetic response control to link performance with metasurface structure, with AI technology playing a central role in this process.

Imaging technology is fundamental to a wide range of scientific and industrial domains, significantly advancing humanity's ability to explore both the microscopic and cosmic scales. From revealing molecular details within the human body to observing distant celestial phenomena, imaging technology has played a crucial role in driving breakthroughs in medicine, astrophysics, security, and more. Traditional optical systems, which are mainly based on refractive and diffractive elements, have been instrumental in enabling multidimensional high-resolution data capture[1,2]. However, these systems are often burdened with inherent limitations, such as bulkiness, material dispersion, and manufacturing complexities. Although computational imaging[3–5] has partially mitigated these constraints through algorithmic post-processing, persistent bulkiness and performance limits continue to pose significant challenges.

Metasurface technology, distinguished by its exceptional ability to manipulate broad electromagnetic properties on a subwavelength scale, has emerged as a promising solution to overcome these long-standing barriers in optical imaging[6–8]. Unlike traditional optics, which relies primarily on refraction or reflection, metasurfaces precisely control electromagnetic waves at the subwavelength scale through carefully engineered nanostructures, enabling multifunctional optical responses. These nanostructures enable tunable control over various electromagnetic responses, offering the potential for ultrathin devices with significantly enhanced functionality. As a subclass of metasurfaces tailored for focusing tasks, metalenses are treated in this work under a consistent terminology framework. By eliminating bulky refractive components and confining optical interactions to the surface, metasurfaces foster new functionalities, such as achromatic imaging, expanded field of view imaging, expanded depth of field imaging, resolution enhancement imaging, multidimensional imaging, optical feature enhancement imaging, holographic imaging, functional integration imaging and compact integration imaging, all achieved within a compact optical layer[9–11]. Especially in recent years, breakthroughs, such as reconfigurable metasurfaces based on phase-change materials[12–15], and high-throughput nanoprinting techniques capable of achieving sub-100 nm resolution across centimeter-scale areas[16–19], have greatly improved the tunability, scalability, and manufacturability of metasurface imaging systems, further strengthening their prospects for next-generation imaging.

Beyond their compact nature, the primary advantage of metasurfaces in imaging systems lies in their capacity for finely tuned electromagnetic

[1]Shenzhen International Graduate School, Tsinghua University, Shenzhen, PR China. [2]Peng Cheng Laboratory, Shenzhen, PR China.
✉e-mail: jin.xin@sz.tsinghua.edu.cn

control[20–22]. By correlating specific imaging requirements with carefully defined electromagnetic responses, metasurface designers can determine the optimal material choices, metaatom geometries, and spatial arrangements. This systematic connection between high-level imaging goals and subwavelength-scale wavefront manipulation ensures that the resulting device meets the desired specifications. Through this structured approach, researchers can minimize guesswork and develop metasurface-based imaging solutions capable of exceeding the limits of traditional optical systems.

Despite the advantages, several challenges remain to realize the full potential of metasurfaces in imaging applications[23]. Designing metasurfaces for imaging, particularly those requiring free-form geometries, multidimensional wavefront control, or high degrees of freedom, often involves navigating vast and highly nonlinear design spaces. In such spaces, a single set of performance metrics can correspond to numerous possible nanoscale configurations. Traditional methods, which rely on trial-and-error or local optimization, struggle to capture the full complexity of these multiparameter interactions, making it difficult to identify solutions that satisfy all specifications simultaneously. In response to these challenges, AI has emerged as a key enabler to translate high-level imaging requirements into viable metasurface designs[24–29]. Machine learning and evolutionary algorithms can efficiently explore large parameter spaces, predict complex electromagnetic responses with minimal manual intervention, and accelerate the design cycle. Furthermore, AI-driven models not only optimize the microstructural layout but can extend to image reconstruction or correction tasks in metasurface-based imaging systems, reducing aberrations and enhancing imaging quality.

Building on these perspectives, this review consolidates the imaging metasurface design into a unified three-stage framework (Fig.1): imaging performance specification, electromagnetic response control, and metasurface structure design. By transitioning from abstract imaging objectives to precise electromagnetic constraints and then to detailed structural designs, the "from performance to structure" paradigm provides an efficient roadmap for translating high-level functional demands into tangible metasurface implementations. Furthermore, this review synthesizes the impressive performance of metasurfaces across six electromagnetic response control methods in nine imaging domains, categorizing three primary design approaches: physically driven, meta-heuristic, and AI-driven, and analyzing six primary encoding strategies and eight common AI techniques. In addition to this structured approach, we explore nine prospective research directions: end-to-end metasurface design, multiobjective metasurface design, manufacturing-aware metasurface design, fast solver-aided metasurface design, large-area metasurface design, metasurface array design, cascaded metasurface design, dynamic tunable metasurface design, and hybrid optics and metasurface design. These directions underscore the continued evolution of metasurface technology and its potential to shape next-generation imaging systems with significantly expanded capabilities, with AI technology playing an increasingly crucial role in translating performance specifications into optimized imaging metasurface systems.

Imaging performance specification

Imaging performance specifications serve as the cornerstone for guiding metasurface design, delineating the required imaging metrics, such as chromatic aberration correction, expanded field of view, depth of field extension, resolution enhancement, multidimensional data capture, optical feature enhancement, holographic field reconstruction, functional integration, and compact device integration across nine distinct imaging domains. These specifications not only define the ultimate performance objectives of the imaging system but also provide clear targets for the manipulation of electromagnetic responses, ensuring that the design process is both focused and actionable. By systematically translating high-level imaging requirements into specific design objectives, researchers can leverage the unique capabilities of metasurfaces to achieve remarkable performance in these domains. This section will comprehensively explore the role of metasurfaces in realizing exceptional performance across these nine imaging domains, emphasizing how the ability to manipulate electromagnetic properties on a subwavelength scale enables breakthroughs in imaging system.

Chromatic aberration correction

Chromatic aberration occurs when different wavelengths of light fail to converge at the same focal point, resulting in blurred or color-fringed images. Traditional optical systems often rely on multi-element lenses with varying refractive indices to correct for chromatic dispersion. Although effective, these systems tend to be bulky and complex. Metasurfaces provide a compact alternative, achieving this by precisely controlling the phase of different wavelengths, which enables the simplification of optical assemblies and enhances achromatic imaging capabilities. However, despite these notable advantages, metasurfaces face persistent challenges, such as the resonant dispersion of individual nanoantennas and the intrinsic dispersion of planar devices, both of which continue to impede the realization of high-quality imaging[30,31]. Consequently, recent research has focused on both refining conventional strategies and developing novel solutions, such as hybrid optical integration, inverse design, and deep learning, to improve the efficiency and versatility of chromatic aberration correction.

To achieve broadband achromatic focusing, the required phase profile must satisfy:

$$\phi(r,\lambda) = \frac{2\pi}{\lambda}\left(\sqrt{r^2+f^2}-f\right),$$

where r is the radial coordinate and f is the focal length. Minimizing chromatic aberration requires

$$\frac{\partial\phi}{\partial\lambda} \approx 0,$$

which places strong constraints on the wavelength dependence of both the material dispersion and the meta-atom geometry. These equations form the theoretical foundation for evaluating and designing chromatic aberration correction in metasurface systems. From the first-principles perspective, the chromatic dispersion behavior of metasurfaces arises from two primary sources: material dispersion and geometric dispersion. The total phase imparted by a meta-atom can be decomposed as

$$\phi(\lambda) = \phi_{\mathrm{mat}}(\lambda) + \phi_{\mathrm{geom}}(\lambda),$$

where ϕ_{mat} originates from the intrinsic wavelength dependence of the refractive index, and ϕ_{geom} results from the effective optical path difference governed by the geometry of the nanostructure. For instance, high-aspect-ratio TiO_2 nanopillars behave as truncated waveguides whose modal effective indices vary with wavelength, giving rise to a strong and controllable $\frac{\partial\phi}{\partial\lambda}$[32]. In contrast, Pancharatnam-Berry (PB) phase-based metasurfaces achieve phase control via in-plane rotation of anisotropic structures, yielding inherently dispersion-free (but polarization-dependent) response. Broadband achromatic metasurface designs often exploit hybrid mechanisms—e.g., stacking multiple metasurfaces, combining geometric and resonant phase components, or integrating with refractive optics—to cancel dispersion across multiple wavelengths[30]. These approaches aim to engineer the total phase response such that $\frac{\partial\phi}{\partial\lambda} \approx 0$ is satisfied globally or locally, thereby achieving efficient achromatic focusing.

Early efforts in metasurface-based chromatic correction focused primarily on phase compensation to align focal points across different wavelengths[33]. For instance, titanium dioxide (TiO_2) nanopillars have been employed to achieve broadband achromatic focusing over the 490–550 nm range[34], while geometric phase control has enabled achromatic performance from 1200 to 1680 nm[33], as shown in Fig. 2a. To further enhance dispersion management, researchers have explored stacking multiple metasurfaces, thereby distributing the overall dispersion control across multiple layers[35,36], as illustrated in Fig. 2b. Beyond cascaded configurations, other advanced phase compensation methods have also been developed to address

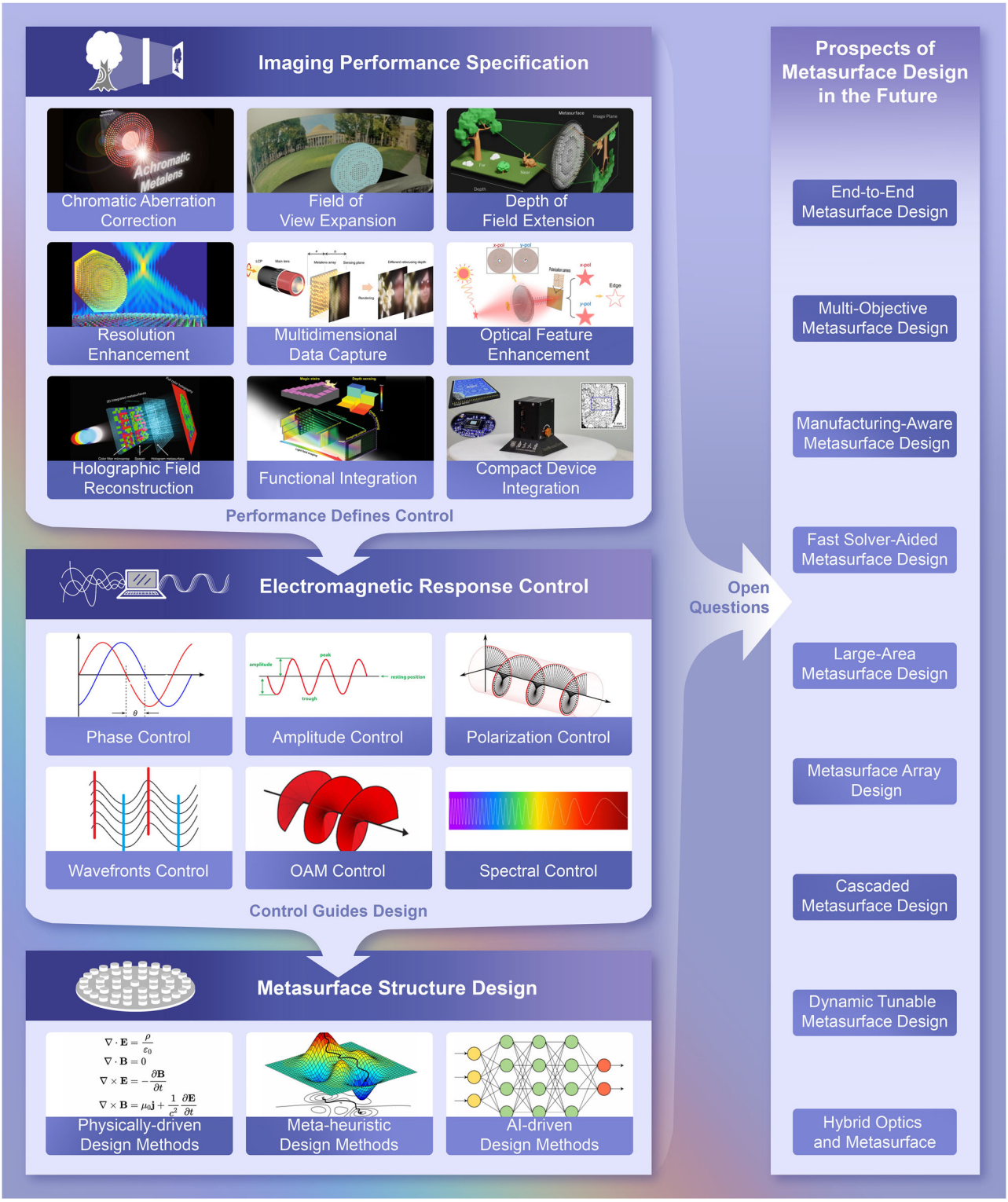

Fig. 1 | Comprehensive design framework for metasurface applications in imaging, encompassing three key stages: imaging performance specification, electromagnetic response control, and metasurface structure design. This framework outlines a systematic approach where imaging performance requirements define the necessary electromagnetic controls, which in turn guide the structural design of metasurfaces. Additionally, the framework highlights potential future directions, underscoring the pivotal challenges and opportunities in metasurface design for imaging applications.

chromatic aberration correction, with a focus on broadband, polarization-insensitive, and high-efficiency operation. For example, Ndao et al.[37] introduced a broadband achromatic metalens based on a photonic fishnet structure, demonstrating an average efficiency above 70% over a continuous spectral range from 640 to 1200 nm. Similarly, Chen et al.[38] and Heiden et al.[39] reported polarization-insensitive achromatic metalenses, underscoring the versatility of metasurface-based designs. Building on these developments, Wang et al.[40] presented a high-efficiency broadband achromatic metalens optimized for the near-infrared biological imaging window. By employing TiO_2 nanopillars with high aspect ratios, they achieved an

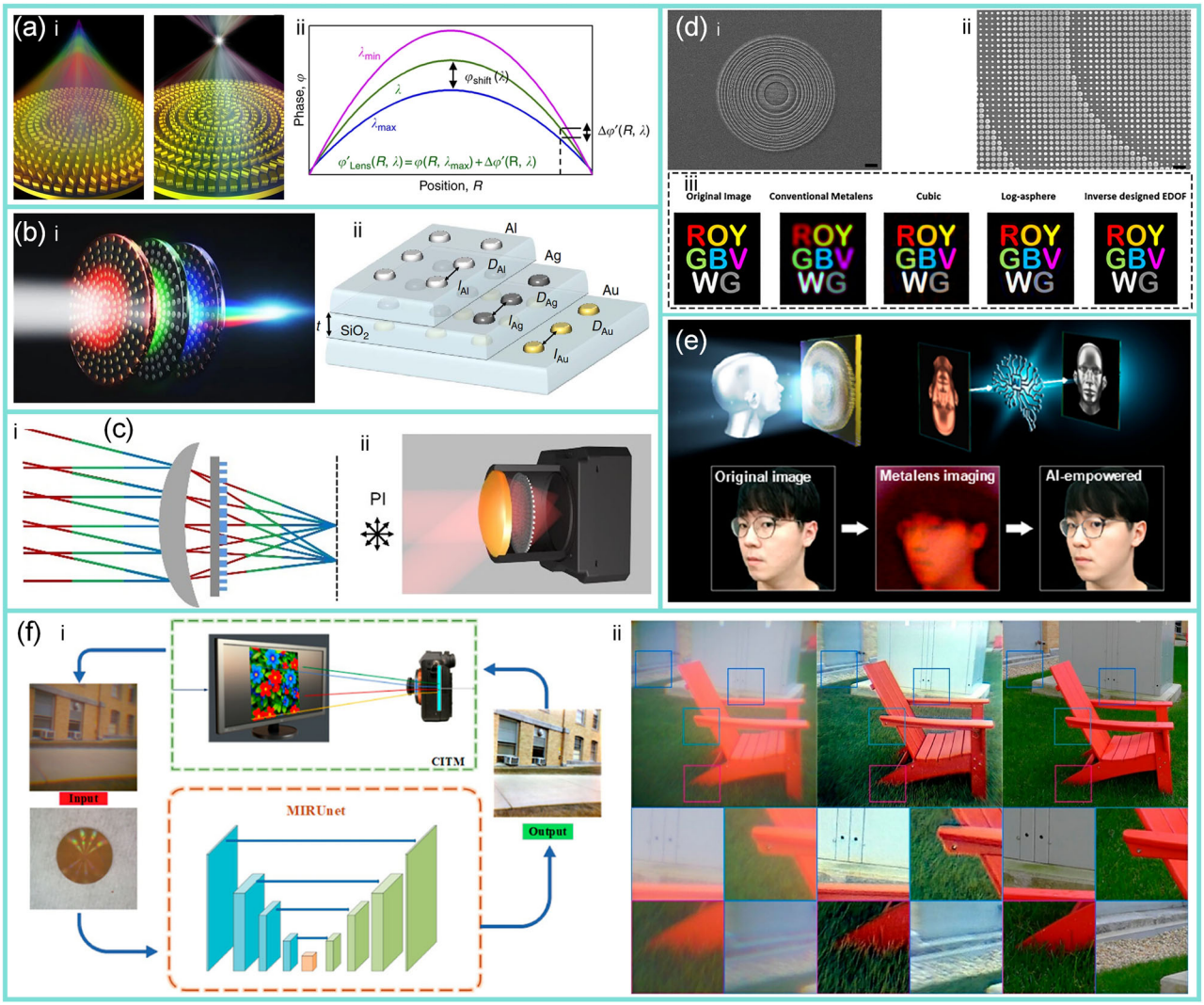

Fig. 2 | Metasurface applications for chromatic aberration correction. **a** Broadband achromatic optical metasurface devices, enabling achromatic performance from 1200 to 1680 nm[33]: i. Schematic for chromatic (left) and achromatic (right) metalenses; ii. Phase profile for broadband achromatic metalens at an arbitrary wavelength. **b** Cascaded metasurfaces for enhanced broadband correction[35]: i. Artist's view of the three-layer lens; ii. Schematic illustration of the layered structure. **c** Combining traditional optics with metasurfaces, featuring a full field-of-view angle surpassing 20° within the 8–12 μm wavelength range[41]. **d** Application of inverse design techniques[42]: i Scanning electron micrograph of inverse-designed metaoptics; ii. Zoom-in scanning electron micrograph of metaoptics; iii. Simulated imaging performance of inverse-designed metaoptics. **e** High-resolution achromatic metalens imaging with sequential AI models[45]. **f** Achromatic single metalens imaging via deep neural network[46].

average efficiency of 77.1–88.5%. Furthermore, hybrid metasurface-refractive optics have been introduced to combine traditional optical components with metasurfaces for superior chromatic aberration correction, Liu et al.[41] designed a hybrid meta-optics doublet for long-wave infrared imaging, effectively mitigating chromatic and coma aberrations by integrating a metasurface corrector with a refractive lens, featuring a full field-of-view angle surpassing 20° within the 8–12 μm wavelength range, as shown in Fig. 2c.

Recent advancements have shifted toward algorithmically optimized imaging metasurface systems, employing both inverse design[42–44] and deep learning[45–48] techniques. Inverse design has been used to realize metalenses with an extended depth of focus and a stable point spread function over a wide bandwidth (Fig. 2d)[42], while genetic algorithms have further enabled achromatic performance spanning 400–1100 nm. These computational strategies are complemented by deep learning approaches, such as autoencoder-based models that correct color distortions (Fig. 2e)[45]. Furthermore, comprehensive image transformation models have been proposed to correct color fringes and enhance resolution in single-wavelength-optimized devices (Fig. 2f)[46]. Despite these advances, robust achromatic performance across various imaging bands—infrared[40,41,49], visible light[45,47,48], and terahertz[50,51]—still requires balancing efficiency, bandwidth, and manufacturability[52,53].

Looking ahead, metasurface-based chromatic aberration correction is poised to achieve broader spectral coverage and more continuous wavelength compensation, encompassing regions from the ultraviolet[54] to the near-infrared[55,56]. Meeting this goal will require maintaining high imaging consistency across wide spectral ranges, while also addressing the complexity of retaining efficiency and precise focusing for multiple wavelength bands. Additionally, controlling the interference caused by multi-band light within a single metasurface structure remains a significant challenge. To overcome these obstacles, future achromatic imaging metasurface system will likely integrate multi-layer architectures, composite materials, and advanced optimization frameworks, particularly those driven by AI. Such approaches will enable more precise phase control, elevated efficiency, and real-time reconfiguration of metasurface parameters, making them well-suited for demanding applications.

Field of view expansion

Expanding the field of view (FOV) is pivotal in numerous imaging applications as it enhances the system's capability to capture a broader perspective, thereby enriching the informational content and analytical utility of the images obtained. However, as the FOV increases, challenges, such as image distortion, aberrations, and resolution loss become more pronounced, especially when aiming to maintain consistent pixel distribution and resolution across large angular spans. Traditional refractive lenses can achieve broader FOV by employing multi-element assemblies, but these systems often become bulky and prone to optical distortions. For instance, standard photographic lenses typically offer a FOV of around 45°, telephoto lenses provide less than 40°, and wide-angle lenses may exceed 60°. In contrast, metasurfaces present a more compact solution by modulating the phase of incident light within a single or few layers, potentially enabling wide-angle imaging without significant performance trade-offs. This section reviews recent developments in wide-FOV metasurfaces, beginning with innovations in single-layer, double-layer, and metasurface array designs, then discussing advances in inverse design and deep learning, and concluding with theoretical constraints on device thickness and angular coverage.

A fundamental constraint on FOV expansion in metasurface optics arises from the off-axis focusing condition. For a metasurface designed to focus at angle θ, the required local phase profile must satisfy:

$$\phi(x) = -k\left(x\sin\theta + \sqrt{x^2+f^2} - f\right),$$

where $k = 2\pi/\lambda$, x is the lateral position, f is the focal length, and θ is the off-axis angle. As θ increases, phase discontinuities become more severe, requiring higher spatial phase gradients and increasing susceptibility to aberrations. This formulation sets the theoretical basis for evaluating angular limitations, aberration accumulation, and device thickness constraints in wide-FOV metasurface designs. Recent advancements in single-layer metalenses have demonstrated their potential for wide-angle imaging without significant losses in resolution or efficiency. For example, one study developed a fisheye metalens with a FOV exceeding 170°, correcting third-order aberrations and achieving a Strehl ratio above 0.8[57] (Fig. 3a). Another approach introduced an aberration-compensated flat lens covering a 32° FOV, effectively addressing both spherical and monochromatic aberrations[58]. Furthermore, efforts to relax diffraction-limited constraints have enabled FOVs larger than 170°, making such metalenses suitable for smartphones and virtual reality applications[59]. Other work has focused on balancing FOV and resolution by applying advanced phase profiles, achieving FOVs greater than 120° for tasks like fingerprint detection[60]. In the infrared domain, polarization-insensitive metalenses have also been demonstrated, achieving FOVs beyond 100°[61].

Beyond single-layer approaches, double-layer metasurfaces have been employed to mitigate aberrations at large incidence angles[62–64]. For instance, a planar camera configuration incorporating a metasurface doublet achieved near-diffraction-limited performance over a 60° × 60° FOV[63] (Fig. 3b). Subsequent work extended this concept to visible wavelengths, correcting both chromatic and monochromatic aberrations[64]. Additionally, metasurface arrays have been investigated to expand the FOV: silicon metalenses integrated with CMOS sensors demonstrated wide-field microscopy capabilities[65] (Fig. 3c), and silicon nitride metalens arrays achieved over 120° FOV in planar wide-angle cameras[66] (Fig. 3d). Furthermore, a bionic compound eye metasurface offering a 120° × 120° FOV was developed for polarization imaging[67].

The incorporation of computational techniques, including inverse design and deep learning, has further expanded the FOV achievable by metasurfaces through optimized phase control and geometry. By combining optical design software with finite-difference time-domain simulations, researchers developed a near-infrared Huygens metalens that preserves high image quality within ±15°[68] (Fig. 3e). Using a damped least-squares method, Fan et al.[69] achieved diffraction-limited focusing beyond 170°. Moreover, a transformer-based neural network has recently been integrated with wide-FOV metalenses, demonstrating over 100° FOV with a 13.5-fold contrast enhancement[70] (Fig. 3f).

Theoretical analyses of wide-FOV metasurfaces have revealed key limitations associated with device thickness and angular coverage. For instance, a thickness constraint for nonlocal metalenses demonstrates the trade-offs among large incidence angles, device thickness, FOV, and lens diameter[71], emphasizing the delicate balance between angular diversity and spatial footprint in multi-channel optical systems. Looking ahead, metasurface-based wide-FOV imaging aims to achieve broader coverage, enhanced optical performance, and scalable, high-precision fabrication. Nonetheless, challenges persist, including the difficulty of large-area manufacturing, the trade-off between performance and manufacturability, and the simultaneous control of aberrations, chromatic dispersion, and focusing ability. Overcoming these barriers will require continued advances in nanofabrication, inverse design and computational optimization, multi-layer architectures, and integrated optical systems. Such innovations will enable superior performance and drive the practical adoption of metasurfaces in a wide range of cutting-edge optical technologies.

Depth of field extension

Achieving a large depth of field (DOF) is essential for maintaining image clarity across a broad range of object distances. Yet conventional optics suffer an inherent trade-off: enlarging the DOF usually requires a longer focal length or a smaller numerical aperture, both of which degrade system compactness or resolution. Diffraction theory gives the approximate limit

$$\mathrm{DOF} \approx \frac{2\lambda f^2}{\mathrm{NA}^2},$$

where λ is the wavelength, f the focal length, and NA the numerical aperture. This equation encapsulates the DOF-resolution compromise in traditional lenses. Metasurfaces circumvent this constraint by tailoring the phase profile $\phi(x)$ at the subwavelength scale to generate axially invariant focal regions—e.g., via multi-focal, varifocal, or extended-PSF designs—thereby extending DOF without sacrificing compactness or lateral resolution.

A key strategy for extending the DOF involves exploiting polarization or other multiplexing methods to enable multi-focal or multi-depth capabilities[72,73] within a single metasurface. For example, spin multiplexing has been integrated with multi-scale convolutional neural networks (CNNs) in bifocal metalens arrays, allowing simultaneous imaging of both near and far scenes across an extreme depth range from centimeters to kilometers (Fig. 4a)[74]. Polarization-sensitive metalenses have also been employed in underwater imaging systems; by focusing orthogonal polarizations at different depths, these designs enhance contrast and extend the DOF under challenging aquatic conditions (Fig. 4b)[75]. Beyond polarization, additional multiplexing approaches leverage chromatic dispersion and orbital angular momentum (OAM). For instance, metasurfaces can exploit dispersion properties to encode depth information via color, enabling compact 3D imaging over the visible spectrum (Fig. 4c)[76]. Another approach utilizes OAM-based division multiplexing for varifocal imaging without mechanical adjustments, covering focal lengths between 5 and 35 mm (Fig. 4d)[77]. Recent developments in polarization-insensitive lenses have further improved robustness under varied illumination conditions: angular modulation techniques extend the DOF while preserving circular-polarization invariance (Fig. 4e)[78], and maintain stable focusing over polarization ranges from 150 to 400 mm[79].

In addition to multiplexing techniques, inverse design and deep learning have greatly accelerated the development of metasurfaces with extended DOF. For instance, topology-shape optimization has been used to realize a focal depth 1.54 times the diffraction limit, achieving a focusing efficiency near 72.6% (Fig. 4f)[80]. Similarly, adjoint-based optimization methods have produced cylindrical metasurfaces with DOFs ranging from 1.5 to 2 times those of conventional designs[81]. Deep learning further refines these systems: neural networks integrated into underwater binocular

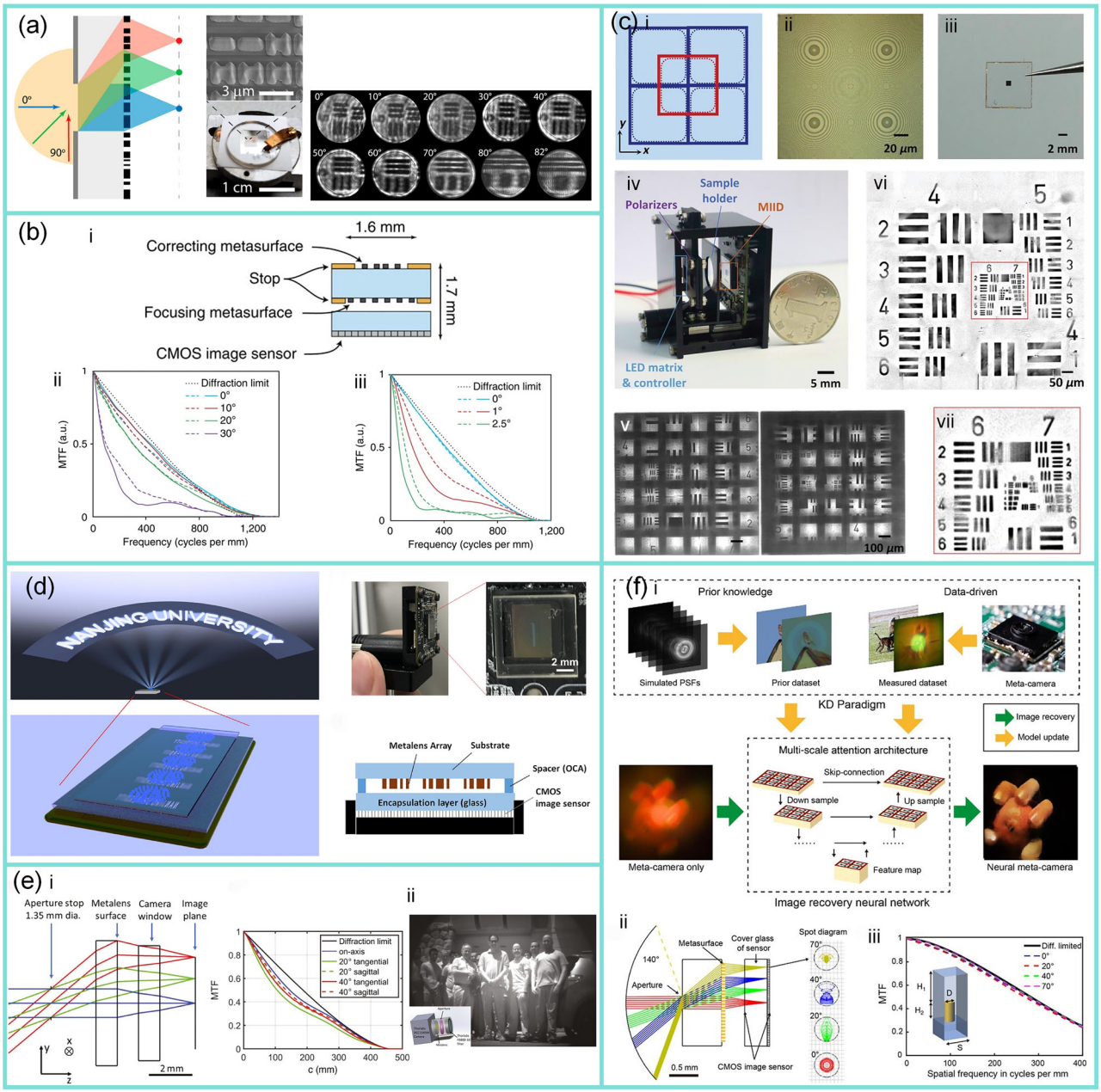

Fig. 3 | Metasurface applications for the field of view expansion imaging. a Single-element diffraction-limited fisheye metalens with a FOV exceeding 170°[57]. **b** Wide-angle metasurface doublet corrected for monochromatic aberrations[63]: i. Schematic drawing of the monolithic metasurface doublet lens; ii. Modulation transfer function (MTF) of the metasurface doublet lens; iii. MTF of the singlet lens. **c** Metalens array-integrated compact imaging devices for wide-field microscopy[65]: i. Phase distribution of the proposed metalens in the x–y plane; ii. Optical microscope image of the proposed metalens; iii. Photograph of the fabricated 6 × 6 proposed metalens array; iv. Photograph of the prototype of metalens-integrated imaging device; v. Raw images of the USAF 1951 resolution chart with LCP (left panel) and RCP (right panel) illuminations; vi. Stitched image from sub-images of (v) through image processing. **d** Planar wide-angle imaging camera enabled by a metalens array[66]. **e** Near-IR wide-field-of-view Huygens metalens[68]: i. Optical layout and nominal MTF; ii. Metalens outdoor image. **f** Ultra-wide FOV meta-camera with transformer-neural-network, demonstrating over 100° FOV with a 13.5-fold contrast enhancement[70]: i. Neural meta-camera mode; ii. Ray-tracing simulation results; iii. Simulated MTF curves at different FOVs.

metalenses have demonstrated micron-level depth accuracy and robust antifouling capabilities (Fig. 4g)[82].

The emergence of compact, multi-functional meta-cameras exemplifies how advanced metasurface techniques can be translated into practical imaging systems. For example, a single-shot 3D depth camera integrates multiple functionalities—including modulators and lenses—into a single metasurface, removing the need for multiple exposures or complex lighting[83]. Moreover, metasurface cameras capable of passively capturing 4D data (2D all-in-focus intensity, depth, and polarization) in one shot have been proposed, demonstrating the potential to streamline imaging systems without sacrificing performance (Fig. 4h)[84].

Looking to the future, metasurface designs will increasingly aim to achieve broader and more continuous DOF ranges, enabling seamless imaging across varying depths with uniform clarity. Yet significant hurdles remain, including the need to preserve high resolution and optical efficiency over extended depth ranges and to control aberrations, such as chromatic dispersion and focusing errors. To overcome these obstacles, future metasurface research will draw upon advanced methods like inverse design,

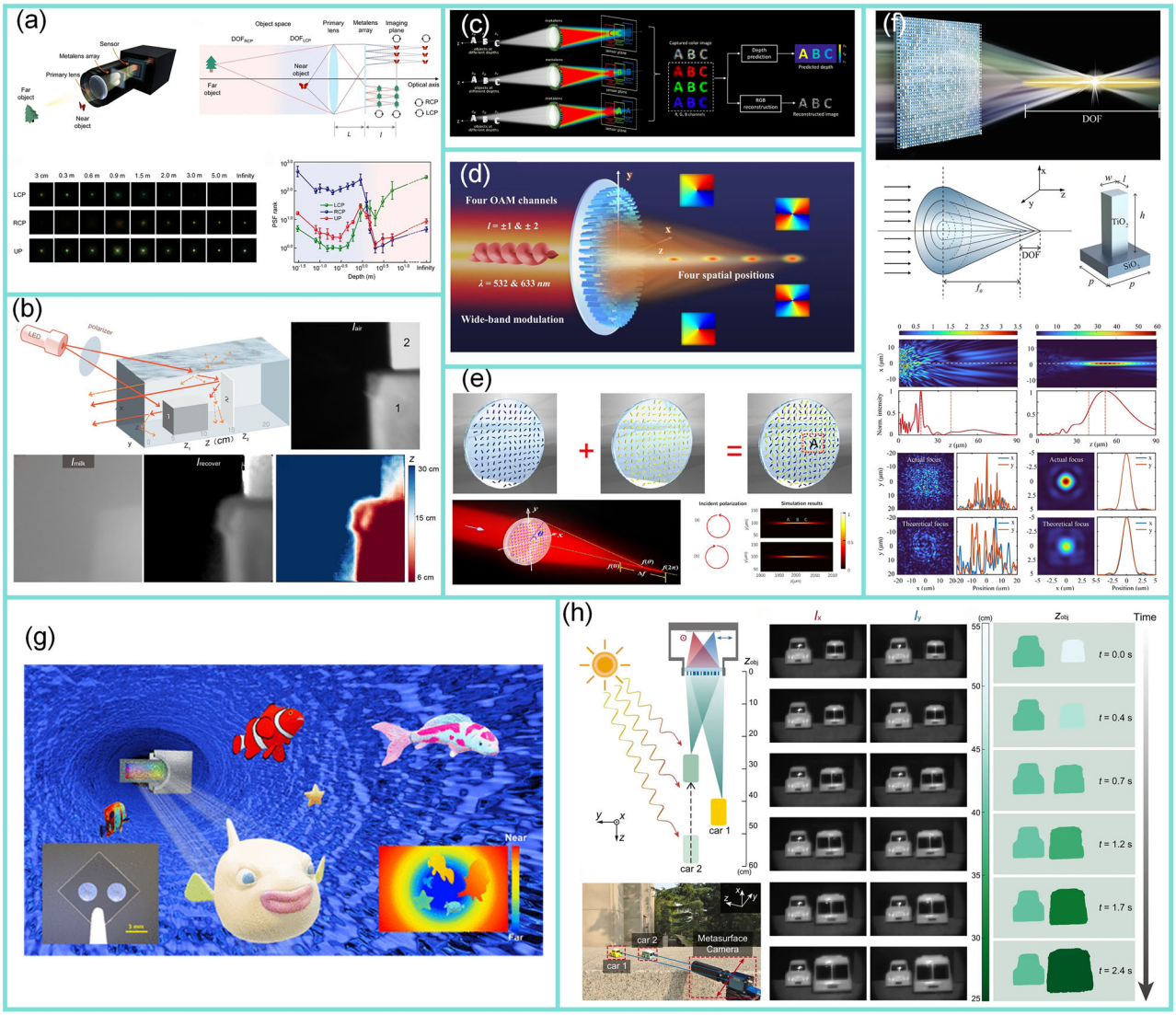

Fig. 4 | Metasurface in extending the depth of field in imaging systems. **a** Trilobite-inspired neural nanophotonic light-field camera with extreme depth-of-field[74]. **b** Metalens-assisted system for underwater imaging[75]. **c** 3D imaging using extreme dispersion in optical metasurfaces[76]. **d** Active multiband varifocal metalenses based on orbital angular momentum division multiplexing, covering focal lengths between 5 and 35 mm[77]. **e** Metasurface lens with angular modulation for extended depth of focus imaging, focusing over polarization ranges from 150 to 400 mm[78]. **f** Designing high-efficiency extended-depth-of-focus metalens via topology-shape optimization[80]. **g** Underwater binocular metalens[82]. **h** Monocular metasurface camera for passive single-shot 4D imaging[84].

multi-layer architectures, and AI-driven optimization. By employing these techniques, metasurfaces can extend their DOF without sacrificing performance, offering versatile and efficient imaging solutions, especially in complex environments where precise depth information is paramount.

Resolution enhancement

High-resolution imaging is critical for delivering clear and precise visual information under diverse conditions[85,86]. The fundamental resolution limit of conventional optical systems is set by Abbe's diffraction criterion:

$$\delta = \frac{\lambda}{2\mathrm{NA}},$$

where δ is the minimum resolvable feature size, λ is the wavelength, and NA is the numerical aperture. Enhancing resolution thus traditionally requires increasing NA or reducing λ, both of which lead to larger, more complex optical assemblies and increased susceptibility to aberrations. Metasurfaces overcome these trade-offs by enabling precise, subwavelength phase manipulation in compact, planar platforms. This capability allows for near- or sub-diffraction-limited focusing, evanescent wave conversion, and non-diffracting beam shaping, underpinning diverse resolution-enhancing strategies, such as high-NA metalens design, super-oscillatory focusing, and far-field reconstruction of subwavelength features.

Four principal strategies have emerged for enhancing resolution in metasurface-based imaging. The first involves reducing the focal spot size by tailoring nanostructures, which can yield sub-diffraction or near-diffraction-limited performance. Metasurfaces facilitate subwavelength focusing by precisely controlling the phase at the nanoscale, enabling resolutions beyond those of traditional high-NA optics. As illustrated in Fig. 5a, TiO_2-based metalenses with high-aspect-ratio nanofins achieve diffraction-limited focal spots smaller than those of conventional objectives[87]. Further gains have been realized through binary amplitude-phase modulation, enabling super-oscillatory focusing with minimal sidelobes[88]. Reflective metalenses employing evanescent-field enhancement enable multifunctional sub-diffraction focusing[89], whereas immersion metalenses designed for visible wavelengths leverage a high NA to improve spatial resolution[90]. Another approach, the "Bessellens," combines lens and axicon functionalities to produce non-diffracting beams for super-

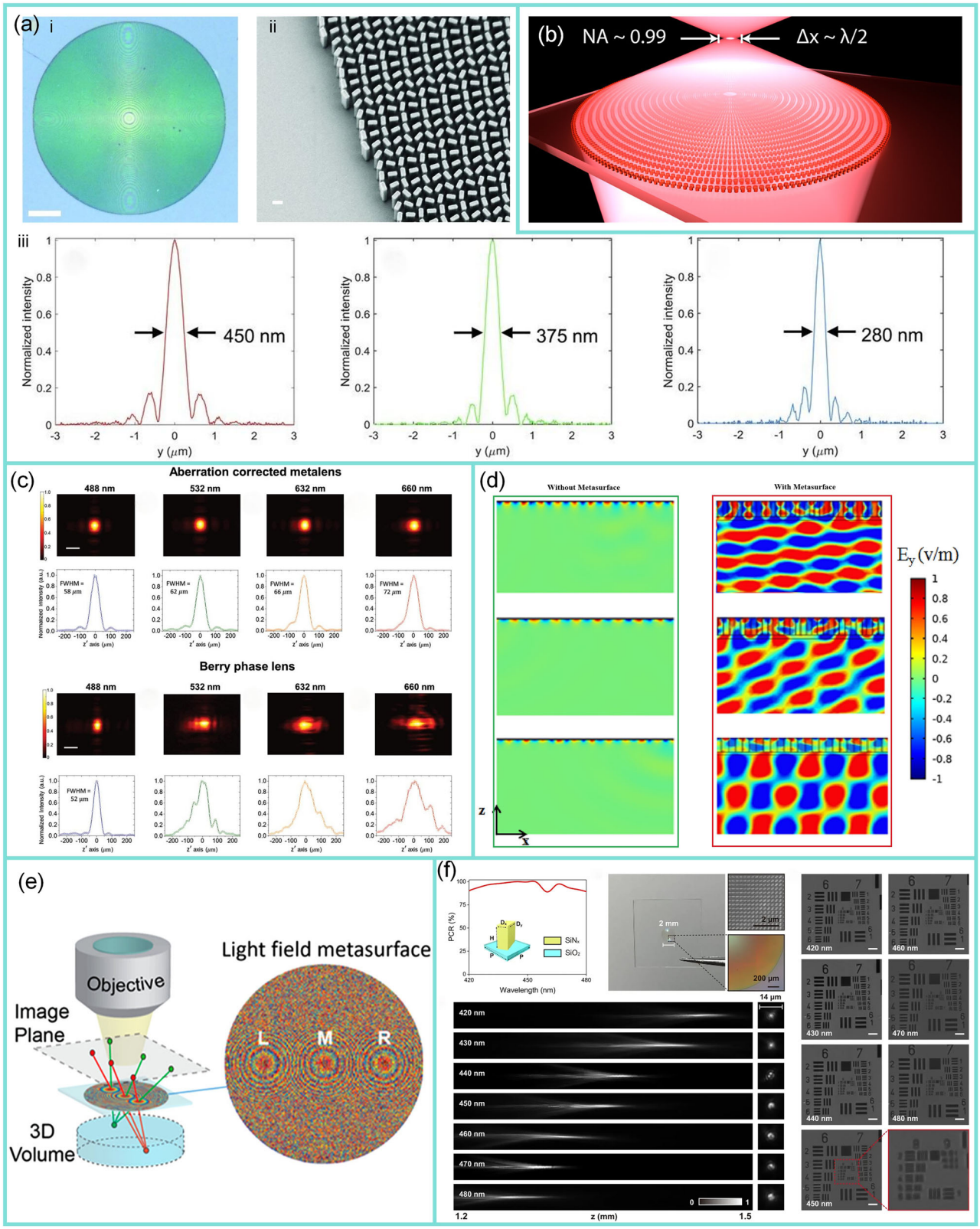

Fig. 5 | Resolution enhancement imaging using metasurfaces. a Diffraction-limited focusing metalens at visible wavelengths[87]: i. Optical microscope image of the metalens; ii. Scanning electron micrograph of the metasurface structure; iii. Normalized intensity profiles for different wavelengths. **b** Metalens with a near-unity NA, exhibiting a subwavelength thickness (~$\lambda/3$) and a focal spot size of 385 nm[94]. **c** Aberration-corrected spectrometers in the visible using dispersion-tailored metasurfaces[96]. **d** High-order continuous dielectric metasurface to convert evanescent waves into propagating modes for super-resolution imaging in the far field, achieving a spatial resolution of $\lambda/5.5$[100]. **e** Metasurface for high-resolution single-particle tracking[102]. **f** High phase detection accuracy imaging with a compact meta-microscope[104].

resolution imaging[91]. Additionally, polarization-based techniques, such as radially polarized illumination combined with circular high-pass apertures—enhance longitudinal field components to yield focal spots below the Abbe diffraction limit[92]. Finally, high-performance GaN metalenses further improve focusing efficiency, enabling diffraction-limited imaging at visible wavelengths[93].

Second, increasing the NA remains a pivotal strategy for improving resolution. Metasurfaces can achieve high NA by precisely controlling phase profiles. As shown in Fig. 5b, a near-unity NA metalens attained a collection angle of 82° at 715 nm, exhibiting a subwavelength thickness (~$\lambda/3$) and a focal spot size of 385 nm[94]. High-aspect-ratio nanoantennas with asymmetric scattering efficiently redistributed light, overcoming conventional phase-mapping losses and enabling confocal imaging of nitrogen-vacancy centers in diamond nanocrystals. By pushing the NA further to 1.4, a metasurface employing partial phase control achieved near-diffraction-limited resolution (~0.32λ) in the visible range[95]. In this design, replacing full $0–2\pi$ phase shifts with partial shifts reduced near-field interactions and allowed for a compact, high-efficiency configuration. The resulting immersion metalens supported broadband anomalous refraction and wavelength de-multiplexing at up to 67% efficiency, underscoring the potential of high-NA metasurfaces.

Next, aberration correction represents a vital approach to achieving high resolution, particularly through mitigating chromatic and spherical aberrations that distort the focal spot. Correcting these aberrations yields a more concentrated focal region, thereby enhancing resolution and producing sharper images. For example, a compact aberration-corrected spectrometer employing dispersion-tailored metasurfaces was demonstrated (Fig. 5c). By engineering the dispersion of a TiO_2-based metasurface lens, high spectral resolution with minimal aberration was achieved over a 200 nm bandwidth in the visible range[96]. This lens, fabricated with nanofins, enabled precise phase control and minimized chromatic aberration, yielding subnanometer resolution at multiple visible wavelengths. In a related effort, a large-scale hybrid metalens combining refractive and diffractive components utilized PB phase to correct chromatic and spherical aberrations[97]. This design addressed 80% of chromatic aberration and 70% of spherical aberration, while high-aspect-ratio nanofins enabled centimeter-scale metasurfaces that outperformed standard refractive lenses, showcasing the potential for compact optical systems.

Evanescent wave manipulation is key to surpassing the diffraction limit, as these waves carry high spatial frequency information that typically decays exponentially and remains inaccessible to conventional far-field imaging. By controlling evanescent waves, metasurfaces can enhance or convert them into propagating modes, thereby recovering sub-diffraction details and enabling high-resolution imaging. For instance, a silver superlens demonstrated that surface plasmon resonance could bolster evanescent waves, achieving sub-diffraction optical imaging[98]. Building on this concept, metalenses composed of anisotropic metamaterials were introduced to amplify evanescent-wave information and project it into the far field, attaining super-resolution imaging beyond the diffraction limit[99]. More recently, high-order continuous dielectric metasurfaces have been shown to convert evanescent waves into propagating modes, reconstructing super-resolution images in the far field with resolution of $\lambda/5.5$ (Fig. 5d)[100]. Additionally, a space-time modulated computational metasurface imager employed temporal modulation to translate high-frequency components into lower-frequency domains, enabling single-pixel super-resolution beyond the Abbe limit[101].

Recent breakthroughs address the enduring trade-offs among resolution, efficiency, and optical complexity, while also reducing mechanical constraints. Holsteen et al.[102] and Conteduca et al.[103] introduced light-field and high-Q metasurfaces, respectively, to merge high resolution with extended sensing volumes or confocal-like imaging. Meanwhile, Pahlevaninezhad et al. cite pahlevaninezhad2022metasurface preserved high lateral resolution over a larger depth range in tomographic applications. In parallel, Wang et al.[104] and Zhou et al.[105] eliminated the need for sample-plane translation by employing dispersion-based or multiplexed phase-shifting illumination, thereby maintaining fine spatial detail without mechanical adjustments.

Altogether, these structural and methodological innovations—encompassing focal spot minimization, large-NA designs, aberration correction, evanescent-wave manipulation, and advanced computational strategies—demonstrate how metasurfaces are extending optical resolution beyond conventional limits in compact, robust form factors. Looking ahead, future metasurface designs will prioritize achieving higher spatial resolution, enabling imaging systems to capture finer details with greater precision. Yet significant challenges remain, including preserving high optical efficiency and suppressing aberrations, such as chromatic dispersion and focusing errors. To surmount these obstacles, researchers will employ advanced methods like inverse design, multi-layer architectures, and AI-driven optimization. These innovations will facilitate high-resolution imaging without sacrificing performance, offering flexible and efficient solutions, particularly in complex environments where precise detail is paramount. By refining these technologies, metasurfaces are poised to transform imaging systems, delivering exceptional resolution and optical efficiency across a variety of demanding imaging applications.

Multidimensional data capture

Capturing multidimensional data in imaging is crucial for comprehensive analysis, as it integrates multiple perspectives and scales simultaneously. Traditional imaging systems primarily record light intensity and color, limiting the richness of the acquired information. These systems often require complex multi-element assemblies to encode additional dimensions, which increases size, cost, and optical aberrations. In contrast, metasurfaces' precise control over phase and amplitude enables the encoding and decoding of multidimensional data within a single captured image, overcoming the limitations of conventional optics and providing compact imaging solutions. Importantly, beyond compactness and structural simplicity, recent metasurface systems also achieve significant functional advantages over traditional approaches. In light-field acquisition, virtual moving metalens arrays preserve spatial sampling while simultaneously doubling both the fill factor and resolving power, leading to a fourfold improvement in image resolution compared to passive microlens arrays[106]. In spectral imaging, quasi-bound-state metasurface spectrometers attain a spectral resolution of 1.7 nm, while delivering more than an order-of-magnitude improvement in photon throughput compared to conventional grating-based systems[107]. For polarization detection, dielectric metasurfaces exceed the classical 50% transmission ceiling of filter-based methods, reaching 65% transmission efficiency and extinction ratios above 23:1[108].

From a structural perspective, metasurfaces enable high-dimensional data capture across multiple domains, beginning with 3D imaging. In active 3D imaging, structured light is projected onto a scene, and depth information is inferred from pattern deformation[109,110]. For instance, a metasurface-based system enhanced depth perception for industrial inspection by projecting structured light[109], while a single-shot technique achieved 3D imaging without requiring multiple exposures[110]. By contrast, passive 3D imaging manipulates the phase and amplitude of incoming light to extract depth and angular information without external illumination[82,111]. In one demonstration, a metasurface-based underwater imaging system harnessed ambient light to infer depth, making it ideal for low-light or submerged environments[82]. Another passive metasurface camera captured both angular and depth data from natural light, offering improved imaging in scenarios where active illumination is impractical[111].

Building on the principles of 3D imaging, metasurfaces have also propelled developments in light-field (4D) imaging, which captures both spatial information and the angular distribution of light rays. An achromatic metalens array composed of GaN nanoantennas was introduced to mitigate chromatic aberration in conventional light-field cameras, achieving full-color, broadband imaging with a diffraction-limited resolution of 1.95 μm (Fig. 6a)[112]. Additionally, a thin nanophotonic array camera integrating

metasurfaces atop the sensor cover glass successfully captured high-quality images over a wide field of view exceeding 100° (Fig. 6b)[113].

Beyond capturing spatial and angular information, metasurfaces can also record spectral data, thereby expanding imaging systems into the spectral domain[55,114–118]. By selectively controlling light-matter interactions across different wavelengths, metasurfaces enable highly efficient spectral acquisition. For instance, colloidal metasurface pixels achieved narrowband spectral selectivity by tuning resonance wavelengths from 580 to 1125 nm[114]. An ultra-compact hyperspectral imager used folded metasurface optics to reach a spectral resolution of about 1.5 nm and an angular resolution of 0.075° within a miniaturized footprint[115]. Additionally, a label-free biosensing platform combined dielectric metasurfaces with hyperspectral imaging to retrieve spectral data from a single image, supporting portable diagnostic applications (Fig. 6c)[116]. Passive and snapshot spectral imaging systems leveraging dynamic and parallel metasurfaces, respectively, offered compact, efficient spectral data acquisition[119,120], while real-time and AI-optimized hyperspectral designs further improved practicality and resolution[121,122]. More recent approaches include snapshot near-infrared and reconfigurable hyperspectral imagers with high spectral fidelity (Fig. 6d)[123], as well as a compact angle-resolved metasurface spectrometer suitable for portable devices[124].

In addition to spectral imaging, polarization imaging is another critical dimension in multidimensional data capture. Polarization conveys essential information about surface characteristics, such as texture and anisotropy, that intensity and color alone cannot reveal. In metasurface architectures, polarization states are most commonly represented using Jones vectors:

$$\mathbf{E}_{\text{in}} = \begin{bmatrix} E_x \\ E_y \end{bmatrix},$$

where E_x and E_y are the complex field components along orthogonal directions. Anisotropic meta-atoms can be modeled as complex Jones matrices:

$$\mathbf{J} = \begin{bmatrix} J_{xx} & J_{xy} \\ J_{yx} & J_{yy} \end{bmatrix},$$

such that the output field is given by $\mathbf{E}_{\text{out}} = \mathbf{J} \cdot \mathbf{E}_{\text{in}}$. This framework enables accurate modeling of polarization-dependent phenomena: for example, PB phase elements implement unitary Jones matrices with spin-dependent off-diagonal terms, while birefringent or resonant structures typically modulate the diagonal elements to enable broadband, polarization-insensitive control. For partially coherent or depolarizing fields, polarization manipulation is more comprehensively described using a 4 × 4 Mueller matrix acting on the Stokes vector.

Matrix-based polarization metasurface imaging systems[125,126] simultaneously capture multiple polarization states, providing detailed insights into an object's physical properties. Full-Stokes imaging polarimetry using dielectric metasurfaces measures all four Stokes parameters at each super-pixel, surpassing the 50% efficiency limit of conventional polarization-filter-based cameras (Fig. 6e)[127]. Additionally, a compact full-Stokes camera employing matrix Fourier optics enables snapshot imaging of complete polarization states without mechanical components[128]. High-efficiency, all-dielectric metasurfaces have been developed for near-infrared full-Stokes detection, integrating both linear and circular polarization filters onto a single chip[129]. Furthermore, bilayer metasurfaces allow observation of a full-parameter Jones matrix, providing independent amplitude and phase control for arbitrary polarization states[130]. Recent innovations include visible-light full-Stokes polarimetry using all-dielectric metasurfaces, enabling spatial separation of polarization components with high efficiency[131], and single-shot, chip-integrated polarization cameras for real-time, high-accuracy imaging[132,133]. A broadband achromatic metasurface polarimeter extends these capabilities to full-color, full-Stokes polarization imaging in the visible range, demonstrating low reconstruction errors (Fig. 6f)[134]. Finally, compact, single-shot full Mueller matrix imaging systems employing metasurfaces facilitate real-time medical imaging and material characterization with high-speed accuracy[125,135].

Metasurfaces are moving toward integrating multiple dimensions of data capture within a compact system. For example, an ultra-compact snapshot spectral light-field imaging setup acquires four-dimensional data —three-dimensional spatial plus one-dimensional spectral—in a single exposure, attaining a spectral resolution of 4 nm and near-diffraction-limited spatial resolution (Fig. 6g)[136]. Similarly, a dispersion-assisted high-dimensional photodetector simultaneously measures intensity, polarization, and spectral information by exploiting thin-film interfaces with spatial and frequency dispersion (Fig. 6h)[137]. Through wavevector-domain projections and a deep residual network for reconstruction, this device performs full-Stokes, broadband characterization in a single measurement. Such integrated approaches underscore how metasurfaces consolidate multiple data dimensions, reducing system complexity and enriching the captured information.

The drive for higher-dimensional perception, particularly in the AI era, underpins the development of intelligent systems that benefit from multimodal information fusion. Future imaging metasurface system will target the capture of additional data dimensions—such as light field, polarization, and phase—to advance multidimensional imaging. The objectives include not only acquiring more information but also refining dimensional precision and integrating these capabilities into compact devices.

Recent developments indicate that metasurfaces are beginning to enable the capture of capturing orbital angular momentum (OAM) by precisely engineering the phase and momentum of light[138–140]. By imposing azimuthal phase gradients or helical wavefronts, metasurfaces can selectively generate, manipulate, and demultiplex multiple OAM modes in a compact and integrable form[141,142]. These capabilities hold significant promise for enhancing information capacity in optical communications and enriching contrast mechanisms in OAM-resolved imaging. In parallel, advances in ultrafast metasurface design[143–145] suggest growing potential for encoding and decoding temporal degrees of freedom, including pulse duration[143], temporal chirp[146], and waveform shape[147]. Through dispersion engineering or time-modulated meta-units, such systems enable femtosecond-scale control of light fields, opening new opportunities in time-resolved spectroscopy, optical pulse shaping, and spatiotemporal focal engineering. Nonetheless, significant challenges persist. Current sensors, primarily designed for intensity data, struggle with dimension coupling and require multi-sensor configurations. To address these limitations, future metasurfaces will employ physical decoupling techniques to isolate distinct optical dimensions, while emerging sensor architectures enable simultaneous multidimensional data capture. Additionally, AI-driven algorithms will optimize data extraction and decoupling, boosting the precision and efficiency of multidimensional imaging systems.

Optical feature enhancement

In many imaging applications, the goal extends beyond mere information acquisition to include direct information processing. Traditional imaging systems primarily focus on capturing light intensity and color, relegating tasks, such as edge detection, image segmentation, and motion recognition to post-capture image processing software. This separation necessitates complex multi-element assemblies, increasing the system's size and cost. Metasurfaces allow for the extraction and enhancement of optical features like edges and specific image segments directly, reducing reliance on external processing and facilitating more compact, efficient imaging systems.

Metasurfaces can adapt to diverse optical feature enhancement applications, from simple edge enhancement to complex three-dimensional scene feature extraction, demonstrating vast potential. For edge detection, three main metasurface approaches are employed: First, spatial differentiation in the Fourier domain enhances high-frequency components of light, as shown in Fig. 7a[148]. The proposed metasurface utilizes a PB phase design to perform

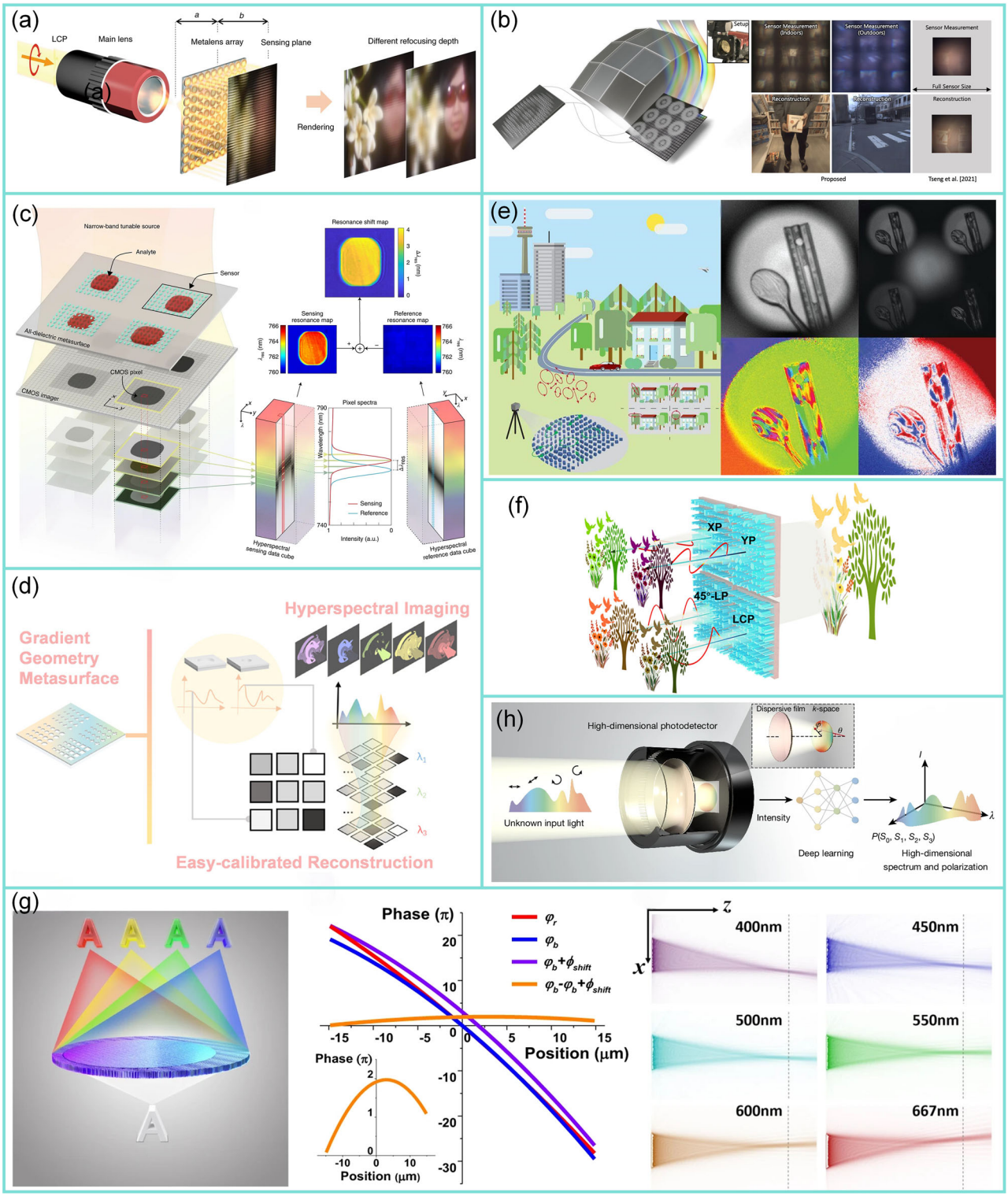

Fig. 6 | Multidimensional data capture enabled by metasurfaces. a Achromatic metalens array for full-color light-field imaging[112]. **b** Thin on-sensor nanophotonic array cameras for wide-FOV light field imaging[113]. **c** Ultrasensitive hyperspectral imaging enabled by dielectric metasurfaces[116]. **d** Reconfigurable snapshot hyperspectral imaging sensor based on gradient geometry metasurface[123]. **e** Matrix Fourier optics enables a compact full-Stokes polarization camera[128]. **f** Achromatic full-Stokes polarimetry metasurface for full-color polarization imaging[134]. **g** Ultra-compact snapshot spectral light-field imaging[136]. **h** Dispersion-assisted high-dimensional photodetector[137].

spatial differentiation in the Fourier plane, enabling broadband edge detection with high optical efficiency and adjustable resolution. Second, the Laplacian operator, a second-order differential operator, captures subtle image changes and facilitates efficient edge extraction in metasurfaces. A flat optical system for image differentiation was presented[149], demonstrating a two-dimensional spatial differentiator that directly converts images into their Laplacian, enabling direct edge detection, as illustrated in Fig. 7b. Third, combining differentiation and integration operations enhances edges while

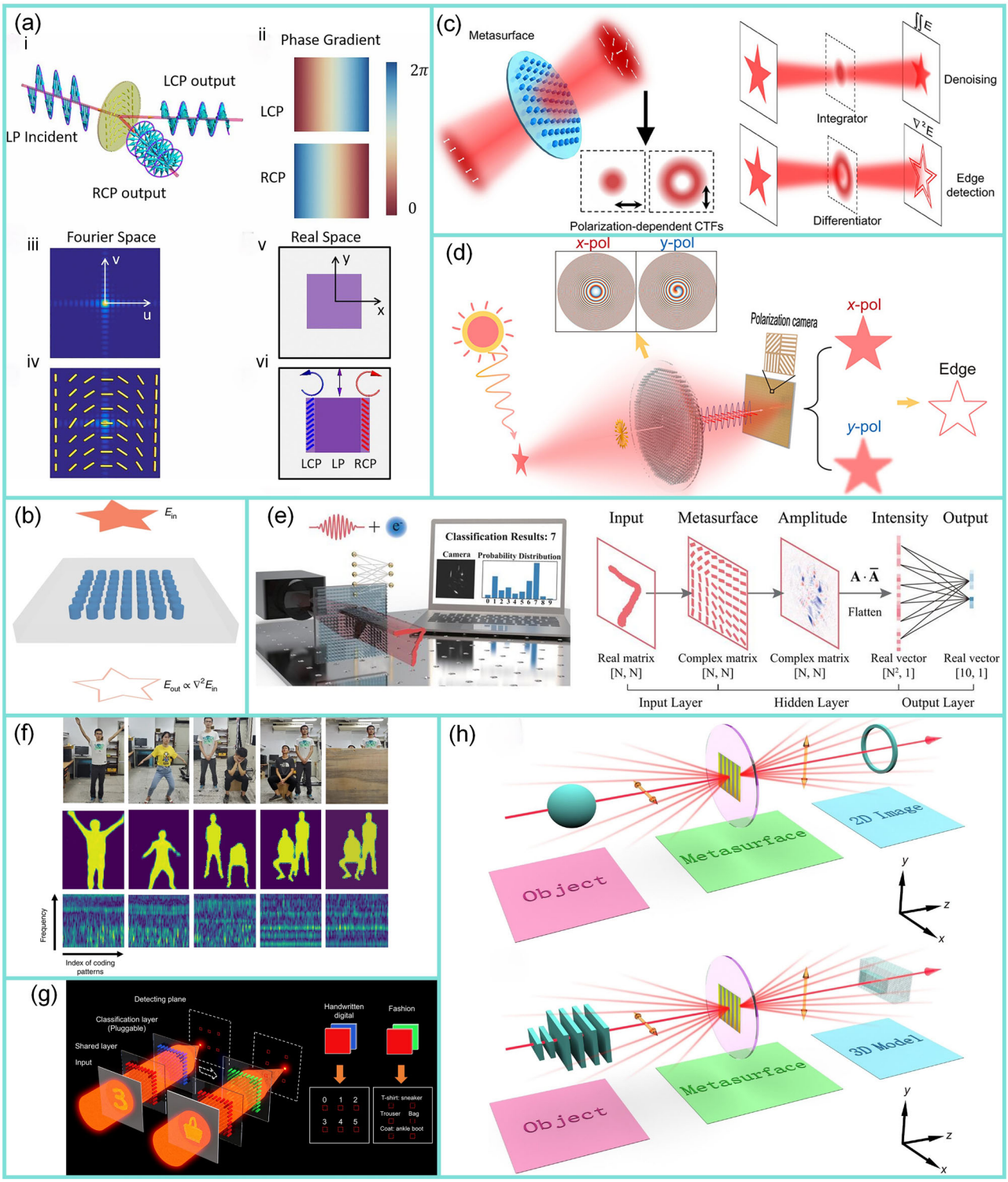

Fig. 7 | Optical feature enhancement using metasurfaces. a Polarization-dependent metasurface for optical field manipulation[148]: i. Incident LP light producing LCP and RCP outputs; ii. Phase gradient control for LCP and RCP; iii. Fourier space and iv. phase distribution for incident light; v. Polarization transformation between real and Fourier spaces; vi. LCP and RCP propagation. **b** Metasurface-based spatial differentiation for edge detection[149]. **c** Concurrent image differentiation and integration processings enabled by polarization-multiplexed metasurface[151]. **d** Metalens for accelerated optoelectronic edge detection under ambient illumination[153]. **e** All-dielectric metasurface empowered optical-electronic hybrid neural networks for MINIST[154]. **f** Gesture and posture recognition using a metasurface[160]. **g** Pluggable multitask diffractive neural networks based on cascaded metasurfaces[162]. **h** All-optical object identification and three-dimensional reconstruction based on optical computing metasurface[164].

smoothing image noise. A metasurface edge encoder for incoherent infrared radiation was developed[150], which generates polarization-dependent optical transfer functions for Laplacian-based edge detection in the long-wave infrared band. By integrating polarization-multiplexed metasurfaces with refractive lenses, they achieved single-shot edge detection in both indoor and outdoor scenes under ambient sunlight, as shown in Fig. 7c. Finally, a polarization-multiplexed metasurface enables concurrent differentiation and integration processing[151], facilitating simultaneous edge enhancement and noise reduction. Metasurfaces have also demonstrated effective edge detection in the visible spectrum. For instance, a two-dimensional isotropic metasurface design[152] overcomes limitations, such as polarization dependence and narrow bandwidth, enabling efficient broadband edge detection across visible wavelengths. Moreover, a polarization-multiplexed metalens system[153] achieves single-shot edge detection under ambient illumination in both indoor and outdoor settings, as illustrated in Fig. 7d.

Metasurface technology has been further applied to feature extraction tasks, such as digit recognition in the MNIST dataset. This dataset benefits from metasurfaces' optical modulation capabilities to efficiently extract key features, transitioning from basic edge detection to more complex tasks like digit recognition[154]. introduced all-dielectric metasurfaces in optical-electronic hybrid neural networks. They designed a network consisting of a TiO_2 metasurface and a fully connected electronic layer. This combination, leveraging nonlocal neural layers and nonlinear transformations, achieved a blind-test accuracy of 98.05% on the MNIST task, as shown in Fig. 7e. This work highlights the potential of integrating metasurfaces with electronic networks for enhanced performance and compactness. Additionally[155], demonstrated a meta-neural-network for real-time, passive deep learning-based object recognition. The system can directly recognize 3D objects without sensor scanning or post-processing.

Subsequently, metasurfaces have been used for more complex optical feature enhancement tasks[156–159]. This technology holds paramount importance in domains, such as health monitoring and intelligent interaction, facilitating critical applications, such as atmospheric CO2 surveillance, pathogen detection in medical diagnostics, and dynamic system adjustments in smart environments. Li et al.[160] proposed an integrated hierarchical system composed of three artificial neural networks that transform measured microwave data into images of the whole human body and instantly recognize hand signs at a Wi-Fi frequency of 2.4 GHz, as illustrated in Fig. 7f. By employing a large-aperture programmable metasurface, they achieved high-resolution imaging and recognition of multiple non-cooperative individuals in real-world settings. Wang et al.[161] designed a transmissive programmable metasurface that dynamically controls electromagnetic focusing to illuminate the forearm and obtain comprehensive echo data.

In complex scenarios, metasurfaces have also been used to simultaneously extract gestures and physiological signals. By processing multimodal signals, metasurfaces can synchronously capture feature information from different signal sources. For instance, He et al.[162] designed a pluggable diffractive neural network that can perform various recognition tasks by switching internal plug-ins, as illustrated in Fig. 7g. By integrating cascaded metasurfaces, they experimentally demonstrated the recognition of handwritten digits and fashion items, showing that the P-DNN enhances the flexibility of optical neural networks and extends their potential in multifunctional applications. Li et al.[163] designed a microwave reconfigurable imaging system based on a programmable coding metasurface to generate radiation patterns required by machine-learning-optimized measurement modes.

Finally, metasurface technology has been further applied to feature extraction in three-dimensional scenes. In three-dimensional scenes, metasurfaces not only need to extract edge information on two-dimensional planes but also combine multidimensional information, such as depth and angle to achieve comprehensive perception of complex three-dimensional environments. Xu et al.[164] established a mechanism for all-optical object identification and applied it to 3D reconstruction, as illustrated in Fig. 7h. Their experimental results showed successful identification and reconstruction of both high-contrast and low-contrast objects. Yang et al.[165] designed a geometric metasurface based on a double-helix point spread function that can achieve depth measurement under incoherent light and two-dimensional edge detection under coherent light.

Metasurface technology has been demonstrated to exhibit a high degree of variability and adaptability in enhancing optical features. Looking ahead, metasurface technology will focus on real-time optical feature enhancement, with the goal of achieving faster, more accurate detection and reducing the need for traditional post-processing. The challenge lies in the direct signal processing on metasurfaces and efficiently extracting key information from them, as current systems are mainly limited to intensity-based data capture. To address these constraints, future metasurfaces will integrate optical computing with AI-driven hardware modules, enabling real-time data processing and direct decision-making. Additionally, the development of integrated optoelectronic modules that combine light manipulation with data processing will allow for more compact, efficient systems, pushing the boundaries of real-time imaging systems.

Holographic field reconstruction

Holographic field reconstruction (HFR) is a pivotal technique in advanced imaging applications, enabling the accurate reconstruction of 3D objects from their light field information. This capability is essential for applications, such as virtual reality (VR)[166–168], augmented reality (AR)[169–171], and data encryption[172–175]. Traditional holographic imaging systems rely on spatial light modulators and bulk optical components to encode and decode both the phase and amplitude of light waves. However, these conventional systems are often constrained by a limited space-bandwidth product (SBP), large physical dimensions, and an inability to perform complex amplitude holography, which undermines the fidelity and scalability of holographic reconstructions. Metasurfaces offer significant advantages by allowing smaller effective pixel sizes, boosting the SBP through multiplexing techniques, and enabling comprehensive control over both phase and amplitude[176–178]. For example, in visual cryptography, vortex-wavelength multiplexed metasurfaces achieve information rates exceeding 1293 bits per hologram—over 2500 times higher than traditional hologram encoding schemes[179]. In 3D holography, angular-spectrum-based metasurfaces extend the achievable depth range from 2 to 95 mm, marking a 47.5-fold improvement over Fresnel diffraction-based methods[180]. Moreover, metasurfaces enable wide-angle reconstructions with viewing angles surpassing ±70°, far exceeding the ~8° limitation of conventional systems constrained by spatial light modulator pixel pitch[181]. These improvements lead to more compact, efficient, and high-performance holographic imaging systems[182–185].

SBP is a crucial parameter in holographic imaging, representing the product of the spatial frequency bandwidth and the field of view that a system can handle. SBP in traditional optical systems is limited by the physical size and resolution of their pixels. Metasurfaces control multiple information channels within a relatively small physical pixel, effectively encoding more optical information in the same area. Various multiplexing methods have been employed in metasurface holography to increase SBP, such as polarization multiplexing, OAM multiplexing, and wavelength multiplexing. For example, polarization multiplexing[7] encodes multiple independent holographic images within a single metasurface by mapping information into different polarization states (Fig. 8a). OAM multiplexing[186] uses the rotational properties of light to encode distinct holograms, thus significantly boosting the information capacity (Fig. 8b). Wavelength multiplexing[187] further extends SBP by generating separate holographic images at different wavelengths, tapping into the spectral dimension (Fig. 8c). Meanwhile, traditional spatial light modulators typically display only pure-phase holograms, preventing complete image reconstruction where amplitude control is crucial. In contrast, metasurfaces can concurrently manipulate phase and amplitude, enabling complex amplitude holographic reconstruction[188–190]. For instance, complex amplitude holography[191] harnesses metasurfaces to reconstruct both amplitude and phase of an optical field, resulting in more detailed and realistic holographic images (Fig. 8d).

Fig. 8 | Holographic field reconstruction using metasurfaces. a Metasurface-based holographic reconstruction using polarization multiplexing[7]. **b** Metasurface orbital angular momentum holography[186]. **c** Wavelength de-multiplexing metasurface hologram[187]. **d** Color holographic display based on complex-amplitude metasurface[191]. **e** Electromagnetic reprogrammable coding-metasurface holograms[192]. **f** On-chip-driven multicolor 3D meta-display[195]. **g** Full-color plasmonic metasurface holograms[197]. **h** Decimeter-depth and polarization addressable color 3D meta-holography[180].

Such dual-mode control is indispensable in high-fidelity holography where preserving the integrity of the optical field is paramount.

Beyond SBP improvements and amplitude-phase control, metasurfaces drive progress in HFR through enhanced programmability, on-chip integration, full-color rendering, and three-dimensional holography. Thanks to their high design flexibility, metasurfaces can be dynamically controlled via external stimuli, such as electric and optical fields or thermal modulation, enabling real-time reconfigurable holographic displays. This adaptability surpasses what is achievable with conventional holographic components. For instance, programmable metasurface holograms[192–194] incorporate diodes within metasurface unit cells, realizing dynamic generation of multiple holographic images. For instance, Li et al.[192] proposed

electromagnetic reprogrammable coding metasurface holograms to achieve dynamic reconfigurability without altering the physical structure of the metasurface, as shown in Fig. 8e. Moreover, the ultrathin profile of metasurfaces allows close integration with other optical or electronic devices, paving the way for on-chip holographic displays[171,195,196]. Such miniaturized systems are lightweight and practical for use in portable electronics and smart glasses, significantly reducing system complexity. For instance, Li et al.[195] demonstrated an on-chip-driven multicolor 3D meta-display, as shown in Fig. 8f. They developed an on-chip meta-hologram driven by guided waves to project multicolor and multiplane images with independent encoding freedoms. By leveraging the propagation-accumulated phase of guided waves and utilizing an optimization algorithm, they successfully encoded multicolor holographic images within the same observation area into a single meta-hologram. Metasurfaces also enable full-color holography within a single layer by carefully manipulating multiple wavelengths. For instance, Wan et al.[197] demonstrated full-color plasmonic metasurface holograms by designing an ultrathin plasmonic metasurface composed of subwavelength nanoslits, as shown in Fig. 8g. In addition, metasurfaces facilitate 3D holographic displays by delivering high resolution and accurate depth cues, essential for realistic VR and AR experiences[174,180,198]. For example, Wang et al.[180] achieved decimeter-depth and polarization-addressable color 3D meta-holography, as shown in Fig. 8h, surpassing the depth limits of traditional holography by employing angular spectrum diffraction theory. And Sun et al.[174] demonstrated high-efficiency, broadband, and low-crosstalk 3D holography by a multi-layer holographic-lens integrated metasurface, enhancing 3D visualization in a lens-free system. Hu et al.[198] realized 3D-integrated metasurfaces for full-color holography. They stacked a hologram metasurface on a monolithic Fabry-Pérot cavity-based color filter microarray to achieve low-crosstalk, polarization-independent, high-efficiency, full-color holography, and microprint. These advances underscore the potential of metasurfaces for developing high-resolution, wide-field, and dynamic holographic imaging systems.

Looking to the future, metasurface technology will likely evolve into one of the most promising approaches for holographic field reconstruction, particularly in AR, VR, and related immersive applications[185,199,200]. More realistic 3D content with detailed depth and texture will elevate user engagement in virtual environments. Realizing a broader FOV while preserving high-quality imaging will also be crucial, offering immersive panoramic experiences. In addition, metasurfaces will advance integrated optical solutions, merging multiple optical functions within a single device to create compact, high-performance systems for AR glasses[171,201,202]. Nevertheless, certain hurdles remain. Chromatic aberration poses a significant obstacle in wide-FOV and high-fidelity 3D holography, diminishing optical quality. Efficiency is another concern: large-area metasurfaces often have lower optical efficiency than traditional components, restricting their use in high-demand holographic applications. Balancing dynamic range with resolution, FOV, and depth precision presents additional trade-offs that can degrade overall system performance. Addressing these challenges will require advanced nanofabrication technologies—such as atomic layer deposition and nanoimprinting—to boost metasurface precision and efficiency. Computational optimization methods, including inverse design and deep learning, will be equally pivotal in mitigating chromatic dispersion and elevating efficiency. Finally, closer integration with optoelectronic platforms promises real-time holographic processing, further enhancing the capabilities of metasurface-based holographic systems.

Functional integration

In modern optical design, functional integration is critical for building efficient, compact imaging systems. Traditional setups often depend on multiple discrete components to perform various optical functions, which increases system size and manufacturing costs. Such approaches also limit flexibility, as each discrete element serves a single purpose. In contrast, metasurfaces—constructed from meticulously engineered microstructures—enable precise manipulation of light to realize diverse and integrated functions on a single platform. This consolidation streamlines optical systems and facilitates novel applications that demand multifunctional capabilities[203–206].

Metasurfaces achieve functional integration through two primary strategies: passive (static) metasurfaces, which maintain a fixed structure[207–210], and active (tunable) metasurfaces, which can adjust their properties in response to external stimuli[208,211,212]. Passive metasurfaces rely on the optical performance determined by the properties of the incident light, such as polarization, wavelength, or intensity, without requiring any change to the metasurface itself. For example, the optical function of passive metasurfaces can be modulated by external parameters, such as incident light polarization or wavelength, allowing different optical functionalities to coexist on the same platform without modifying the metasurface structure. In contrast, active metasurfaces can actively change their structure in response to external stimuli like temperature or voltage, enabling real-time reconfiguration of the metasurface's optical functions, offering more flexibility in applications requiring adaptive functionality.

Passive metasurfaces typically achieve functional integration through three distinct strategies. The first strategy is simultaneous acquisition of multiple data modalities, enabling a single metasurface to concurrently capture diverse forms of information. For example, Kwon et al.[213] demonstrated a metasurface-based system that simultaneously captures quantitative phase and intensity data, facilitating label-free cellular imaging and rapid diagnostics (Fig. 9a). Similarly, Intaravanne et al.[214] developed a compact metasurface platform integrating edge enhancement, polarization detection, and standard imaging modalities, enabling real-time, multimodal sample characterization (Fig. 9b). The second strategy leverages spatial multiplexing, wherein distinct spatial regions of a single metasurface perform separate optical functions simultaneously. For instance, Dai et al.[215] proposed a bi-channel metasurface capable of simultaneously processing near-field imaging and manipulating far-field wavefronts, generating optical vortices and holograms under different polarization conditions (Fig. 9c). Likewise, Guo et al.[216] integrated holographic imaging and spot-cloud projection functionalities onto a unified metasurface, achieving combined high-density spatial sensing and advanced imaging capabilities (Fig. 9d). The third strategy involves designing metasurface geometries that inherently support multiple functionalities across varying environmental conditions without dynamic structural modulation. For example, Chen et al.[217] demonstrated a static metasurface array capable of switching functions between light field imaging and structured-light projection, enabling effective depth perception across both bright and low-light scenarios (Fig. 9e). Similarly, Wang et al.[218] designed an asymmetric composite metasurface that simultaneously integrates infrared and microwave stealth functionalities, achieving multi-band camouflage and wavefront control without altering its physical structure (Fig. 9f).

Active metasurfaces achieve functional integration primarily through three modulation strategies. The first approach utilizes mechanical modulation, wherein flexible substrates or microelectromechanical systems (MEMS) induce structural deformation or localized strain in metasurfaces, dynamically tuning their electromagnetic responses without permanent structural changes[219,220]. For example, Li et al.[220] demonstrated a mechanically adaptive intelligent metasurface platform that integrates functionalities, such as electromagnetic illusion, carpet cloaking, and data transmission through real-time deformation recognition and adaptive electromagnetic response programming, as shown in Fig. 9g. The second approach employs field-effect modulation, where external electric fields dynamically alter carrier concentrations in active materials, enabling rapid, low-power modulation of optical properties, such as refractive index[221,222]. This strategy is particularly advantageous due to its fast response speeds and compatibility with CMOS technology, suitable for scalable device integration. For example, Lan et al.[221] implemented a GaN-based high-electron-mobility transistor metasurface architecture, which dynamically modulates terahertz wavefronts by precisely controlling carrier densities in two-dimensional electron gases, as shown in Fig. 9h. The third approach leverages phase-change materials, whose optical properties significantly alter in response to temperature or external stimuli, thus enabling

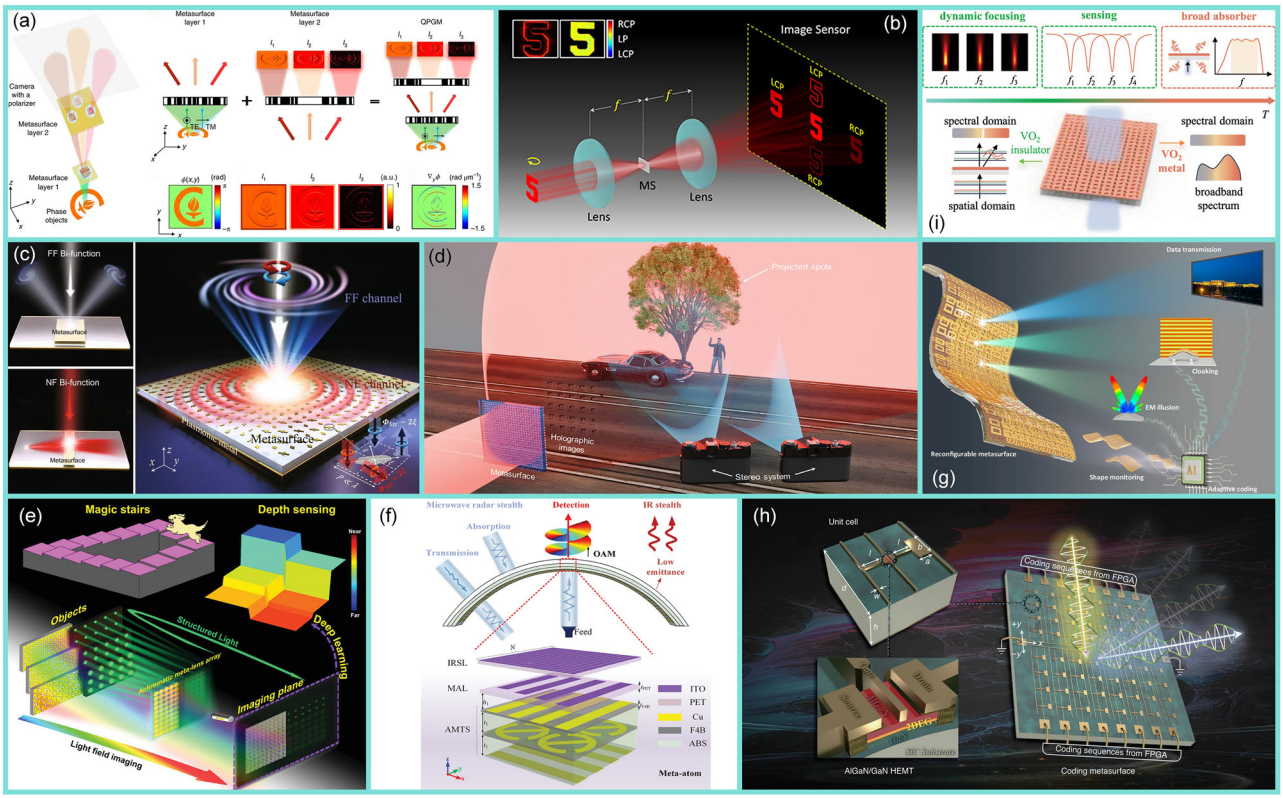

Fig. 9 | Functional integration of metasurfaces for diverse applications across static and dynamic strategies. a Single-shot quantitative phase gradient microscopy using a system of multifunctional metasurfaces[213]. **b** Metasurface-enabled 3-in-1 microscopy[214]. **c** Multiplexing near- and far-field functionalities with high-efficiency bi-channel metasurfaces[215]. **d** Multifunctional metasurface: holography and spot cloud projection[216]. **e** A Meta-Device for both passive and active depth detection[217]. **f** Detection and anti-detection with microwave-infrared compatible camouflage using asymmetric composite metasurface[218]. **g** Flexible intelligent microwave metasurface with shape-guided adaptive programming[220]. **h** Real-time programmable metasurface for terahertz multifunctional wave front engineering[221]. **i** Dynamic nonlocal metasurface for multifunctional integration via phase-change materials[211].

multifunctional, reconfigurable optical platforms[211,212,223]. For instance, Yu et al.[211] presented a vanadium dioxide (VO_2)-based nonlocal metasurface capable of dynamically switching among distinct optical functionalities—including dynamic focusing, optical sensing, and broadband absorption—by thermally induced phase transitions, as shown in Fig. 9i. These dynamic modulation strategies significantly enhance metasurface versatility and responsiveness, opening avenues for real-time adaptive optics and multifunctional photonic systems.

Beyond imaging, metasurfaces have increasingly enabled functional integration in domains, such as optical communications, energy harvesting, and electromagnetic stealth. In optical communication systems, reconfigurable metasurfaces incorporating phase-change materials, graphene, and varactor diodes allow for dynamic and multiplexed modulation of amplitude, phase, and polarization, thereby supporting functionalities including beam steering, broadband absorption, and polarization conversion[224–226]. For energy harvesting, metasurface platforms have been coupled with triboelectric nanogenerators or broadband thermal absorbers to simultaneously enable environmental energy conversion, vibration suppression, and controlled thermal emission[227–229]. In stealth-related applications, metasurfaces facilitate electromagnetic signature reduction via microwave absorption, RCS suppression, and dynamically tunable infrared emissivity, with recent demonstrations achieving multispectral concealment while preserving optical transparency[230–232]. Looking forward, metasurface research will prioritize integrating multiple imaging functions. Future designs will emphasize dynamic functionality switching, adapting to environmental changes and operational demands, a feature essential for adaptive optics and intelligent imaging. Additionally, the capacity for real-time or autonomous adjustments will become increasingly important, enabling metasurfaces to reconfigure functions without user intervention. However, significant challenges remain, particularly with respect to post-manufacturing tunability and sensitivity to external environmental factors. To address these issues, advances in dynamic adjustment mechanisms, adaptive fabrication materials, and integrated intelligent control systems will be essential, ultimately facilitating the seamless functional integration required for the next generation of metasurfaces.

Compact device integration

Metasurfaces, due to their micro- and nano-scale design advantages, have demonstrated significant potential for high-level integration in imaging applications. Compared to traditional optical devices, metasurfaces can achieve complex light manipulation within extremely confined spaces and can be integrated at multiple levels with other optical components, sensors, and entire systems[233–236]. This integration significantly enhances the functional performance of imaging systems while maintaining compactness. Therefore, exploring the integration methods of metasurfaces in imaging is critical for the development of next-generation optical systems.

In imaging applications, the integration methods of metasurfaces can be broadly categorized into three main approaches. The first approach involves integrating metasurfaces with existing optical components, which enhances the system's light field manipulation capabilities and improves overall imaging performance. By combining metasurfaces with traditional optical devices, this method leverages the microstructural advantages of metasurfaces to compensate for the limitations of conventional components, enabling more precise control of light waves. For example, Pahlevaninezhad et al.[237] developed a nano-optic endoscope for high-resolution optical coherence tomography, where a metalens was integrated into an endoscopic optical coherence tomography probe. This integration allowed the system to achieve near-diffraction-limited focusing, eliminating

spherical aberration and astigmatism (Fig. 10a). Similarly, Reshef et al.[10] introduced the concept of an optical "spaceplate," which replaces the space between lenses in traditional imaging systems. This integration results in ultra-thin imaging systems with compression factors of up to 4.9 (Fig. 10b).

The second category of integration focuses on embedding metasurfaces directly onto sensors, such as CMOS imaging sensors, to enhance the functional capabilities at the perception layer. This integration improves the efficiency and precision of optical information acquisition by combining the light-field manipulation of metasurfaces with the sensing capabilities of the sensors. As a result, the overall complexity of optical systems is reduced, while imaging quality is significantly enhanced. For example, Zuo et al.[133] developed a chip-integrated metasurface full-Stokes polarimetric imaging sensor, termed MetaPolarIm, by integrating an ultrathin metasurface polarization filter array onto a visible imaging sensor. This design enabled single-shot full-Stokes imaging with high measurement accuracy (Fig. 10c). Similarly, Luo et al.[238] presented metasurface-enabled on-chip multiplexed diffractive neural networks (MDNNs) operating in the visible spectrum. This approach demonstrated a multi-channel classifier framework capable of simultaneously recognizing handwritten digits and fashion items (Fig. 10d).

The third category of integration focuses on system-level integration, where metasurfaces are comprehensively incorporated into the entire imaging system architecture to achieve broader functional optimizations. This holistic approach allows metasurfaces to play a pivotal role in complex imaging systems, enhancing overall performance and expanding the system's application scope. For instance, Xu et al.[65] developed metalens-integrated compact imaging devices for wide-field microscopy by directly mounting silicon metalenses onto CMOS image sensors. This integration enabled ultra-thin, lightweight, and flat optical designs with a resolution of approximately 1.74 wwm and an extended field of view (Fig. 10e). Similarly, Xiong et al.[121] introduced a dynamic brain spectrum acquisition system that uses a real-time ultraspectral imaging chip integrated with reconfigurable metasurfaces, enabling high temporal, spatial, and spectral resolution necessary for capturing dynamic brain spectra (Fig. 10f). These system-level integrations emphasize the potential of metasurfaces to revolutionize optical systems by enabling high-performance, real-time spectral imaging and ultra-thin microscopy devices.

In metasurface-enabled computational imaging, current algorithmic frameworks can be broadly categorized into two paradigms: independent optimization frameworks and end-to-end optimization frameworks. The independent approach decouples optical design from computational reconstruction—metasurfaces are first designed to satisfy general optical constraints, while reconstruction algorithms (e.g., deconvolution or compressed sensing) are later tailored to the resulting point-spread function or measurement model[136,217,239]. This modularity offers flexibility and interpretability but often leads to sub-optimal system-level performance. In contrast, end-to-end frameworks jointly optimize the metasurface structure and the downstream neural reconstruction network within a unified pipeline, using differentiable physical simulators or learned surrogates[177,240,241]. This tightly coupled strategy enables task-specific design, reduces reconstruction artifacts, and improves robustness under fabrication or environmental perturbations, making it especially suitable for broadband, multimodal, or dynamic imaging scenarios.

Looking ahead, metasurface technology is set to enable the integration of multiple complex optical functions into compact devices, allowing for smaller devices to perform more sophisticated tasks. The future will see the efficient integration of metasurfaces with traditional optical components, combining the unique strengths of both approaches. While metasurfaces provide advanced capabilities for precise light manipulation, traditional optical elements still offer unparalleled stability and high efficiency. Therefore, the key challenge will be optimizing the synergy between metasurfaces and conventional optics to maximize performance while maintaining compactness. However, this integration faces significant challenges, including the need for high precision in manufacturing and the optimization of functional coordination to prevent interference between components. Overcoming these challenges will require advancements in multi-functional integration technologies, computational design, and intelligent control systems. By addressing these issues, metasurfaces will revolutionize optical imaging systems, enabling high-performance, miniaturized devices suitable for a wide range of applications.

Electromagnetic response control

The precise manipulation of electromagnetic characteristics—namely, phase, amplitude, polarization, wavefronts, OAM, and spectral properties—is fundamental to the advancement of sophisticated imaging systems. Electromagnetic waves in imaging can be described by:

$$\mathbf{E}(x,t) = \mathrm{Re}\left\{\mathbf{E}_0 e^{i(kx-\omega t+\phi)}\right\}$$

where $\mathbf{E}_0$ represents the amplitude vector, k the wave number, ω the angular frequency, and ϕ the phase. Metasurfaces offer unprecedented control over these parameters, enabling enhancements in resolution, contrast, and multifunctionality within compact device architectures. This chapter delves into these six key electromagnetic response controls, examining how metasurfaces tailor these fundamental properties to optimize light-matter interactions and achieve superior imaging performance.

Phase control

Phase control is a cornerstone in optical engineering, essential for manipulating light wavefronts to achieve desired imaging functionalities. The phase of an electromagnetic wave signifies its position within the oscillatory cycle, significantly influencing interference, diffraction, and wavefront shaping phenomena. In traditional optical components, phase control is achieved by varying the geometric dimensions or refractive index of materials to introduce spatially varying optical path lengths, thus inducing phase delays. Unlike conventional bulk optical elements, metasurfaces achieve phase modulation through the precise engineering of meta-atoms—subwavelength scatterers that locally alter the phase of transmitted or reflected light[242–245]. This phase manipulation is accomplished via mechanisms, such as resonant phase, propagation phase, and geometric phase.

Resonant phase involves designing the geometric parameters of meta-atoms (such as their size, shape, and material) to resonate at specific frequencies[246–248]. When the frequency of incident light matches the resonant frequency of the meta-atom, a sharp phase shift occurs. This effect arises from the interaction between the incident light and the resonance modes of the meta-atom. Metals, due to their free electrons, exhibit plasmonic behavior, leading to significant phase shifts at certain resonant frequencies[33,249]. For example, when a meta-atom is designed to resonate at a particular wavelength, the light's phase will change abruptly at this resonance frequency. This phenomenon is especially effective for controlling the phase of light at specific frequencies and can be manipulated by adjusting the size or shape of the meta-atom.

Propagation phase is achieved by adjusting the propagation path of light through the meta-atom structure[243,250,251]. This is often accomplished by varying the height or arrangement of the meta-atoms to change the optical path length, resulting in a phase shift. The phase shift due to propagation in a material with refractive index n_{eff} and thickness h is given by:

$$\phi = \frac{2\pi}{\lambda_0} n_{\mathrm{eff}} h,$$

where λ_0 is the wavelength of light in free space. The effective refractive index n_{eff} depends on the material properties and geometry of the meta-atom. By designing the meta-atom to have different heights or other structural variations, the phase can be controlled over a broad range of wavelengths.

Geometric phase control (PB phase) occurs when circularly polarized light interacts with anisotropic meta-atoms[252,253]. As the orientation of the meta-atoms is rotated in the plane of the metasurface, a spatially varying geometric phase is induced, which depends on the geometry and the

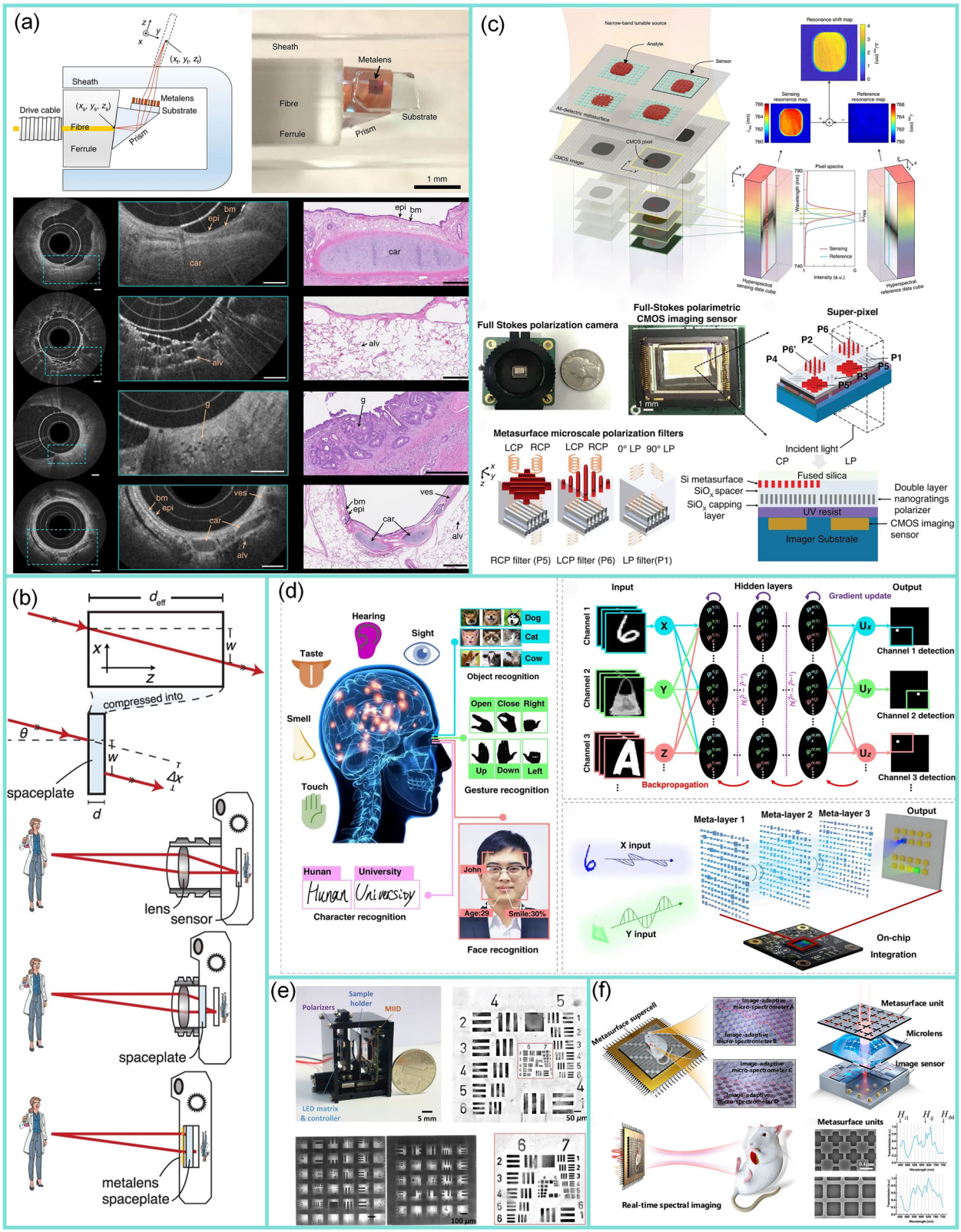

Fig. 10 | Compact device integration using metasurfaces. a Nano-optic endoscope for high-resolution optical coherence tomography in vivo[237]. **b** An optic to replace space and its application towards ultra-thin imaging systems[10]. **c** Chip-integrated metasurface full-Stokes polarimetric imaging sensor[133]. **d** Metasurface-enabled on-chip multiplexed diffractive neural networks in the visible[238]. **e** Metalens-integrated compact imaging devices for wide-field microscopy[65]. **f** Dynamic brain spectrum acquired by a real-time ultraspectral imaging chip with reconfigurable metasurfaces[121].

rotation angle of the meta-atom. This effect is particularly useful for manipulating the polarization state of light, enabling applications, such as beam steering and holography. The geometric phase does not depend on the wavelength of light but rather on the relative rotation of the meta-atom with respect to the incident light's polarization[254,255]. By carefully designing the geometry and arrangement of the meta-atoms, the phase of the transmitted or reflected light can be efficiently controlled.

Detour phase modulation achieves phase shifts by strategically introducing lateral offsets (or "detours") of subwavelength scatterers or apertures within each periodic metasurface unit cell. This spatial displacement generates a local linear phase gradient governed by momentum conservation within the lattice, leading to controlled diffraction effects[190,256–258]. Unlike resonant and propagation phases, which rely on internal resonances or optical path length differences within meta-atoms, detour phase modulation operates via extrinsic diffractive interactions. Due to this diffraction-based mechanism, detour phase exhibits intrinsic advantages, including broadband performance, robust angular tolerance, and inherent polarization insensitivity. Moreover, detour phase modulation can be synergistically combined with geometric phase control—by concurrently adjusting both meta-atom displacement and orientation—to achieve comprehensive manipulation of the phase and polarization states of diffracted light[225,259]. This versatility greatly enhances the design flexibility for advanced metasurface functionalities.

In the field of imaging, the core functionality of metasurfaces lies in their ability to precisely control the phase of light, thereby influencing its propagation. Resonant phase control leverages the resonance effects of nanostructures to induce sharp phase shifts, offering high modulation depth and flexibility[260]. However, this approach is constrained by a narrow bandwidth and demands high-quality factor materials for optimal performance. Geometric phase control, in contrast, achieves phase manipulation by altering the geometric symmetry of the nanostructures. This method inherently enables polarization multiplexing and exhibits high efficiency, though it suffers from limited phase modulation depth and a strong dependence on the polarization state of the incident light. Propagation phase control adjusts the geometric dimensions of dielectric pillars to achieve phase coverage, enabling broadband operation and high efficiency. Nonetheless, its phase modulation accuracy is restricted by the precision of the fabrication process. Beyond isolated phase modulation strategies, hybrid phase control, which combines multiple phase mechanisms, such as geometric and propagation phase, offers enhanced flexibility and functionality in wavefront modulation[261,262]. This can be achieved via spatial interleaving of distinct meta-atoms or co-design of meta-units supporting multiple responses simultaneously. Such strategies enable broadband, polarization-insensitive, and multifunctional control, underpinning recent advances including achromatic metalenses with 77.1–88.5% efficiency across the near-infrared range[40], full-space dual-channel meta-hologram[263], energy-controllable polarization routing[264], and multi-channel meta-holography via spectral-polarization decoupling[265]. The exploration and integration of more fundamental principles for phase control, particularly those that combine these mechanisms, will be crucial for developing more versatile, precise, and scalable phase modulation techniques, paving the way for more advanced metasurface applications in imaging and beyond.

Amplitude control

Amplitude control is a critical element in optical engineering, essential for managing the intensity distribution of light within imaging systems[190,210,266–268]. Precise modulation of light's amplitude plays a vital role in influencing key parameters, such as image contrast, brightness, and dynamic range—factors that directly enhance overall image quality. Metasurfaces offer various mechanisms for controlling the amplitude of electromagnetic waves, including absorption modulation, interference effects, and resonant coupling. These techniques enable the creation of spatially varying amplitude profiles, which are crucial for applications, such as high-contrast imaging, adaptive illumination, and selective filtering. By tailoring these mechanisms, metasurfaces can modulate light with high spatial resolution, providing advanced capabilities for optical systems.

Absorption modulation involves designing meta-atoms that selectively absorb or transmit light at specific wavelengths or spatial regions[269,270]. By varying the absorption properties across the metasurface, it becomes possible to precisely control the intensity of transmitted or reflected light. This method is particularly useful in applications where controlled attenuation or enhancement of specific light wavelengths is required. In contrast, interference effects[271,272] exploit phase differences between interacting waves, which can result in constructive or destructive interference, thereby modulating the amplitude. This principle allows for dynamic adjustments to the amplitude profile based on the phase relationships embedded in the metasurface. Resonant coupling[250,273] leverages the resonances of meta-atoms to enhance or suppress light transmission or reflection at specific spectral regions. By tuning the geometry and material properties of the meta-atoms, metasurfaces can achieve the desired resonant responses, modulating the amplitude of incident light with high spatial resolution.

These amplitude modulation mechanisms enable metasurfaces to create spatially varying amplitude profiles with high resolution, which are essential for high-contrast imaging systems. By enhancing the visibility of features against varying background intensities, metasurfaces improve the performance of imaging systems, resulting in clearer images with better dynamic range. In adaptive illumination systems, amplitude control can optimize lighting conditions in real-time, improving image clarity and reducing noise. Looking ahead, the simultaneous control of both amplitude and phase presents a highly promising avenue for advancing optical technologies[190,274–276], enabling more sophisticated and versatile light manipulation in imaging systems and beyond.

Polarization control

Polarization control is a crucial element in optical imaging[2,277,278], significantly enhancing the functionality and versatility of imaging systems. The polarization state of light, which defines the orientation and ellipticity of its electric field vector, directly influences key aspects, such as image contrast, information capacity, and the ability to distinguish between different materials or structures. Metasurfaces, through their precise design of anisotropic nanostructures, provide unprecedented control over the polarization. Unlike traditional bulk optical components, metasurfaces manipulate polarization by locally altering the polarization state via geometric and material engineering of meta-atoms—subwavelength scatterers that impose specific polarization transformations[279–281]. The primary mechanisms for polarization control in metasurfaces include geometric phase, anisotropic resonances, and polarization conversion.

Geometric phase control leverages the in-plane rotation of meta-atoms to impose a spatially varying Pancharatnam-Berry phase, enabling polarization-multiplexed wavefront manipulation. For circularly polarized light, a meta-atom rotated by an angle θ introduces a geometric phase shift of $\pm 2\theta$ for left-handed and right-handed circular polarizations (LCP and RCP), respectively. This intrinsic chirality-phase duality allows a single metasurface to encode dual-phase profiles, such as $\Phi_{\mathrm{LCP}}(x, y)$ and $\Phi_{\mathrm{RCP}}(x, y) = -\Phi_{\mathrm{LCP}}(x, y)$, which is crucial for polarization-multiplexed holography and dual-channel beam steering[282,283]. Anisotropic resonances exploit orthogonally polarized eigenmodes in meta-atoms to achieve polarization-selective amplitude modulation. By engineering resonance detuning along orthogonal axes (e.g., x: electric dipole resonance at λ_1, y: magnetic dipole resonance at λ_2), metasurfaces can independently manipulate TE- and TM-polarized waves. This capability is a cornerstone for polarization-division multiplexing in compact spectropolarimetric systems[284,285]. Polarization conversion utilizes symmetry-broken meta-atoms (e.g., L-shaped or elliptical nanostructures) to induce phase retardation between orthogonal linear polarization components (e.g., $\Delta\phi_x - \Delta\phi_y = \pi/2$ for quarter-wave plates). This enables the dynamic generation of various polarization states, including linear ↔ circular ↔ vectorial, providing additional degrees of freedom for hybrid polarization multiplexing. By simultaneously

controlling both incident and converted polarization states, metasurfaces can achieve multi-functional operations[286–288].

These polarization control mechanisms significantly enhance the capabilities of imaging systems, enabling polarization-sensitive imaging that can differentiate between materials based on their unique polarization responses[151,289]. This leads to improved contrast and the ability to detect subtle structural details that would otherwise be indistinguishable. In biomedical imaging, polarization control aids in identifying anisotropic tissues and visualizing biological structures with greater clarity[286,290]. Furthermore, polarization manipulation enables the compact, multifunctional optical elements capable of supporting polarization multiplexing[7,291,292], where multiple information channels are transmitted simultaneously using different polarization states, which increases the overall information capacity. However, achieving precise polarization control through metasurfaces presents several challenges, such as fabrication tolerances, which must be carefully managed to ensure the desired polarization response. Additionally, balancing polarization control with other electromagnetic responses, such as phase and amplitude modulation, necessitates sophisticated design strategies.

Wavefront control

Wavefront control is a critical aspect of optical engineering that enables the precise shaping and manipulation of light wavefronts[293–295]. By altering the spatial distribution of phase, amplitude, and polarization of incident light, wavefront control enhances optical systems and improves their performance. The primary mechanisms for wavefront manipulation using metasurfaces include phase gradient engineering, multi-layer stacking, and dynamic modulation.

Phase gradient engineering[296,297] is one of the fundamental techniques for wavefront control, utilizing spatially varying phase shifts to guide the propagation of light. By introducing a phase gradient across the metasurface, anomalous reflection and refraction are induced, enabling functionalities like programmable lensing and beam deflection. Multi-layer stacking extends this concept by layering multiple metasurfaces[298,299], each contributing different phase and amplitude modifications to the incident light. This approach facilitates complex wavefront engineering, such as three-dimensional imaging and multi-focal lensing, which would be challenging to achieve with single-layer designs. Additionally, dynamic modulation[300,301] integrates tunable materials and active components into the metasurfaces, enabling real-time adjustments to the wavefront.

Metasurfaces offer significant potential for precise wavefront control, making them highly suitable for advanced imaging systems[302,303]. However, achieving high-fidelity wavefront shaping remains challenging due to the sensitivity of metasurfaces to fabrication imperfections, which can introduce phase errors and distortions, ultimately degrading imaging performance. Furthermore, the complexity of multi-layer metasurface structures presents challenges, as inter-layer coupling effects are difficult to control. Looking ahead, the integration of phase gradient engineering, multi-layer stacking, and dynamic modulation presents a promising approach for achieving dynamic and wide-range wavefront control. These innovations enable the realization of complex wavefront profiles, making them invaluable for applications in high-resolution imaging and adaptive optics.

OAM control

(Orbital angular momentum) OAM control provides a powerful method to enhance the functionality of optical systems. Metasurfaces offer a compact and efficient platform for manipulating the OAM of light beams, enabling the generation and control of light fields with specific angular momentum[186,304,305]. By tailoring OAM states, metasurfaces can produce light beams with customized phase profiles, which are essential for applications, such as high-resolution imaging, optical manipulation, and quantum information processing. The ability to precisely control the OAM of light allows metasurfaces to encode information onto light.

Metasurfaces achieve OAM control by introducing spatially varying phase shifts across the incident light beam, which generates helical phase fronts. These phase shifts result in a light beam with a spiral phase structure, characterized by a topological charge, which defines the amount of OAM carried by the beam. A key mechanism for generating and controlling OAM states is the geometric phase[306–308], which is sensitive to the orientation of anisotropic meta-atoms. When circularly polarized light interacts with rotated meta-atoms, a phase shift proportional to twice the rotation angle is imparted, creating specific OAM states. Additionally, metasurfaces can support anisotropic resonances that selectively enhance or suppress particular polarization components[309,310], which is crucial for generating distinct OAM states. Furthermore, metasurfaces enable OAM multiplexing[77,304,305], where multiple OAM channels can be simultaneously encoded and transmitted, thereby enhancing the information capacity of optical systems.

Despite the significant potential of metasurfaces for precise OAM control, several unique challenges need to be addressed. Even small deviations in the design of the meta-atoms or in material properties can lead to undesired OAM states, compromising the efficiency and fidelity of OAM generation. Additionally, achieving robust OAM control often requires careful coordination with other optical functionalities, such as phase and amplitude modulation, which demands sophisticated design strategies to ensure seamless integration. However, the ability of metasurfaces to engineer complex OAM profiles offers transformative potential for high-resolution, high-contrast, and multifunctional imaging applications, significantly enhancing optical system capabilities.

Spectral control

Controlling the spectral properties of light is essential for advancing multispectral and hyperspectral imaging systems[117,311,312], which capture information across a wide range of wavelengths beyond the visible spectrum. Metasurfaces provide a compact and efficient platform for tailoring the spectral response of optical systems. By precisely engineering the interaction of light with subwavelength scatterers, metasurfaces enable selective detection and manipulation of specific wavelengths. These applications benefit from the ability to obtain more accurate data and deeper insights by utilizing the rich spectral information that metasurfaces provide.

Metasurfaces achieve spectral control by engineering meta-atoms with specific resonant properties, such as electric and magnetic dipole modes, to selectively interact with different wavelengths. This allows for the creation of narrowband filters, broadband transmitters, or wavelength-selective modulators, essential for applications in hyperspectral imaging and spectroscopy[313,314]. Multi-resonant designs extend this capability by enabling metasurfaces to support multiple resonant modes across different spectral regions, allowing for more versatile spectral control. This is particularly important in applications, such as hyperspectral imaging, where precise capture of a wide range of wavelengths is crucial. Furthermore, metasurfaces enable spectral multiplexing[315–317], allowing for the simultaneous manipulation of multiple spectral channels. This capability enhances the information capacity in optical systems, particularly in advanced imaging and display technologies, where multiple wavelengths can be used to carry separate data streams, thereby improving system throughput and efficiency.

Looking ahead, the future of spectral control using metasurfaces lies in advancing their integration into multifunctional optical systems with even greater precision and flexibility[114,116,318]. One promising direction is the development of dynamic and tunable metasurfaces that can adapt to changing spectral requirements in real-time. Additionally, the combination of multi-layer metasurfaces and advanced AI-driven design holds great potential for enabling ultra-precise spectral control across broad wavelength ranges, facilitating the development of hyperspectral sensors with higher resolution and sensitivity. These advances will enable new capabilities in imaging and sensing, such as detailed molecular detection and complex material characterization, pushing the boundaries of current multispectral and hyperspectral technologies.

Metasurface structure design

Translating desired electromagnetic performance into realizable structures requires robust design methodologies. The design of metasurfaces is a

cornerstone in the development of advanced optical devices, enabling precise control over electromagnetic waves. To systematically achieve this translation, current strategies are categorized into physics-driven, meta-heuristic, and AI-driven approaches. Each approach plays a crucial role in tailoring the interaction of light with matter at the nanoscale, optimizing metasurfaces for specific optical functions and embodying the "from performance to structure" design paradigm.

Designing a metasurface involves configuring numerous sub-wavelength meta-atoms to exhibit various novel physical phenomena. The fundamental challenge in metasurface design is to optimize the structural parameters of these meta-atoms to achieve desired reflection or transmission properties. Traditional design processes rely heavily on full-wave simulation software and numerical algorithms to derive electromagnetic characteristics, necessitating iterative adjustments based on the intuition and experience of researchers. This trial-and-error approach is both time-consuming and resource-intensive. Furthermore, when redesigning similar meta-atoms for different electromagnetic responses, the optimization process must be repeated from scratch. These limitations have prompted the exploration of more automated and efficient design techniques, such as meta-heuristic algorithms and AI, which aim to streamline the design process by leveraging computational power and advanced optimization strategies.

Physically-driven design methods

In metasurface design, physically-driven methods rely on theoretical modeling of light-matter interactions to optimize optical properties. These approaches are grounded in classical physical laws, such as the propagation and diffraction of light, enabling precise control over the direction, phase, and reflection of light waves. The advantage of physically-driven methods lies in their strong physical interpretability, as they are based on well-established principles. However, their limitations are evident when applied to complex, high-dimensional design tasks, where flexibility and computational efficiency become significant challenges. Despite these drawbacks, physically-driven design remains a powerful tool for metasurface engineering, particularly when physical explainability is paramount.

A cornerstone of metasurface design is the generalized Snell's law, introduced by Capasso et al.[261] at Harvard University, as shown in Fig. 11a and Zhou Lei et al.[319] at Fudan University, as shown in Fig. 11b. This extension of the classical Snell's law accounts for the influence of metasurface geometries and material properties on light propagation, offering a broader framework for controlling light's refraction and reflection at the interface with structured surfaces. Unlike the traditional Snell's law, the generalized form incorporates the effects of surface topology and electromagnetic response, enabling more sophisticated control of light directionality. This advancement significantly broadens the design space for metasurfaces, providing a more comprehensive theoretical foundation for controlling light behavior in a variety of applications. The refraction and reflection behavior of light on a 2D metasurface can be deduced and is mathematically expressed by the generalized Snell's law:

$$\begin{cases} \sin\theta_r - \sin\theta_i = \frac{\lambda_0}{2\pi n_i}\frac{d\varphi}{dx} \\ n_t \sin\theta_t - n_i \sin\theta_i = \frac{\lambda_0}{2\pi}\frac{d\varphi}{dx} \end{cases}$$

where θ_i and θ_t are the angles of incidence and transmission, respectively, n_i and n_t are the refractive indices of the incident and transmitted media, λ_0 is the wavelength of the incident light in vacuum, and $\frac{d\varphi}{dx}$ represents the spatial phase gradient imparted by the metasurface. This generalized Snell's law demonstrates that a metasurface with a well-designed phase gradient can deflect incident light in any desired direction, enabling functionalities, such as beam steering and anomalous refraction. From the perspective of the Huygens-Fresnel principle, each meta-atom on a metasurface acts as a secondary wave source. The collective radiation fields from these meta-atoms interfere constructively or destructively in space, forming any desired light field distribution.

Phase control is a crucial aspect of metasurface design, directly influencing the way light interacts with the structure. The three main phase manipulation mechanisms—resonant phase[247], geometric phase[320], and propagation phase[321]—each offer distinct advantages, limitations, and suitable applications. The resonant phase relies on plasmonic resonance, where phase shifts are induced when the incident light matches the resonance frequency of the metasurface, as shown in Fig. 11c. The geometric phase exploits the polarization dependence of light, allowing for flexible and precise phase control through the rotation of anisotropic nanostructures, as shown in Fig. 11d. The wide tunability of geometric phase, often spanning a full 2π shift, provides flexibility, but it is typically restricted to circularly polarized light. The propagation phase manipulates phase shifts by introducing optical path differences, dependent on the material's thickness and refractive index, as shown in Fig. 11e. It provides the advantage of being polarization-insensitive, unlike resonant and geometric phase methods. However, it requires precise phase distribution control, often necessitating detailed electromagnetic simulations to accurately model high-order resonances and material properties. Hybrid approaches, such as combining resonant + geometric phase or propagation + geometric phase[261,262], as shown in as shown in Fig. 11f[262], leverage the advantages of multiple mechanisms, offering solutions for both narrowband precision and flexible polarization control, or broadband phase modulation with polarization insensitivity, expanding the metasurface design space.

The parameter scanning process is a crucial step that bridges theoretical models with practical design[322–324]. In this phase, the metasurface geometry—such as unit cell size, shape, and arrangement—is systematically varied, and numerical simulations are employed to predict the resulting optical performance. This iterative process helps identify optimal configurations by exploring how changes in the structural parameters affect the light-matter interaction. While effective for narrowing down potential designs, parameter scanning can become computationally intensive, particularly when the design space is large.

In conclusion, physically-driven design methods provide a robust theoretical framework for metasurface engineering, ensuring high precision and interpretability in controlling optical properties. While these methods are effective for addressing fundamental design challenges, their applicability is limited for more complex or high-dimensional design problems. The combination of physical principles with other advanced design techniques, such as machine learning or heuristic algorithms, is often necessary to overcome these limitations and enhance design flexibility, offering a pathway to more innovative and versatile metasurface applications.

Meta-heuristic optimization design methods

Meta-heuristic optimization design methods encompass a broad spectrum of algorithmic strategies aimed at efficiently exploring and optimizing the intricate design spaces inherent in metasurface engineering[251,325,326]. These methods integrate both gradient-based techniques, such as adjoint optimization, and meta-heuristic algorithms like genetic algorithms (GAs), particle swarm optimization (PSO), and ant colony optimization (ACO). Additionally, hybrid approaches that combine these optimization strategies with deep neural networks (DNNs) have emerged, leveraging the strengths of both gradient-based and data-driven methodologies. This subsection delves into these prominent numerical optimization methods, elucidating their principles, applications, advantages, and limitations in the context of optimizing meta-atom configurations for advanced optical functionalities.

Adjoint optimization is a gradient-based technique that has emerged as a powerful tool for designing large-scale, multifunctional metasurfaces[327–329]. By formulating metasurface design within a partial differential equation (PDE)-constrained framework, this method relies on two full-wave electromagnetic simulations per iteration (forward and adjoint) to compute the gradient of an objective function with respect to potentially thousands of design parameters. In contrast to finite-difference approaches, which would require separate simulations for each parameter, adjoint optimization efficiently scales to high-dimensional design spaces, making it particularly suitable for metasurfaces consisting of numerous meta-atoms or

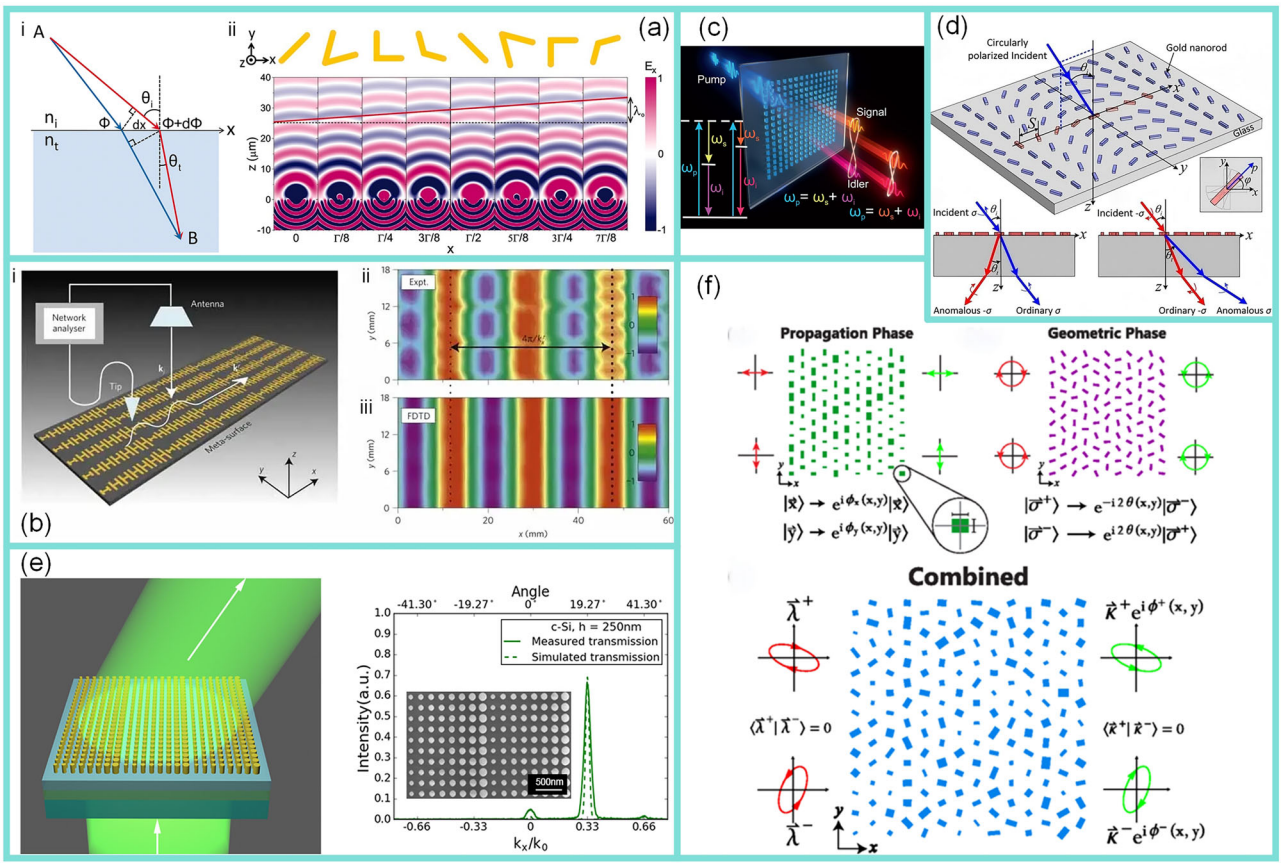

Fig. 11 | Physically driven metasurface design methods. a Generalized laws of reflection and refraction by the Capasso group[261]. **b** Gradient-index meta-surfaces as a bridge linking propagating waves and surface waves[319]. **c** Resonant metasurfaces for generating complex quantum states using a resonant phase metasurface[247]. **d** Dispersionless phase discontinuities for controlling light propagation[320]. **e** Efficient silicon propagation-phase metasurfaces for visible light[321]. **f** Independent phase control of arbitrary orthogonal states of polarization using propagation and geometric phase metasurfaces[262].

incorporating multiple functionalities[327,330]. Adjoint optimization methods can also capture near-field and far-field interactions at the full-device level. Traditional periodic or unit-cell approximations often neglect inter-cell coupling and therefore do not accurately account for complex electromagnetic interactions across the entire metasurface. By solving Maxwell's equations globally[331,332], adjoint optimization optimally tunes each meta-atom to meet specified performance metrics. Moreover, it can be extended to multi-objective scenarios[329,333], allowing designers to integrate phase control, polarization control, and spectral engineering into a single optimization framework. Nevertheless, as a gradient-based method, adjoint optimization is prone to converging to local minima, underscoring the need for careful initialization or hybrid approaches that combine global searches with local refinement. Moreover, the accuracy of gradient calculations is contingent on robust electromagnetic simulations, making them sensitive to errors in mesh generation, boundary conditions, or material modeling.

GAs, inspired by the principles of natural selection and genetics, have been extensively employed to optimize the geometric and material parameters of metasurfaces[334–337]. By representing meta-atom configurations as chromosomes, a population of candidate solutions undergoes selection, crossover, and mutation, thereby evolving over successive generations. In metasurface applications, this global search capability is particularly useful for navigating high-dimensional or discontinuous design spaces, since GAs do not rely on gradient information. For example, Cai et al.[334] demonstrated the efficient exploration of complex meta-atom topologies to improve transmission efficiency and phase control, as shown in Fig. 12b. GAs can also accommodate both discrete and continuous variables and readily extend to multi-objective formulations, making them well-suited for multifunctional metasurface designs. However, they can be computationally expensive, especially when large populations and many generations are required. Moreover, tuning parameters, such as population size, crossover rates, and mutation probabilities is critical to avoid premature convergence to suboptimal solutions.

Ant colony optimization (ACO) is a nature-inspired metaheuristic that models the collective foraging behavior of ants, allowing artificial agents (ants) to explore complex design spaces while depositing and following pheromone trails[324,338,339] In metasurface design, ACO often encodes discrete parameters, such as meta-atom positions, shapes, or interconnections as nodes or paths, enabling a combinatorial search for optimal electromagnetic responses. For instance, Zhu et al.[338] employed ACO to optimize three-dimensional plasmonic metasurface elements, achieving high diffraction efficiencies by systematically navigating the large solution space, as illustrated in Fig. 12c. The evolving pheromone distribution guides subsequent ants toward more promising regions, thereby improving performance metrics, such as beam-steering fidelity and phase uniformity. Compared to gradient-based or purely random searches, ACO is well-suited for discrete and combinatorial problems, and it can adapt to dynamic scenarios where objectives or constraints change over time. Nonetheless, the algorithm can be computationally demanding, since it requires iterative pheromone updates, and its effectiveness heavily depends on parameter tuning (e.g., pheromone evaporation rates, colony size). Moreover, inadequate balancing between pheromone reinforcement and exploration may cause premature convergence.

Particle swarm optimization (PSO), inspired by the flocking behavior of birds or schooling of fish, iteratively refines a swarm of candidate solutions by sharing both individual and global experience[325,340,341]. Each particle updates its velocity and position based on its own previous best

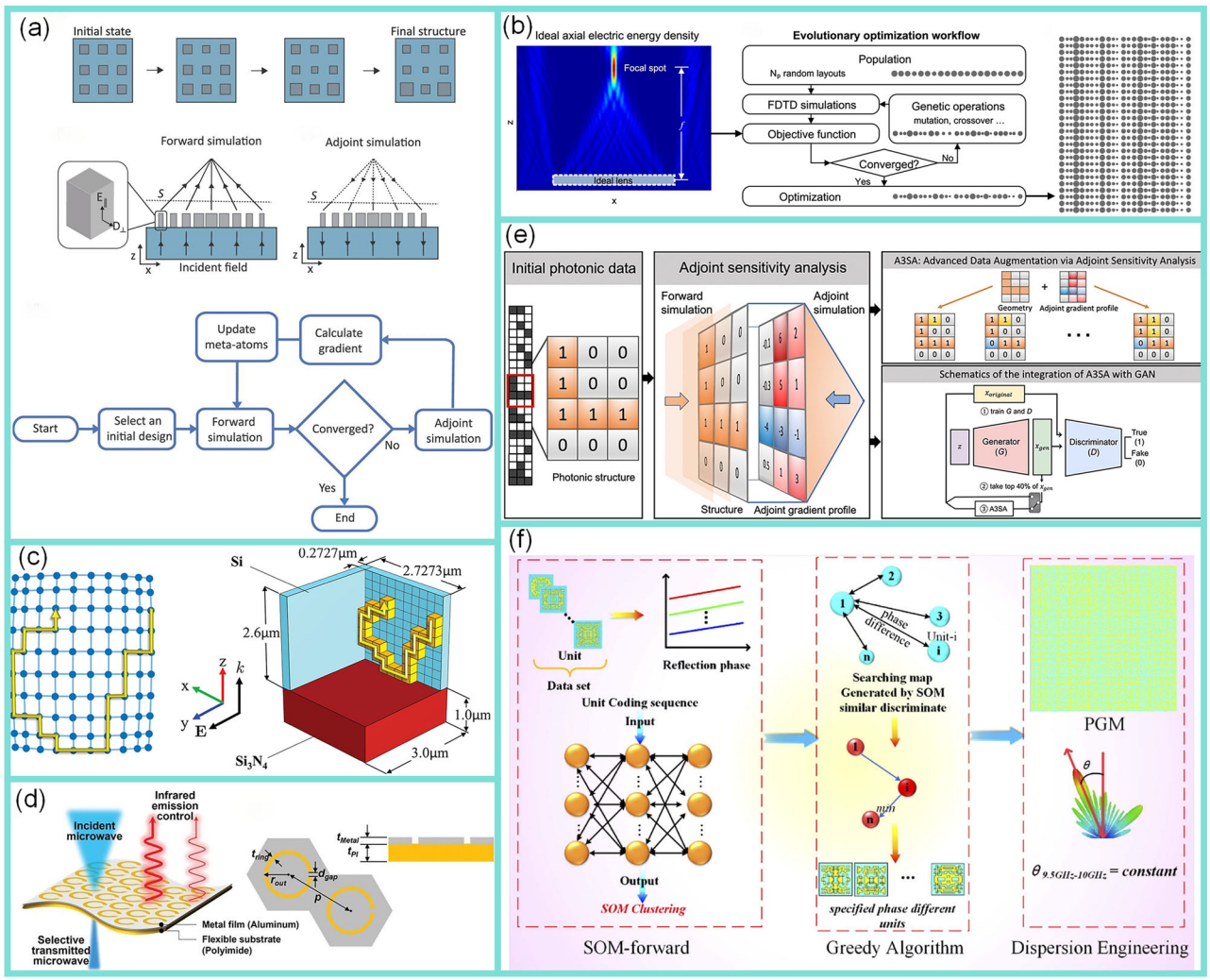

Fig. 12 | Meta-heuristic optimization metasurface design methods. a Large-scale parametrized metasurface design using adjoint optimization[327]. **b** Inverse design of metasurfaces with genetic algorithms[334]. **c** Optimal high-efficiency 3D plasmonic metasurface elements revealed by lazy ants[338]. **d** Flexible metasurface for microwave-infrared compatible camouflage via particle swarm optimization[340]. **e** Hybrid optimization methods integrating the adjoint method with machine learning techniques[332]. **f** Metasurface design via a greedy algorithm empowered by a self-organizing map neural network[345].

performance and that of its neighbors, striking a balance between exploration and exploitation of the design space. In metasurface applications, parameters, such as meta-atom geometry, spacing, and material properties can be encoded into each particle's position vector. For instance, Nam et al.[340] employed PSO to design flexible metasurfaces for microwave-to-infrared camouflage, optimizing the spatial arrangement and physical dimensions of meta-atoms to achieve selective transmission and emission characteristics, as illustrated in Fig. 12d. PSO is lauded for its conceptual simplicity and relatively rapid convergence compared to genetic algorithms, yet it is susceptible to premature convergence, particularly in complex multimodal landscapes. Its performance also depends on carefully tuned parameters, such as the inertia weight and cognitive/social coefficients.

Hybrid optimization methods that combine meta-heuristic algorithms with machine learning models, such as DNNs, have emerged as powerful strategies for improving efficiency and robustness in metasurface design[342–344]. By leveraging the global exploration capability of meta-heuristics and the predictive power of data-driven models, these approaches can more effectively navigate high-dimensional design spaces while reducing the number of full-wave simulations. For instance, Kang et al.[332] introduced a framework that couples the adjoint method's gradient-based optimization with generative adversarial networks (GANs) for data augmentation, significantly lowering computational overhead while accelerating photonic device design (Fig. 12e). Similarly, Zhu et al.[345] integrated a greedy algorithm and a self-organizing map (SOM) neural network to mitigate chromatism in metasurfaces, achieving precise control over electromagnetic properties (Fig. 12f). These hybrid methods offer faster convergence and fewer required simulations, but introduce additional complexity in model training and parameter tuning. Their overall success depends heavily on the availability of high-quality training data, as well as careful calibration of hyperparameters to avoid issues like overfitting or suboptimal fusion of the algorithmic components. Nonetheless, they represent a promising avenue for metasurface design[346–348].

In summary, meta-heuristic optimization algorithms provide robust global search capabilities and flexible handling of discrete, continuous, or multi-objective challenges in metasurface design[349,350]. Their adaptability makes them well-suited for highly complex or non-convex design landscapes, especially where gradient information is limited. However, computational overhead can become prohibitive for large-scale full-wave simulations, and performance frequently hinges on careful tuning of parameters, such as population size, mutation rates, or pheromone evaporation. While these constraints introduce additional complexity, recent advances—particularly the integration of machine learning and data-driven

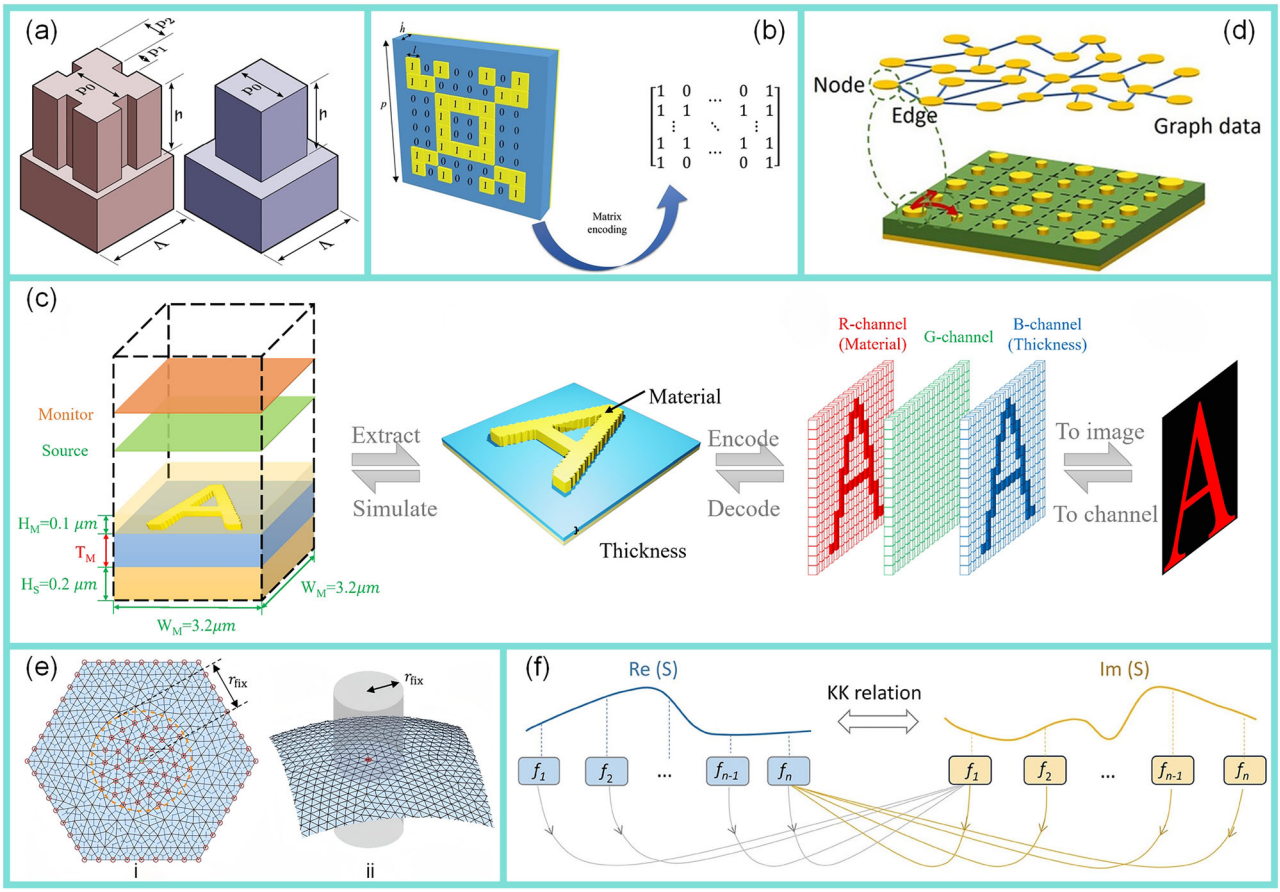

Fig. 13 | Different encoding methods for AI-driven metasurface design. **a** Parametric encoding based on geometrical parameters for metasurface design[355]. **b** Vector encoding to represent high-dimensional metasurface parameters in optimization tasks[358]. **c** Image encoding that represents metasurface design as pixel matrices for optimization with deep learning[360]. **d** Graph encoding used to model the interactions between metasurface elements in a network structure[363]. **e** Mesh encoding to discretize metasurfaces into grid-based elements for high-precision simulations[364]. **f** Sequence encoding to model metasurface designs through ordered data for use in sequence-based neural networks[365].

approaches—show promise in mitigating computational burdens and enhancing convergence.

AI-driven design methods

AI-driven design methods have emerged as a pivotal advancement in the field of metasurface design, offering unprecedented capabilities in automating and optimizing the design process[24,25,351,352]. By integrating sophisticated machine learning and deep learning techniques, these methods navigate the complex, high-dimensional design spaces characteristic of metasurfaces, enabling the creation of highly optimized and multifunctional structures tailored to specific electromagnetic responses[353]. The effectiveness of AI-driven metasurface design fundamentally relies on two core aspects: the encoding and decoding process and the underlying neural network architectures. This subsection provides an in-depth exploration of these two aspects, illustrating how AI methodologies are transforming metasurface design through novel approaches to data representation and model deployment.

Encoding and decoding in AI-driven metasurface design. In an AI-driven metasurface workflow, encoding encompasses transforming both the structural design parameters and the desired electromagnetic responses into representations suitable for learning and optimization. Decoding then recovers the physical metasurface geometry or the predicted response from those representations, ensuring the final design or analysis remains consistent with the original objectives.

Parametric encoding. Parametric encoding relies on a limited set of predefined parameters (for instance, shape dimensions or material constants) to describe a metasurface[354,355]. Here, the input might be a small set of geometric variables, while the output could be key performance metrics (e.g., reflection coefficients at specific frequencies). For instance, Huang et al.[355] represent the metasurface with only a few geometric parameters, optimizing these parameters to realize the desired functionality and thereby confining the design space to a limited set of physically meaningful variables while accelerating the convergence process, as shown in Fig. 13a. Because each parameter directly correlates with a physical attribute, designers can more easily decode the resulting model back into actual device structures and correlate those with the measured or simulated electromagnetic responses. However, parametric encoding struggles with highly complex or free-form designs. Expanding the parameter set can address more intricate geometries, but doing so erodes the simplicity and interpretability that make parametric methods appealing.

Vector encoding. Vector encoding unifies a large set of design parameters or response metrics into a single high-dimensional vector[356–359]. For instance, each component of the input vector may define a distinct geometrical feature across the metasurface, while the output vector could represent measured or simulated spectral profiles over numerous frequencies. As an illustration, Qiu et al.[358] formulate the metasurface design as a two-dimensional 0–1 matrix, where each entry indicates the presence or absence of a specific material and consequently expands the design dimension

significantly for enhanced layout flexibility, as shown in Fig. 13b. This unified representation handles complex or irregular designs more flexibly than parametric encoding, but tends to obscure direct physical interpretation, making it harder to map individual vector entries back to specific design features or response bands. Even so, vector encoding excels in tasks where the design and response spaces are both high-dimensional, and data-driven models can more readily learn correlations between them.

Image encoding. Image encoding transforms metasurface layouts and their responses into pixel or voxel grids[360–362]. For periodic or quasi-periodic structures, the input might be a 2D map depicting geometric features, and the output could be spatial field patterns or spectral heatmaps. This approach leverages established image-processing algorithms to detect and manipulate spatial patterns. For instance, Zeng et al.[360] embed thickness, meta-atom distribution, and material properties into different channels of an image, thereby accommodating a variety of neural network architectures and substantially broadening the design space, as shown in Fig. 13c. However, high-resolution image grids can be memory-intensive, especially if the goal is related to complex, 3D field responses. Image encoding is thus most beneficial when spatial patterns dominate the design logic and the resolution demands remain manageable.

Graph encoding. Graph encoding emphasizes interrelationships among metasurface elements[363], often crucial for capturing near-field coupling or large-scale interactions. Nodes could represent distinct meta-atoms or patches, and edges encode mutual coupling or physical adjacency. On the input side, the graph describes the structural topology, while the output could be the corresponding collective electromagnetic behavior, such as field distributions or multi-frequency scattering parameters. For example, Wu et al.[363] transform the metasurface into a graph structure that models not only individual meta-atoms but also their mutual coupling relationships for a more holistic optimization, as shown in Fig. 13d. Although graph-based methods are powerful for complex and non-periodic metasurfaces, they call for specialized neural network architectures (like GNNs) and can grow computationally expensive with increasing numbers of nodes and edges.

Mesh encoding. Mesh encoding discretizes the metasurface into a grid or mesh of smaller elements[364], where each element's properties and field responses are explicitly modeled. Consequently, the input could be local material parameters assigned to each mesh cell, and the output might be detailed electromagnetic fields or reflection/transmission coefficients at each cell boundary. For instance, Kwon et al.[364] employ a triangular mesh to represent the metasurface design, facilitating detailed modeling of geometric features and ensuring compatibility with high-precision electromagnetic simulations, as shown in Fig. 13e. This fine-grained approach is advantageous for simulating physical phenomena with high accuracy, using techniques like finite element or finite-difference time-domain methods. Yet, as mesh density grows, so does computational complexity, making it challenging to decode large meshes into physically realizable designs without a substantial computational budget.

Sequence encoding. Sequence encoding treats metasurface configurations and their associated responses as ordered sequences[365]. One might record the addition or modification of unit cells step by step, with each sequence entry denoting both a geometric action and its partial electromagnetic outcome. This format suits models like recurrent neural networks or Transformers, which excel at capturing long-range dependencies. For example, Zhang et al.[365] utilize a sequence-based representation to capture spectral correlations and accommodate potential frequency-transfer tasks[366,367], effectively leveraging sequential neural networks for iterative design processes, as shown in Fig. 13f. However, while sequences naturally encode the temporal or iterative nature of design steps, they can lose spatial context if the layout is not inherently linear. Ensuring the final decoded device accurately reproduces the desired field or spectral response can therefore be more demanding, particularly for large-scale metasurfaces.

By selecting an appropriate encoding-decoding strategy for both structural inputs and electromagnetic outputs, AI-driven metasurface design can achieve higher accuracy, faster convergence, and more transparent interpretation of results. Crucially, the chosen representation must allow the reconstruction (or decoding) to faithfully reflect the original design and response objectives, ensuring that any learned relationships hold true in physical realization. Achieving such consistency typically involves aligning the input-output encoding schemes so that each predicted parameter or field component can be reliably mapped back to a tangible device setting. As a result, reproducibility and unification across encoding and decoding stages become central to advanced metasurface research, offering a pathway toward not only more efficient but also more trustworthy AI-assisted photonic design.

The selection of appropriate models in AI-driven metasurface design. In AI-driven metasurface design, the choice of deep learning methods critically influences design efficiency, optimization accuracy, and adherence to physical constraints. Given the diverse data structures, optimization targets, and physical limitations inherent in metasurface research, different deep learning approaches exhibit distinct strengths and drawbacks. Therefore, a structured taxonomy is necessary to clarify how each method addresses design objectives, handles data modalities, and incorporates electromagnetic or fabrication constraints.

We categorize existing deep learning techniques for metasurface design into eight primary classes based on their application scenarios: (1) Fundamental neural network-based models, (2) Advanced Neural Network Models, (3) Sequence-based models, (4) Graph-based methods, (5) Generative models, (6) Reinforcement learning models, (7) Physics-Informed Models, and (8) AI Enhancement Models. While this classification highlights the specific problem settings each category can tackle, many practical systems integrate multiple methods to balance performance, computational demands, and physical feasibility. Hence, a thorough understanding of the commonalities and differences across these eight categories is crucial for selecting or combining suitable approaches.

Fundamental neural network models primarily solve straightforward regression or classification problems, establishing a direct mapping between design variables and target performances. Advanced neural network models extend these foundational models by enhancing representational capacity—often adding specialized layers or attention mechanisms to handle more complex phenomena. Sequence-based models incorporate temporal or iterative aspects into the design process, while graph-based methods naturally encode spatial couplings among meta-atoms. Generative models open up possibilities for synthesizing entirely new metasurface configurations from learned distributions, and reinforcement learning focuses on adaptive decision-making through trial-and-error interactions with the environment. Importantly, physics-informed and constraint-aware frameworks integrate electromagnetic equations or fabrication limits directly into the learning process, bridging the gap between data-driven inference and physical consistency. Lastly, AI enhancement models, such as transfer learning, and explainable models, can further enhance scalability and robustness.

Fundamental neural network-based models. Deep learning has proven effective for addressing both forward and inverse problems in metasurface design, especially when the underlying task involves relatively direct parameter-to-performance mappings. As shown in Fig. 14a, a bidirectional DNN can link plasmonic nanostructure geometries to far-field optical spectra in both directions, substantially streamlining the design and characterization process[368]. Building on this framework, a physics-informed DNN that embeds Lorentzian constraints allows accurate prediction of frequency-dependent dielectric properties in all-dielectric metamaterials without sacrificing physical realism, as illustrated in Fig. 14b[369].

Beyond simple parameter input, CNNs are adept at handling spatially structured data and capturing localized interactions within metasurface

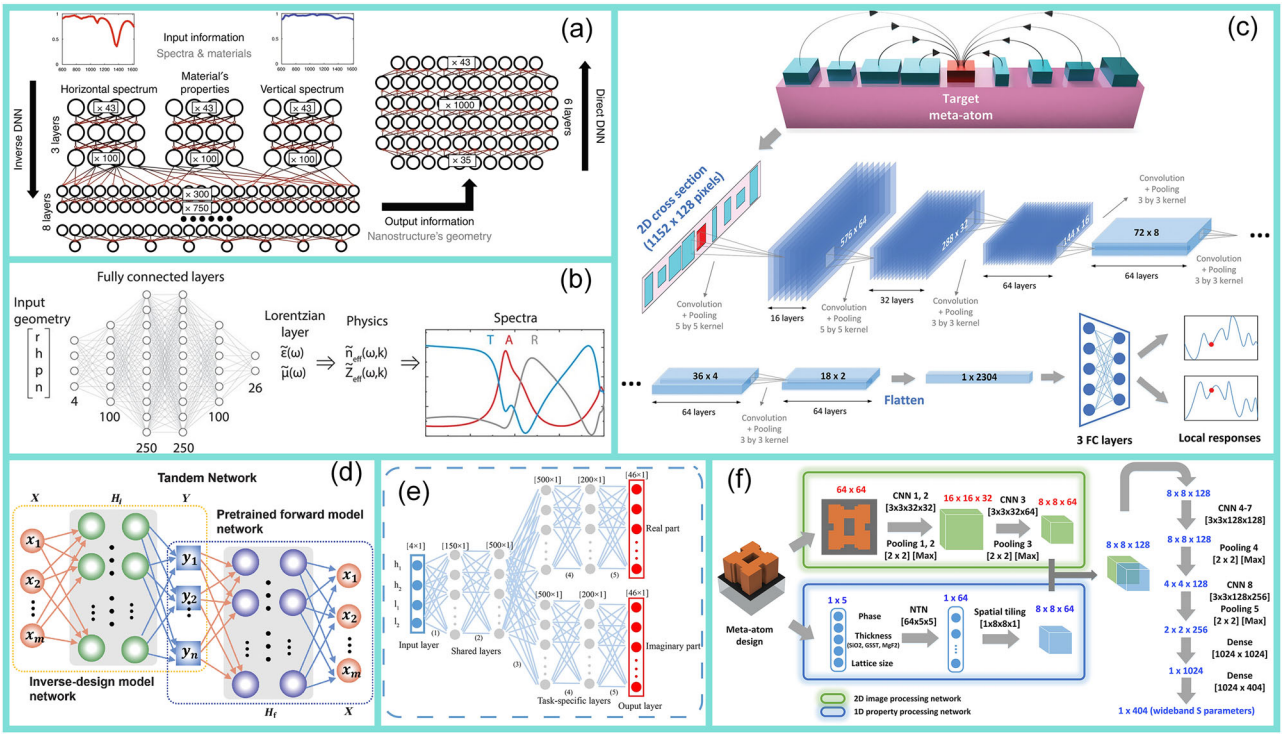

Fig. 14 | Applications of fundamental neural network models in metasurface design. a Bidirectional DNN architecture for plasmonic nanostructure design, addressing both forward and inverse problems by linking geometrical parameters with far-field spectra[368]. **b** Physics-informed DNN incorporating Lorentzian constraints to predict frequency-dependent dielectric properties in all-dielectric metamaterials[369]. **c** CNN-based prediction of mutual coupling effects in metasurfaces, improving phase and amplitude accuracy beyond periodic boundary assumptions[370]. **d** CNN optimization of metasurface structures to enhance tandem solar cell efficiency through light management[371]. **e** Multi-headed CNN architecture for modeling light--matter interactions in dielectric nanostructures, achieving enhanced nonlinear optical responses[11]. **f** Fusion CNN model integrating forward and inverse networks for the design of active metasurfaces with embedded functionalities[372].

arrays. Figure 14c showcases a CNN trained to account for mutual coupling effects, overcoming the limitations of periodic boundary assumptions and achieving higher accuracy in phase and amplitude prediction[370]. Similarly, a CNN-based optimization for tandem solar cells, shown in Fig. 14d, leverages the metasurface's geometry to manage light more effectively, thereby enhancing overall device efficiency[371]. For more complex light–matter interactions, multi-headed CNN architectures can model nonlinear optical phenomena (Fig. 14e), offering a deeper view into device-level physics[11]. Finally, fusing forward and inverse network modules, as in Fig. 14f, enables adaptive metasurface designs that incorporate active elements while maintaining computational efficiency[372].

In short, these fundamental neural-network approaches lay the groundwork for many AI-driven metasurface designs, offering a balance between ease of implementation and predictive power. Specifically, by serving as differentiable surrogate models for complex electromagnetic responses, fundamental neural networks—such as bidirectional DNNs and CNNs—enable efficient backpropagation of electromagnetic performance criteria, such as phase, amplitude, and polarization, into precise adjustments of metasurface geometry. This capability substantially reduces reliance on computationally intensive full-wave simulations, facilitating rapid exploration and optimization of large design spaces while ensuring accurate electromagnetic response control. However, as metasurface applications grow increasingly elaborate—requiring multi-band operation, polarization control, or large-scale non-periodic layouts—further refinements may be needed. These refinements often involve hybridizing fundamental networks with advanced architectures or embedding additional physical constraints.

Advanced neural network models. Recent advancements in deep learning have fueled the development of more sophisticated models for metasurface design, aiming to tackle challenges, such as global relationship modeling, nonlinear mappings, data dimensionality reduction, fabrication robustness, and multi-network integration. Compared to fundamental neural networks, these advanced methods typically incorporate deeper or more specialized architectures that can encode complex physics, reduce design uncertainties, and handle large parameter spaces. In practice, they often balance higher computational overhead with stronger expressive capabilities, thereby enabling efficient generation of intricate metasurfaces.

Transformer-based frameworks[373–375] offer a robust mechanism to capture long-range dependencies among design variables, significantly enhancing local near-field intensities by harnessing quasi-bound states in continuum (quasi-BIC) effects, as shown in Fig. 15a[373]. By predicting electric field distributions and subsequently performing inverse optimization, Transformers streamline the iterative design of metasurfaces for applications like surface-enhanced Raman scattering. However, their training may demand large, high-quality datasets to fully exploit attention mechanisms and handle diverse geometries. Recent advances further demonstrate that Transformer-based models enable real-time inverse design across multiple spectral and polarization regimes, offering both scalability and adaptability for complex metasurface functionalities[375,376].

Autoencoders, characterized by their encoder–decoder structure, have proven highly effective in compressing high-dimensional data into concise, informative representations, facilitating efficient exploration and optimization in complex metasurface design spaces[377–379]. An illustrative application is demonstrated in Fig. 15b[378], where an autoencoder learns compact, low-dimensional embeddings of polarization-dependent optical responses, enabling the efficient generation of multi-channel polarization holograms. Despite their strength in dimensionality reduction and representation learning, autoencoders can potentially omit fine-grained structural details, necessitating careful tuning or incorporation of additional physical constraints to maintain precision in practical metasurface implementations.

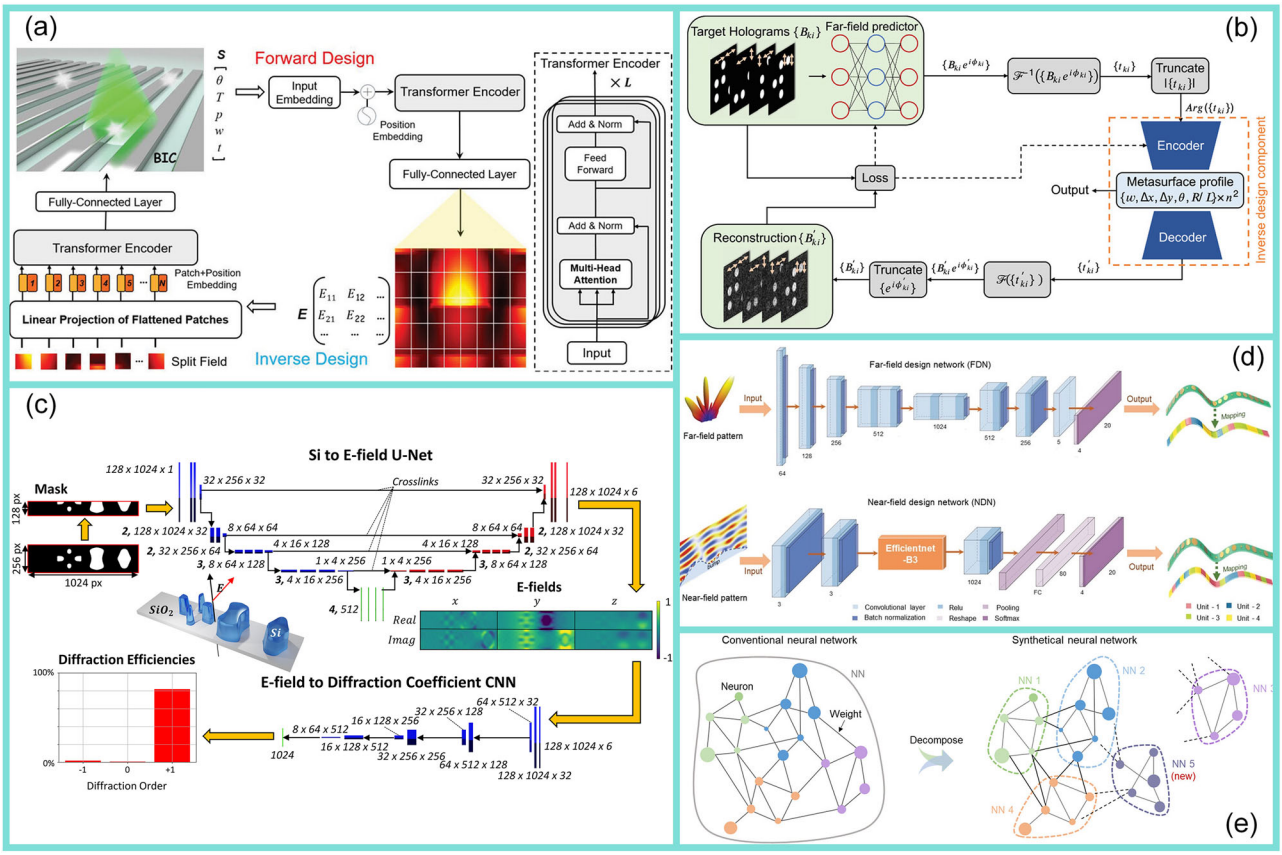

Fig. 15 | Applications of advanced neural network methods in metasurface design. a Transformer-based framework for designing all-dielectric surface-enhanced Raman scattering metasurfaces, optimizing electric field distributions and enhancing Raman signals through quasi-BIC coupling[373]. **b** Autoencoder-assisted optimization of polarization holograms, enabling multi-channel storage and reconstruction by learning polarization-dependent optical features[378]. **c** U-Net model applied to establish robustness against fabrication uncertainties in metasurface design, ensuring stable performance despite manufacturing defects[380]. **d** In Situ Customized Illusion Enabled by Global Metasurface Reconstruction using network fusion[521] **e** Network fusion of multiple neural networks for broadband metasurface inverse design, enabling real-time optimization by integrating pre-trained networks[381].

U-Net architectures, characterized by their encoder-decoder structures and multi-scale feature extraction capabilities, are particularly effective at capturing spatial hierarchies and fine-grained structural information in metasurface designs. This ability allows *U*-Nets to efficiently identify and predict subtle geometric variations, which makes them highly suitable for addressing fabrication uncertainties, as shown in Fig. 15c[380].

Finally, network fusion strategies integrate multiple models for dynamic inverse design, ensuring rapid adaptation to broad bandwidths or changing performance metrics. For example, Jia et al.[381] proposed a global metasurface reconstruction framework by fusing two convolutional neural networks—Far-field design network and near-field design network —to achieve customized optical illusions based on user-defined near-field or far-field specifications, as shown in Fig. 15e. This network fusion approach efficiently addresses the complexity of meta-atom couplings and significantly accelerates the inverse design process, eliminating extensive iterative optimization inherent in traditional methods. Jia et al. introduced a novel synthetical neural network approach in later research[381], dynamically assembling multiple inverse neural networks via an assembly neural network to efficiently tackle broadband metasurface inverse design tasks, as shown in Fig. 15f. Network fusion enhances metasurface design efficiency, reduces data dependency, and effectively captures complex inter-element electromagnetic couplings, enabling rapid adaptation to diverse and dynamic design tasks. However, orchestrating several neural networks raises concerns about model consistency and overfitting, prompting the need for robust calibration and cross-validation protocols.

In summary, advanced neural network models address key limitations of basic architectures by incorporating attention mechanisms, dimensionality reduction, or multi-network ensembles. Specifically, transformer-based frameworks enhance electromagnetic response control by effectively capturing long-range interactions within metasurface arrays, enabling accurate predictions of complex near-field phenomena and resonant behaviors. Autoencoders facilitate efficient exploration of metasurface design spaces through dimensionality reduction, significantly improving the speed and accuracy of identifying optimal electromagnetic responses. U-Net architectures ensure robustness in electromagnetic performance by precisely modeling fine-scale geometric variations and manufacturing imperfections. Furthermore, network fusion strategies dynamically integrate multiple specialized networks to adaptively handle complex, broadband electromagnetic requirements, substantially accelerating inverse design and optimization processes. They are particularly useful in scenarios requiring large-scale optimizations, multi-physics constraints, or high resilience to manufacturing errors. Yet, they may also introduce more hyperparameters, heavier computational loads, and reliance on extensive training datasets.

Sequence-based models. Sequence-based models leverage temporal or ordered data structures to capture evolving design patterns or spectral correlations in metasurface engineering. Unlike feedforward architectures, these recurrent or hybrid networks consider the sequential nature of design updates or spectral variations, enabling more direct handling of dynamic or iterative design processes.

For instance, LSTM networks have demonstrated direct predictions of polarization sensitivity in nanofin metasurfaces, thereby performing inverse design with minimal reliance on computationally expensive simulations, as

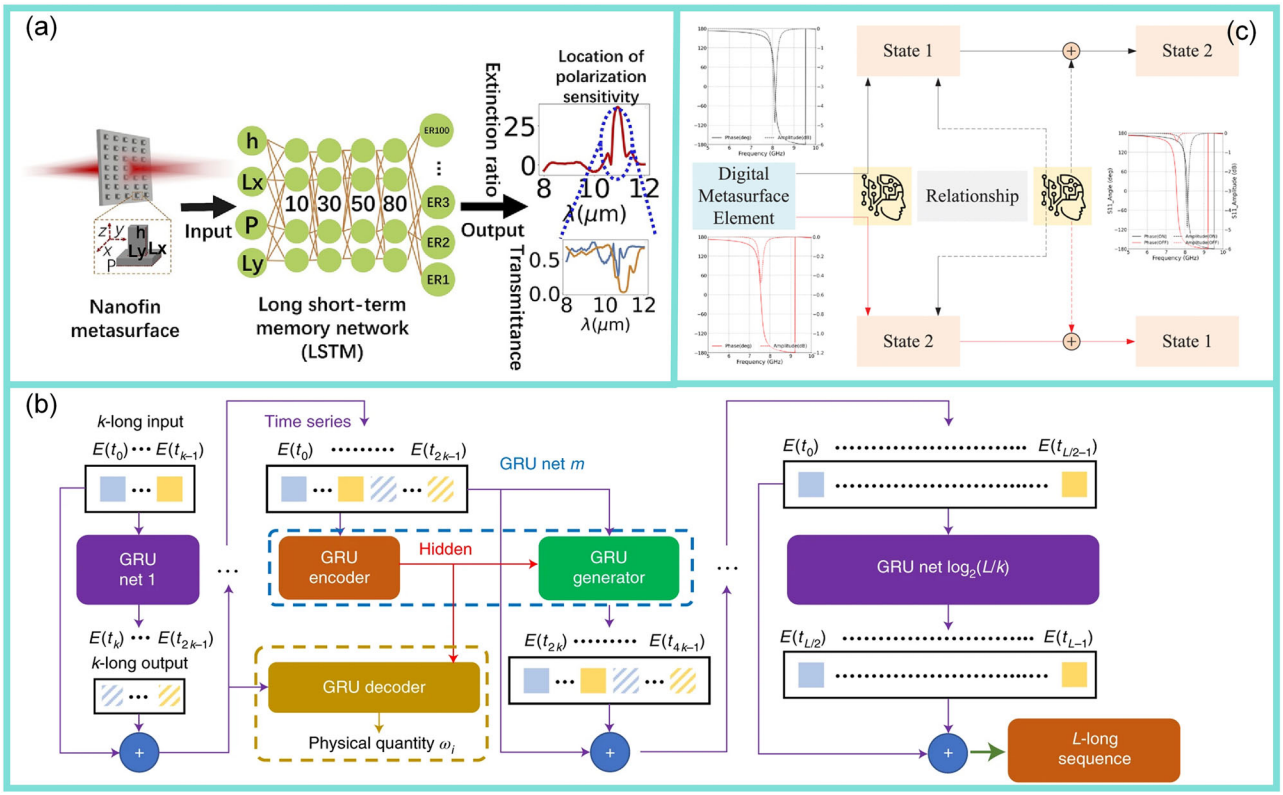

Fig. 16 | Applications of sequence-based models in metasurface inverse design. **a** Long short-term memory neural network for directly inverse design of nanofin metasurface[382]. **b** GRU-based method utilizing the Kramers-Kronig relation to leverage the physical correlation between the real and imaginary parts of spectral data[383]. **c** Hybrid CNN-LSTM-DNN approach for space-time coding digital metasurfaces design[384].

shown in Fig. 16a[382]. By taking extinction ratio as a core feature, LSTMs mitigate the non-uniqueness issue in inverse problems, though they may still struggle when design spaces become extremely large or nonlinear. Meanwhile, GRU-based methods exploit physical correlations in spectral data, such as the Kramers-Kronig relation, as shown in Fig. 16b[383], offering a more compact memory mechanism and potentially faster convergence compared to LSTM. These models are particularly helpful in cases requiring real-time analysis of spectral shifts.

In addition, hybrid CNN-LSTM-DNN architectures can simultaneously extract spatial features and capture temporal relationships, as demonstrated by space-time coding digital metasurfaces (Fig. 16[384]). Such integrated methods are valuable when designing metasurfaces that must adapt across multiple operating conditions, yet they can be more complex to train and tune due to the increased number of parameters. Sequence-based models collectively enhance electromagnetic response control by explicitly capturing temporal dependencies and spectral correlations inherent in metasurface design processes. By effectively modeling ordered interactions among sequential parameters—such as wavelength-dependent optical responses or iterative design updates—these architectures substantially reduce simulation overhead and accelerate the inverse design of dynamically tunable metasurfaces. Sequence-based models significantly enhance prediction accuracy for wavelength-dependent or dynamically tunable structures. Their recurrent architectures inherently model complex correlations within electromagnetic spectra, thus reducing reliance on computationally expensive simulations. However, these models often require substantial sequential training data and may struggle to accurately represent spatial interactions.

Graph-based models. Graph-based models have emerged as a potent tool for representing metasurfaces where localized interactions between meta-atoms significantly influence global performance[385,386]. By treating each unit cell as a graph node and mapping its relationships (edges) according to physical adjacency or coupling strength, these methods naturally incorporate spatial correlations that might be overlooked by conventional grid-based or sequence-based representations.

A typical GNN model characterizes coupling effects in large-scale metasurfaces by assigning geometric or material attributes to node features and inverse-distance measures to edges (Fig. 17[387]). Such GNNs can be augmented with diffraction theory or near-field transformations, boosting their predictive accuracy for real-world deployments. Alternatively, graph convolution layers can focus on scattering properties, as shown in Fig. 17[388], enabling scalable modeling that adapts seamlessly to different array sizes or shapes. Although these methods capture complex interactions, they often demand careful architectural design to avoid over-smoothing (where node features become indistinguishable) or excessive computational overhead.

Graph Attention Networks (GANets) extend this framework by learning attention weights that dynamically weigh the importance of each edge in multifunctional metasurfaces (Fig. 17c[389]). This approach refines inverse design by letting the model selectively focus on crucial interactions for specific wavelength bands or polarization states. However, the added flexibility also increases model complexity and parameter count, which may necessitate larger training datasets or more rigorous validation strategies.

Overall, graph-based models excel in scenarios involving strong coupling effects or irregular, large-scale layouts. By explicitly modeling spatial dependencies and inter-unit electromagnetic interactions as graph-structured relationships, these methods inherently enhance electromagnetic response control. This approach allows precise characterization of local coupling effects, enabling efficient optimization of global metasurface performance by accurately predicting and manipulating near-field and far-field responses. They serve as a complementary alternative to image-like encodings or sequence-based representations, especially when local-to-global interactions play a decisive role in metasurface performance. Balancing the benefits of detailed spatial modeling against the computational

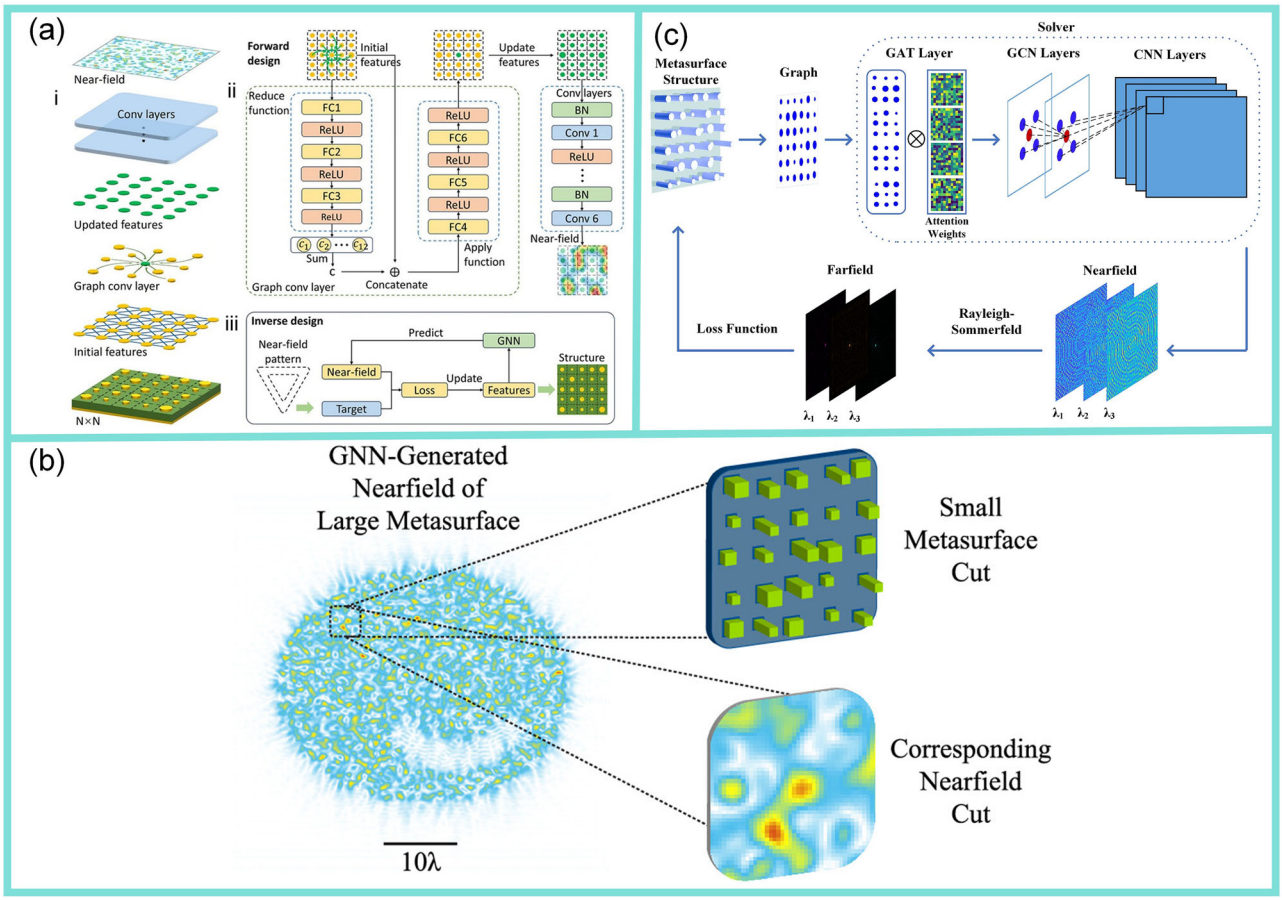

Fig. 17 | Applications of graph-based methods in metasurface design. a Graph Neural Network (GNN) for characterizing coupling effects in intelligent metasurfaces, modeling each unit as a node and defining inter-unit relationships with distance-based edges[387]. **b** GNN-based modeling of electromagnetic scattering in metasurfaces, predicting near-field distributions via graph convolution layers[388]. **c** Graph Attention Network for inverse design of multifunctional metasurfaces, adjusting the importance of interactions between units to improve multi-wavelength performance[389].

cost of large-scale graph operations remains an active area of research, underscoring the ongoing innovation in AI-driven metasurface design.

Generative models. Generative models are particularly attractive for metasurface design because they can efficiently explore high-dimensional parameter spaces to produce novel configurations that satisfy specific optical or electromagnetic criteria[390–394]. Variational autoencoders (VAE), for instance, compress intricate metasurface patterns into a continuous latent space, enabling the creation of new absorber designs that exhibit broadband absorption (Fig. 18a[395]). VAEs typically excel at smooth interpolation between known configurations, but they may struggle with capturing fine-grained details unless carefully regularized or combined with physics-based constraints.

Progressing to more expressive frameworks, GANs directly map target spectra or performance metrics to plausible metasurface layouts[392,396,397], bypassing extensive trial-and-error design, as Liu's work shown in Fig. 18b[390]. Although GANs can generate highly diverse patterns, training instability and mode collapse remain challenges, especially when balancing electromagnetic fidelity against structural variation. Extensions like Wasserstein GAN (Fig. 18c[398]) alleviate some training issues by introducing an Earth Mover's distance, facilitating more stable learning of phase-change absorbers for molecular fingerprint detection. The Anchor-Controlled GAN (Fig. 18d[360]) further refines design diversity by incorporating spectral overlap coefficients and cluster-guided controllers, effectively exploring multiple structural configurations that fulfill similar target responses. Such anchor-based strategies improve interpretability and allow designers to incorporate partial physics constraints in the generative loop.

Beyond GANs, Flow-based models offer a reversible mapping between partial and complete field information, making them well-suited for recovering electromagnetic data in complex or partially obstructed domains (Fig. 18e[399]). By modeling an explicit probability density, flow-based approaches can integrate physical priors more easily, though they often require careful architecture design to handle large-scale metasurface layouts. Finally, hybrid models that combine VAEs and GANs (Fig. 18f[400]) aim to reap the benefits of both latent-space smoothness and realistic sample generation, reducing computational overhead while retaining high design diversity.

These advanced generative models substantially broaden the metasurface design space, enabling the discovery of novel and structurally diverse solutions. By leveraging latent-space representations, adversarial training mechanisms, and explicit density estimation, generative models systematically enhance electromagnetic response control. They enable designers to efficiently navigate complex parameter spaces, predict optimal configurations, and directly generate high-performance metasurface layouts, thereby significantly reducing iterative optimization steps and computational costs associated with traditional electromagnetic simulations. However, they also impose new challenges, including maintaining physical realism within generated designs, and ensuring compatibility with practical manufacturing constraints.

Reinforcement learning models. Reinforcement Learning (RL) has gained significant attention in various domains due to its ability to optimize decision-making processes in dynamic, uncertain environments. Initially developed for robotics[401–403], gaming[404–406], and autonomous

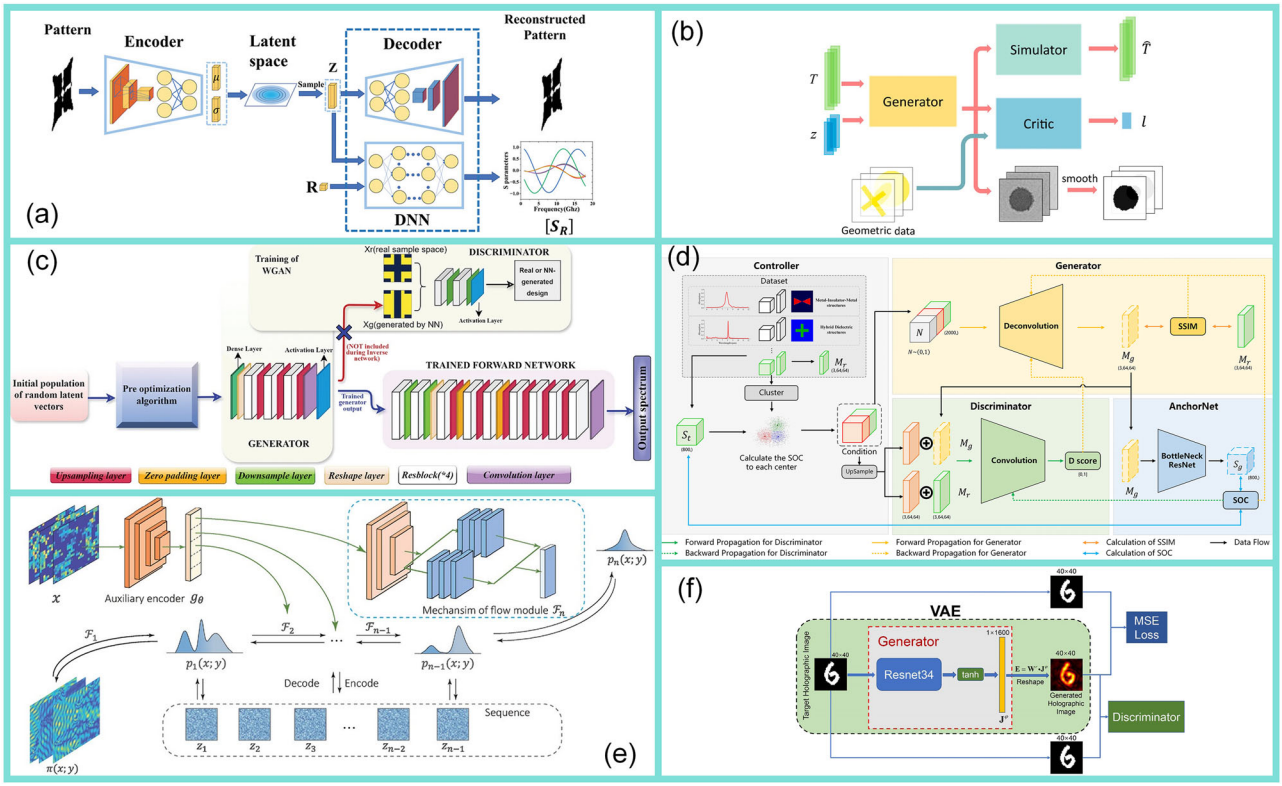

Fig. 18 | Applications of generative models in metasurface design. a VAE-based model for metasurface-based absorber design, generating new patterns for enhanced broadband absorption[395]. **b** GAN-based framework for inverse design of metasurfaces, directly generating metasurface patterns from optical spectra[390]. **c** Wasserstein GAN applied to phase-change material absorbers for molecular fingerprint detection, optimizing absorption spectra[398]. **d** Anchor-Controlled GAN for improved electromagnetic fidelity and structural diversity, guided by spectral overlap coefficients[360]. **e** Flow-based model for full-field electromagnetic information recovery in inaccessible or low-resolution regions[399]. **f** Hybrid VAE-GAN approach that combines the strengths of both latent-space encoding and realistic sample generation[400].

driving[407–409], RL techniques have shown great promise in fields where sequential decision-making or continuous adaptation is required. In metasurface design, RL offers a compelling solution for addressing the complexities of high-dimensional design spaces and dynamic performance requirements. Even if the exploration process involves testing many suboptimal designs, RL's ability to eventually converge to a high-performance metasurface from a large design space holds significant value.

RL has shown significant promise for metasurfaces design[410–412]. For example, double-deep Q-learning (DDQN), for instance, has been applied to optimize metasurface holograms by selecting among material or geometric parameters that maximize holographic efficiency, as shown in Fig. 19a[413]. Similarly, Deep Q-Network (DQN)-based methods navigate large parameter spaces for solar absorber design, achieving high absorption at visible wavelengths while minimizing infrared absorption (Fig. 19b[414]). Such approaches benefit from RL's capacity for handling discrete actions or configurations without requiring differentiable cost functions. For continuous or more complex freeform tasks, deep reinforcement learning frameworks translate metasurface beam deflection or dynamic wavefront shaping into Markov decision processes (Fig. 19c[415]), though the computational cost of training can be substantial due to repeated full-wave simulations.

More advanced methods like proximal policy optimization (PPO) and asynchronous advantage actor-critic (A3C) enable dynamic metasurface control, either by adjusting geometry in real time (Fig. 19d[416]) or designing asymmetric polarization converters beyond traditional transmission limits (Fig. 19e[417]). RL can also handle feedback-based reconfiguration, where bias voltages or tunable elements are continuously adapted to meet changing performance requirements (Fig. 19f[418]).

Reinforcement learning significantly enhances electromagnetic response control in metasurface design by systematically navigating high-dimensional parameter spaces, optimizing sequential design decisions, and dynamically adapting device configurations. By iteratively interacting with simulated or real electromagnetic environments, RL efficiently discovers high-performance metasurface structures that traditional optimization methods may overlook, thereby enabling robust and adaptive wavefront manipulation and electromagnetic functionalities. Despite these advantages, RL methods often demand large-scale exploration and numerous reward-based updates, which can be resource-intensive. Balancing exploration (searching new configurations) and exploitation (fine-tuning known good designs) is key to realizing RL's full potential in metasurface engineering. As metasurface designs become more complex, there is a need for more efficient simulators or surrogate models that can accelerate RL training. Future research will likely focus on improving the scalability of RL methods for large metasurface arrays, integrating RL with physics-informed approaches to reduce simulation costs.

Physics-informed models. Physics-informed and constraint-aware models explicitly encode electromagnetic principles or fabrication limits into the neural network or optimization loop[419–421]. These models play a pivotal role in ensuring that AI-generated metasurface designs are physically feasible and can be manufactured in practice. Unlike purely data-driven approaches, which may generate abstract designs that lack physical relevance, physics-informed models incorporate fundamental physical laws, such as Maxwell's equations, either directly or indirectly into the design process, thereby enforcing constraints that ensure manufacturability and functional viability. Notably, recent advances demonstrate that embedding Maxwell's equations

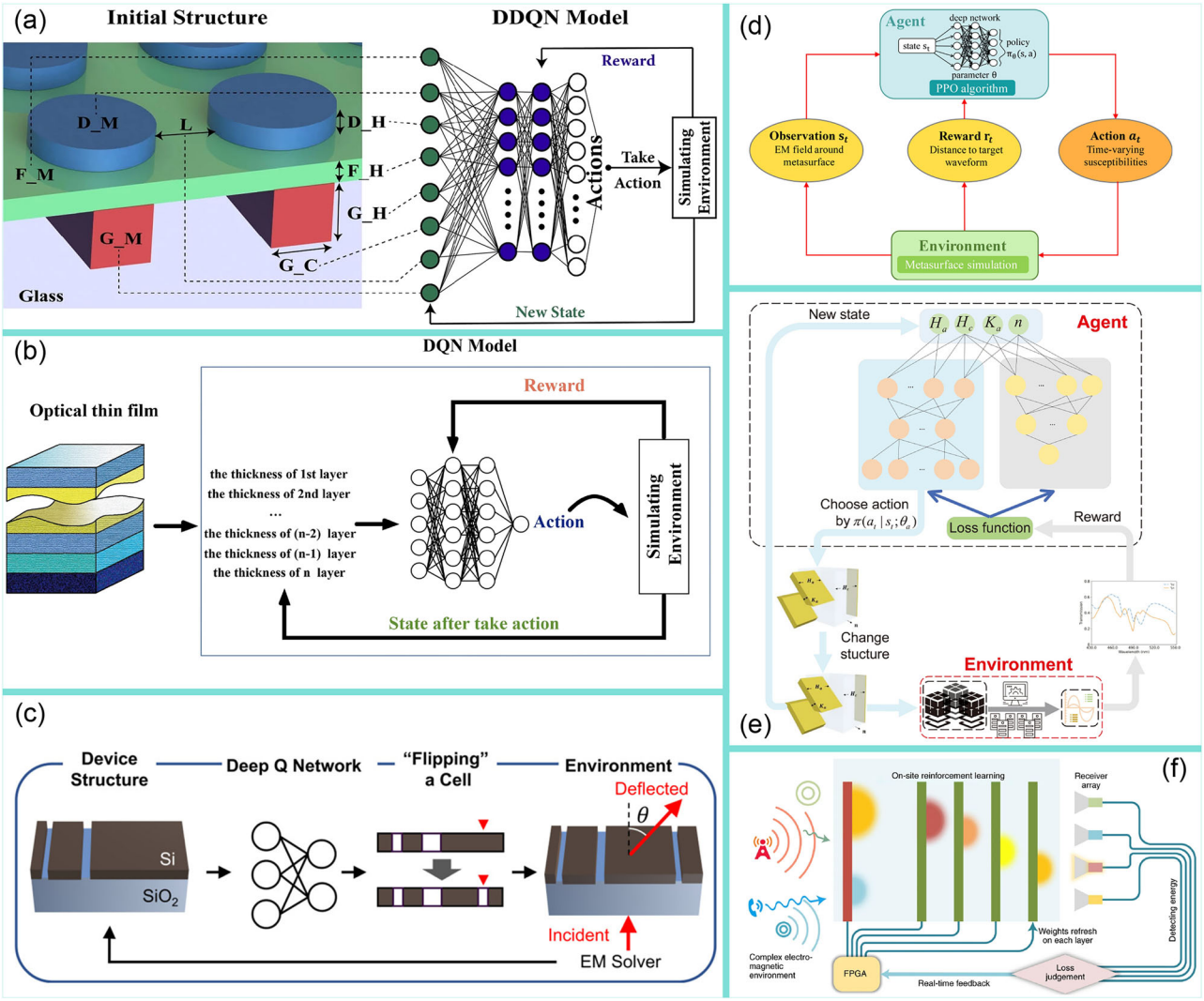

Fig. 19 | Applications of reinforcement learning methods in metasurface design. **a** DDQN for optimizing metasurface holograms[413]. **b** DQN-based method for designing perfect solar absorbers[414]. **c** Deep Reinforcement Learning for freeform metasurface beam deflection[415]. **d** Proximal Policy Optimization (PPO) for dynamic metasurface control[416]. **e** Asynchronous Advantage Actor-Critic (A3C) for asymmetric polarization converters[417]. **f** Feedback-based RL for reconfigurable metasurface control[418].

directly into neural network loss functions—such as via Helmholtz residuals[422] or Lorentz-type dispersion constraints[369]—significantly enhances the physical fidelity and generalization of inverse design models. These physics-informed networks inherently enforce electromagnetic principles, such as energy conservation, causality, and material dispersion, thereby enabling robust prediction across diverse regimes with reduced data requirements[423,424].

Surrogate-based optimization accelerates the design process by approximating expensive simulations with pre-trained forward models[3,55,425,426]. For example, Ma et al.[426] developed a deep learning-based surrogate model to automatically learn the complex relationship between metasurface structure parameters and optical responses, enabling direct mapping from optical design goals to physical structures. This approach establishes an end-to-end design framework, embedding deep learning models into the optimization loop to generate metasurface structures that meet the design requirements directly from the goals, as shown in Fig. 20a. And Huang et al.[355] accelerated simulation results and facilitated gradient-based optimization by replacing RCWA simulations with a DNN surrogate model using pre-collected simulation data, as shown in Fig. 20b. Surrogate-based physics-driven methods enable rapid, differentiable design optimization by approximating costly simulations while allowing direct goal-to-structure mapping for efficient automated metasurface synthesis. Despite these advantages, surrogate models inherently suffer from approximation errors due to limited training data coverage and potential biases, which can lead to exacerbated inaccuracies in the metasurface design.

Adjoint and topology optimization methods are key physics-informed approaches in metasurface design. These methods enable gradient-based fine-tuning by calculating the adjoint variables, ensuring physical feasibility while optimizing performance[427–429]. For example, Jiang et al.[427] computed the efficiency gradient of forward and adjoint variables through electromagnetic simulations, using them for backpropagation in neural networks to learn the physical relationship between geometry and optical response, as shown in Fig. 20c. And Davoodi et al.[423] proposes a physics-integrated deep topology optimization framework that synergizes Maxwell-constrained neural networks with tight-binding-derived topological invariants (e.g., winding numbers), ensuring electromagnetic consistency while distinguishing trivial and topological photonic modes, as shown in Fig. 20d[423]. Adjoint and topology optimization methods can optimize the metasurface design without relying on collected datasets. However, their computational cost can be high, especially for large-scale designs with complex geometries, as they require repeated electromagnetic simulations.

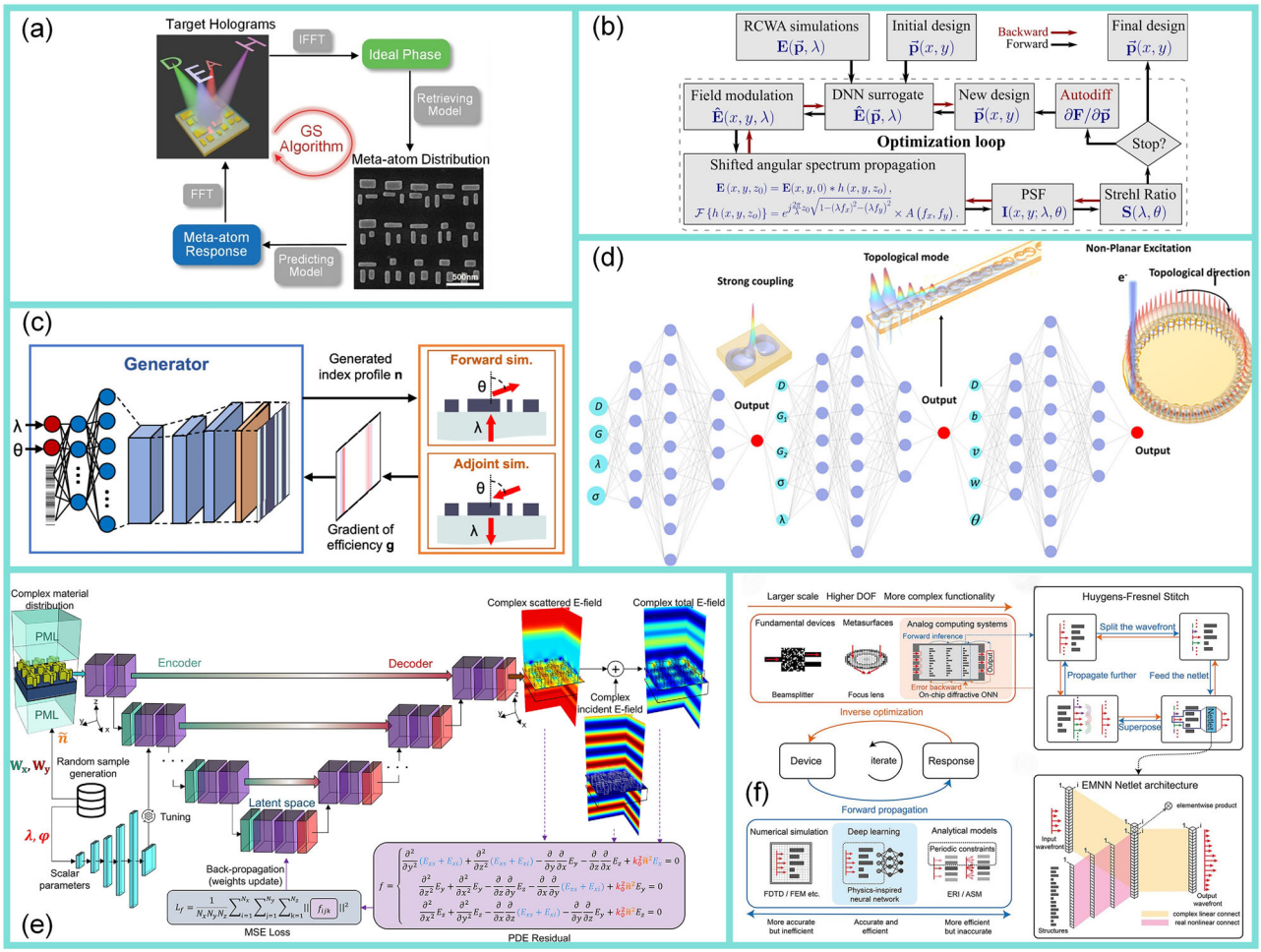

Fig. 20 | Physics-informed models in metasurface design. a Surrogate model-based optimization[426]. **b** Broadband thermal imaging using metaoptics with DNN-based surrogate model[355]. **c** Global optimization of dielectric metasurfaces using a physics driven neural network[427]. **d** Physics-informed Neural Networks for diffraction and polarization effects[423]. **e** Physics-informed deep learning for 3D modeling of light diffraction from optical metasurfaces[422]. **f** Huygens-Fresnel physics-inspired photonic inverse design[419].

We can also directly integrate fundamental physical principles into the metasurface design process using deep learning frameworks[419,422,430]. For example, Medvedev et al.[422] developed a physics-informed deep learning approach for 3D modeling of light diffraction in optical metasurfaces, where PDEs are embedded directly into the loss function to accurately simulate both near-field and far-field responses, as shown in Fig. 20e. Similarly, Shao et al.[419] proposed a physics-inspired deep learning architecture called the electromagnetic neural network (EMNN), which consists of two components: the EMNN Netlet, which serves as a local electromagnetic field solver, and the Huygens-Fresnel Stitch, which concatenates local predictions. This architecture enables rapid, accurate full-wave field predictions based on arbitrary input fields and non-fixed geometries, as illustrated in Fig. 20f. Directly integrating physical principles into deep learning models for metasurface design can lead to physically accurate solutions, but it often requires careful approximations, tricks, and simplifications to make the approach computationally feasible and practically applicable.

In conclusion, the integration of physics-driven AI methodologies has ushered in a paradigm shift for metasurface design, effectively bridging the gap between data-driven black-box approaches and physical realizability. Surrogate models, adjoint optimization, and physics-embedded neural networks collectively address critical challenges in computational efficiency, physical consistency, and manufacturing constraints. By explicitly embedding Maxwell's equations and material constraints into neural architectures or optimization loops, these physics-informed methods significantly enhance electromagnetic response control, ensuring both accurate prediction of complex optical behaviors and direct compliance with physical limitations. Such rigorous incorporation of physical insights drastically reduces the search space, accelerates convergence to optimal solutions, and guarantees realistic, manufacturable metasurface designs. Nevertheless, challenges persist in balancing computational costs, mitigating error propagation in surrogate models, and enhancing generalizability across multi-band or multi-functional designs. Future research could focus on hybrid approaches that synergize physics-based priors with few-shot learning techniques, develop unified frameworks for multi-physics constraints, and establish standardized benchmarks for evaluating model robustness. The convergence of interpretable AI and domain-specific physical modeling holds particular promise for designing next-generation metasurfaces with unprecedented functionalities.

AI enhancement models. Although AI has achieved significant advancements in metasurface design, inherent limitations within AI models still persist, such as issues related to generalization, interpretability, and data efficiency[431]. As a result, there has been a growing focus on AI enhancement models in the metasurface design field, aiming to address these challenges. These models aim to overcome the fundamental shortcomings of current AI approaches, including limitations in model adaptability, transparency, and the need for large datasets. Specifically, three key approaches have emerged to tackle these issues: transfer learning, active learning, and explainable AI,

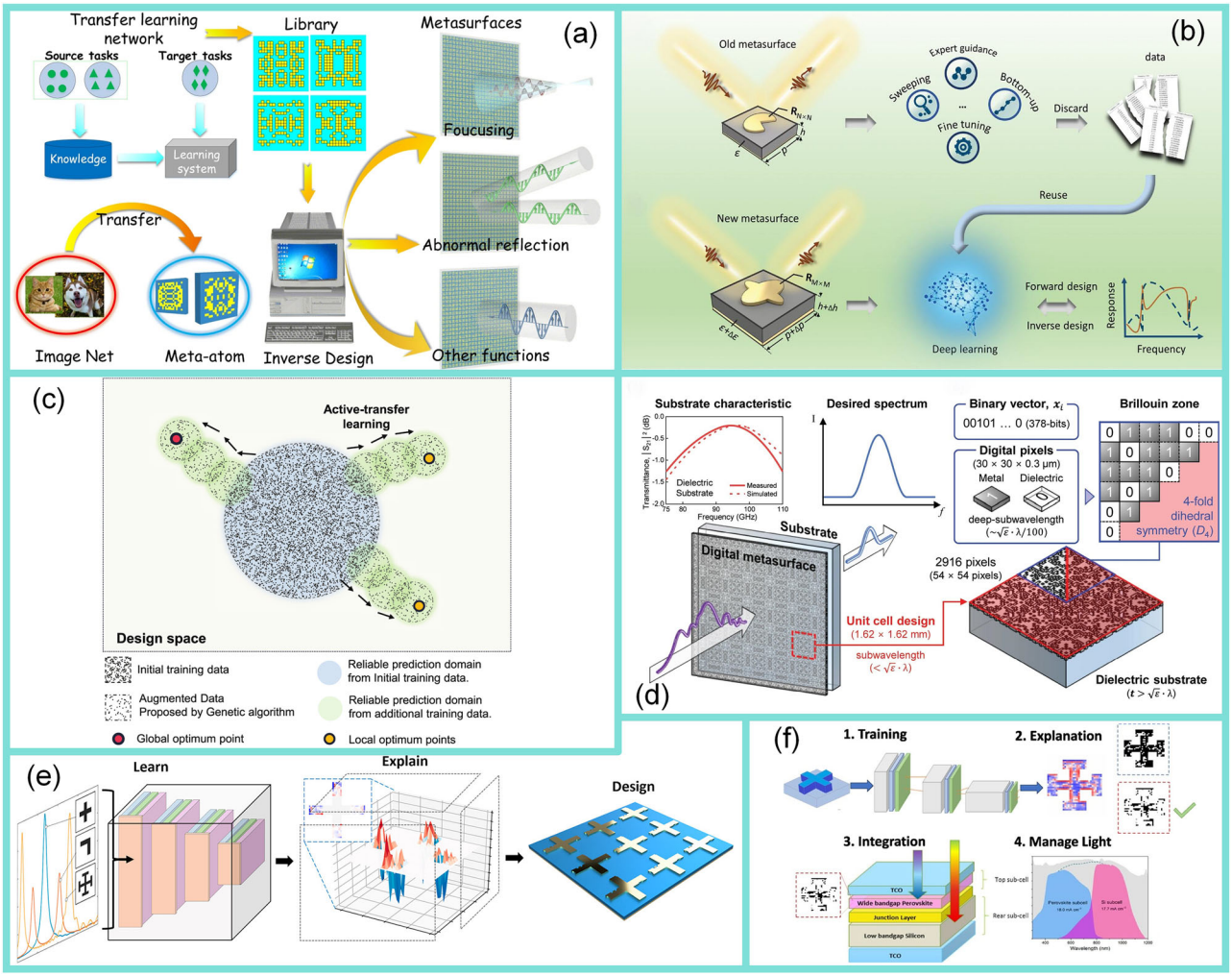

Fig. 21 | AI enhancement models for metasurface design. a Transfer learning for rapid phase-to-pattern inverse design[438]. **b** Heterogeneous transfer learning across different metasurface tasks[439]. **c** Active transfer learning with data augmentation for exploring novel materials[446]. **d** Active learning-based binary optimization for high-frequency metasurface design[445]. **e** XAI with SHAP analysis to elucidate nanophotonic structure behavior[450]. **f** CNN-driven metasurface optimization for solar cell enhancement, validated by SHAP-based interpretability[451].

each playing a crucial role in enhancing the performance, flexibility, and interpretability of AI systems in metasurface design[432–435].

Transfer learning enables AI models to leverage knowledge from related tasks, reducing the need for large datasets[436,437]. In metasurface design, where acquiring diverse training data is difficult, transfer learning allows models to adapt quickly to new design tasks, improving efficiency and reducing computational costs, which is particularly important for complex, data-scarce design spaces[366,432,433,438,439]. Recent quantitative studies have demonstrated its efficacy: PTLOR-Net reduces training data requirements by a factor of 10 while maintaining predictive accuracy across diverse optical regimes[440]; cross-domain transfer learning in terahertz biosensors achieves comparable performance with 50% fewer samples[441]; and inverse design of multifunctional metasurfaces benefits from 30 to 50% data savings while preserving design fidelity[434,442]. Recent studies have demonstrated that transfer learning not only reduces training data demands but also improves model accuracy and robustness across varied metasurface tasks. For example, Zhu et al.[438] proposed a fast design method for functional metasurfaces using transfer learning, achieving high accuracy in generating metasurface patterns from phase profiles, demonstrated in 2D focusing and abnormal reflection applications, as shown in Fig. 21a. And Zhang et al.[439] introduced heterogeneous transfer learning for efficient metasurface design, reducing error by up to 50% and enabling faster design across diverse geometries and parameterizations, as shown in Fig. 21b. In metasurface design, knowledge gleaned from simpler or related problems can be repurposed to expedite inverse design in more complex scenarios. However, ensuring compatibility between source and target domains remains a challenge, as large discrepancies in geometry or material properties can diminish the benefits of transfer.

Active learning optimizes the learning process by selecting the most informative data points for labeling, significantly reducing the data requirements[443,444]. In metasurface design, where simulations or experimental data are resource-intensive, active learning accelerates model training by focusing on the most critical data, enhancing design efficiency while minimizing data collection efforts[445–447]. For example, Kim et al.[446] introduced a deep learning framework combining active transfer learning and data augmentation to efficiently explore material design spaces, achieving near-optimal solutions with minimal data and overcoming the limitations of traditional generative models, as shown in Fig. 21c. In later work, Kim et al.[445] proposed a W-band frequency selective surface design method using active learning-based binary optimization, achieving optimal binary state configurations for distinct FSS profiles with transmittance peaks at 79.3 GHz and Q-factors of 32.7, as shown in Fig. 21d.

Explainable AI (XAI) enhances the interpretability of complex models, making their decision-making processes transparent[448,449]. In metasurface design, XAI is crucial for understanding the relationship between structural parameters and optical performance, facilitating model trust and guiding

design improvements[450–452]. For example, Yeung et al.[450] proposed the use of XAI through convolutional CNNs to predict and explain the electromagnetic response of metal-dielectric-metal metamaterials, revealing underlying physics and identifying key spatial regions influencing absorption peaks in nanophotonic structures, as shown in Fig. 21e. And Razia et al.[451] utilized XAI in conjunction with CNN-based optimization to design metasurfaces for tandem solar cells, using SHAP to interpret CNN predictions and gain insights into the design's impact on efficiency, achieving significant improvements in absorption and performance, as shown in Fig. 21f. Such interpretability not only fosters greater trust in AI-driven design pipelines but can also yield physical insights that inspire new device concepts or refine existing designs.

In conclusion, by re-using prior electromagnetic knowledge across tasks, adaptively sampling the most informative design points, and revealing the physical saliency of learned features, these strategies directly sharpen control over amplitude, phase, and polarization responses—often achieving comparable optical performance with an order-of-magnitude fewer simulations and markedly higher design interpretability. While AI enhancement models like transfer learning, active learning, and explainable AI address key issues, such as data efficiency and model generalization in metasurface design, there are still significant challenges to overcome. Issues like computational resource demands, scalability, and the diversity of training data remain under-explored in the context of metasurface design. Future research should focus on these aspects to further improve the practical application of AI.

The aforementioned AI models have demonstrated remarkable versatility across the full spectrum of metasurface design scales, from optimizing individual unit-cell structures[355,372,453,454] to configuring global metasurface layouts[363,374,455] and even enabling holistic system-level co-design[177,241,456,457]. By leveraging hierarchical architectures and differentiable surrogate models, these methods facilitate the co-optimization of local scattering physics and global wavefront objectives within a unified computational graph. In contrast, conventional multiscale strategies—such as nested topology optimization—often suffer from poor scalability, slow convergence, and design space fragmentation due to their sequential nature and exponential growth of parameters[458]. Building upon these foundational advantages, recent advances have enabled genuinely multiscale—or even cross-scale—optimization, wherein deep learning frameworks directly couple nanostructure-level physics with system-level optical targets without the need for intermediate hand-off stages. For example, Yeung et al.[455] developed a tandem-residual neural network that efficiently explores a 3-trillion-point design space of metal-insulator-metal supercells, enabling spectral goals to be mapped directly to broadband, multiplexed absorber configurations. Ha et al.[420] introduced a physics-data-driven "intelligent optimizer" that incorporates local coupling corrections within 5×5 meta-atom blocks and propagates them across centimeter-scale apertures, achieving the design and fabrication of a high-efficiency 1-cm metalens system in only a few hours. Extending to full-system control, Chi et al.[241] proposed an end-to-end framework that jointly optimizes nano-geometry and macroscopic layout to realize multi-wavelength, tri-polarization holography, achieving a sixfold improvement in structural similarity compared to sequential design strategies. They underscore how modern AI architectures have transformed electromagnetic-response control from a fragmented, iterative task into a continuous, gradient-informed pipeline—paving the way for the integrated, multiscale optimization paradigms.

From the learning paradigm perspective, AI models discussed above can be broadly categorized into supervised and unsupervised approaches. Supervised models—such as CNNs[370,371], GNNs[387,389], and Transformers[375,376]—require paired structure-response data and excel in deterministic inverse design tasks where accurate geometric-to-optical mappings are essential. In contrast, unsupervised learning methods—including VAEs[395,459], GANs[392,396], and flow-based models[399,460]—do not rely on labeled pairs but instead learn latent distributions of high-performing metasurface patterns from unannotated data. These models are particularly advantageous in design scenarios characterized by non-uniqueness, such as multi-functional metasurfaces with degenerate solutions, or when labeled datasets are scarce due to the high cost of full-wave simulations. In such contexts, unsupervised generative models enable rapid exploration of the solution space, synthesis of diverse structures, and incorporation of implicit physical priors, thereby offering enhanced generalization and data efficiency.

In summary, this section presents a comprehensive overview of the diverse deep learning models used in metasurface design, categorized into eight primary approaches: Fundamental Neural Network-Based Models, Advanced Neural Network Models, Sequence-Based Models, Graph-Based Methods, Generative Models, Reinforcement Learning Models, Physics-Informed Models, and AI Enhancement Models. Each of these methodologies offers unique strengths, addressing specific challenges such as spatial coupling, nonlinearity, dynamic optimization, and physical feasibility. However, these methods also face limitations, including computational overhead, data dependencies, and challenges in managing complex geometries and multi-physics constraints. Consequently, hybrid approaches, which combine multiple models, are often necessary to balance performance, computational efficiency, and physical consistency. Looking ahead, the future of metasurface design will likely benefit from advancements in large-scale deep learning models for more efficient multi-dimensional design space exploration. Diffraction neural networks and physics-constrained deep learning models are pushing the boundaries of simulating complex optical behaviors while integrating fundamental physical principles. Moreover, the development of multi-physics optimization strategies, where electromagnetic, mechanical, and thermal simulations converge, will enhance the robustness and applicability of metasurfaces across various domains. These innovations are expected to enable the design of adaptive, multifunctional metasurfaces that can meet the next-generation imaging systems.

Prospects of metasurface design in the future

Building on the comprehensive design framework presented in our "From Performance to Structure" approach, this section explores potential advancements and emerging trends in next-generation imaging metasurface design. While some of these ideas may align with ongoing research, they reflect the dynamic and rapidly evolving nature of metasurface engineering, offering a forward-looking perspective grounded in our framework.

End-to-end metasurface design

This subsection explores an end-to-end metasurface design approach, inspired by the holistic framework, which integrates desired optical functionalities directly into the final metasurface configuration. Leveraging AI algorithms, this methodology aims to streamline the design process, enabling comprehensive optimizations that surpass traditional stage-by-stage design.

End-to-End (E2E) metasurface design methods[177,241,457] aim to integrate the design of imaging metasurface structures with the image reconstruction process into a unified optimization framework, thereby achieving synergistic enhancements in overall system performance. Metasurface-assisted imaging systems face numerous challenges, including manufacturing limitations, material losses, and structural complexities, which result in low-quality raw imaging data. These issues prevent the full potential of the metasurface's superior electromagnetic response control from being realized, thereby degrading image clarity and accuracy. To address these challenges, computational imaging methods[461–463] have emerged, significantly enhancing image quality through advanced reconstruction algorithms. However, computational imaging methods primarily focus on optimizing the image reconstruction algorithms themselves, neglecting the intrinsic interdependencies between metasurface design and image reconstruction processes.

In metasurface-assisted imaging systems, the design of the metasurface and the image reconstruction process are deeply interconnected. The quality of the raw data acquired by the metasurface directly impacts the performance of image reconstruction algorithms, making it crucial to jointly optimize both aspects for optimal system performance. E2E design

methods, which optimize metasurface structures and image reconstruction algorithms simultaneously, have emerged as an important research direction to maximize overall system efficiency.

Several studies[457,464–467] have made notable advancements in E2E metasurface design. For example, Tseng et al.[468] devise a fully differentiable learning framework that learns the metasurface physical structure in conjunction with a neural feature-based image reconstruction algorithm, presenting a high-quality, nano-optic imager that combines the widest field-of-view for full-color metasurface operation. And Yin et al.[177] proposed an inverse design framework that directly links metasurfaces with reconstructed images using a loss function to guide metasurface updates, enabling multi-dimensional multiplexed metasurface holography. Similarly, Xia et al.[469] jointly optimized coded aperture metasurfaces and residual self-attention networks for snapshot full-Stokes imaging, significantly improving imaging quality and efficiency, though challenges remain in geometric control and manufacturing precision. To break the trade-off in imaging, Seo et al.[240] demonstrated deep-learning-driven E2E metalens imaging, overcoming the trade-off between broadband focusing efficiency and operating bandwidth to achieve high-quality, aberration-free full-color imaging. Zhu et al.[470] introduced a direct field-to-pattern monolithic design method using residual encoder-decoder convolutional neural networks, which accelerated holographic metasurface design by reducing unit coupling. In the latest research, Chi et al.[241] proposed a neural network-assisted end-to-end design framework that facilitates global, gradient-based optimization of multi-functional meta-optics layouts for full light field control, harnessing the dispersive full-parameter Jones matrix, orthogonal tri-polarization multi-wavelength-depth holography.

Despite these advancements, current E2E design methods face significant challenges, such as the need for large, high-quality training datasets, limited generalization across diverse design tasks, and high computational costs associated with comprehensive AI models. Moreover, effectively integrating the objective functions of metasurface design and image reconstruction remains a critical challenge to ensure mutual enhancement during optimization. Future research should focus on developing more efficient and robust E2E optimization frameworks. Key directions include enhancing data diversity and quality using techniques like GANs to improve model generalization; optimizing network architectures, such as integrating GNNs, to better capture the complex relationships between design parameters and image outcomes; reducing computational costs through model compression and acceleration; improving model interpretability by developing transparent AI models that clarify the connections between metasurface design and image reconstruction; and integrating multi-objective optimization strategies to consider both design parameters and image quality metrics. These advancements are expected to significantly improve the performance and efficiency of next-generation metasurface-assisted imaging systems, enabling higher quality and more efficient optical imaging.

Multi-objective metasurface design

Multi-objective metasurface design[471–473] aims to optimize multiple electromagnetic responses—such as amplitude, phase, polarization, and spectral characteristics—within a single metasurface structure[474]. While metasurfaces inherently offer extensive tunability at the subwavelength scale, fully harnessing this potential necessitates a comprehensive approach that simultaneously addresses the interdependencies among different performance metrics. However, this complexity remains a significant challenge, as optimizing these coupled properties requires more than simply addressing them in isolation.

Although previous studies have demonstrated metasurfaces that address multiple functionalities, many existing designs still focus on only a limited subset of electromagnetic dimensions[72,138,475–477]. The majority of current approaches employ stepwise or segmented optimization strategies, which often fail to provide a unified framework for truly multi-objective, multi-dimensional electromagnetic control. As a result, while some progress has been made in optimizing certain aspects, the joint optimization of amplitude, phase, polarization, and spectral responses insufficiently explored, limiting the ability of metasurfaces to meet the demands of complex, real-world applications.

Achieving multi-objective metasurface design is challenging due to the complex coupling between different electromagnetic objectives. For example, optimizing amplitude for transmission efficiency often compromises phase accuracy, while expanding operational bandwidth may reduce polarization selectivity. Traditional methods, such as linear weighting or sequential design, fail to capture these interdependencies, resulting in sub-optimal solutions. Hence, a more systematic optimization approach is needed, one that treats amplitude, phase, polarization, and spectral response as interconnected objectives rather than isolated targets. Future research should focus on decoupling and analyzing the relationships between these parameters from a physical principles perspective. Understanding the underlying coupling mechanisms between multiple electromagnetic objectives is essential for effective optimization. Additionally, from the encoding and decoding perspective, new methods are needed to handle these high-dimensional, multi-dimensional electromagnetic responses simultaneously. These responses, represented in different dimensions—pose a challenge for integration into a unified design framework. Moreover, in terms of data collection, there is a need for the generation of richer, more diverse multi-dimensional datasets that capture the full complexity of these interactions. This data will serve as a foundation for training models that can handle the intricacies of multi-objective optimization. Algorithmically, leveraging advanced multi-objective evolutionary algorithms, swarm intelligence, and reinforcement learning, will be key to navigating high-dimensional design spaces and efficiently identifying Pareto-optimal solutions. These algorithms can enable designers to explore the trade-offs between competing performance criteria and select the best solutions according to specific application requirements. Additionally, surrogate-assisted AI methods can further accelerate the optimization process, making it feasible to explore large design spaces with reduced computational overhead. By overcoming these challenges, multi-objective metasurface design can unlock the full potential of metasurfaces for sophisticated light manipulation, driving advances in metasurface design for next-generation imaging.

Manufacturing-aware metasurface design

The pursuit of highly functional metasurfaces has driven the development of high-degree-of-freedom design methodologies, such as free-form metasurfaces[288,392,478–480], which enable precise electromagnetic wave manipulation across various parameters. However, the practical realization and scalability of these advanced designs are hindered by significant fabrication challenges, including stringent precision requirements, process complexity, and high production costs. These manufacturing constraints limit the widespread application of metasurfaces.

In response to these challenges, recent studies have incorporated fabrication considerations directly into the metasurface design process[454,481–484]. For instance, Zhang et al.[454] introduced a Bayesian neural network approach to quantify uncertainties arising from material properties and geometric precision during fabrication, thereby enhancing the robustness of the design by simulating manufacturing-induced errors. Similarly, Ueno et al.[481] proposed a fabrication-friendly method for dual-band optical collimators, leveraging CNNs and a meta-atom selector to address fabrication limitations, such as minimum feature sizes, ensuring that metasurfaces remain manufacturable using current nanofabrication technologies. Huang et al.[482] further advanced this approach by generating random-shaped meta-atoms with smooth boundaries, resolving issues like sharp edges and small feature sizes that often complicate micro/nano-fabrication processes. Additionally, Pitilakis et al.[483] co-designed reconfigurable metasurfaces with integrated circuit chips, enabling dynamic wavefront manipulation while adhering to manufacturing constraints. Moreover, Zhang et al.[484] demonstrated broadband holograms that maintain high tolerance to fabrication errors, ensuring consistent performance across a wide wavelength range even in the presence of geometric deviations.

Looking ahead, future research should prioritize the development of comprehensive optimization frameworks that integrate both fabrication constraints and electromagnetic performance objectives. In constraint characterization, advancements must focus on differentiable manufacturing models that encode multi-physics limitations—such as stochastic edge roughness in lithography or elastic deformation in nanoimprinting—into topology-aware design spaces, enabling AI to natively "understand" fabrication boundaries. Algorithmically, hybrid physics-data frameworks should emerge, combining reinforcement learning-driven topology generators with adversarial networks to eliminate non-manufacturable features (e.g., overhangs, acute angles) while embedding historical process deviation data as penalty functions through transfer learning. Additionally, the synergy between advanced manufacturing technologies—such as nanoimprint lithography, high-precision photolithography, and 3D printing—and innovative design methodologies is essential for achieving higher fabrication precision and reducing production costs. Last but not least, we should also construct multimodal fabrication-performance databases (e.g., e-beam lithography dose-topography mappings, 3D-printed interlayer stress-optical response correlations) and synthetic data engines to overcome small-sample learning limitations. In summary, manufacturing-aware metasurface design plays a pivotal role in bridging the gap between theoretical innovations and their practical implementations. By embedding fabrication constraints directly into the design process and adopting robust optimization strategies, future metasurfaces can achieve improved performance, enhanced reliability, and greater commercial viability, paving the way for significant advancements in next-generation imaging.

Fast solver-aided metasurface design

Simulation plays a critical role in the design and optimization of metasurfaces by enabling the prediction of electromagnetic responses and facilitating the iterative refinement of designs. Traditional methods like Finite-Difference Time-Domain (FDTD), Finite Element Method (FEM), and Rigorous Coupled-Wave Analysis (RCWA) are commonly used, but these methods, while accurate, are computationally expensive and time-consuming, especially for complex structures. Given the high degree of freedom and inherent complexity of metasurface structures, the ability to perform fast and accurate simulations is essential. Rapid simulation tools not only accelerate the design process but also allow for the exploration of more complex, high-performance metasurface configurations.

To achieve fast simulations in metasurface design, two primary strategies have emerged. The first strategy focuses on developing physics- and mathematics-based solvers to enhance the computational efficiency of solving Maxwell's equations. Advanced numerical techniques[485–488], such as the fast multipole method (FMM)[489,490] and the method of moments (MoM)[491,492], have been optimized to reduce computational complexity while maintaining high accuracy. FMM accelerates the computation of long-range interactions by employing multipole expansions, significantly reducing the computational burden. MoM discretizes the structure into a set of integral equations, efficiently handling complex geometries. These methods enable the simulation of large-scale, high-frequency metasurface structures within feasible timeframes, supporting more comprehensive design explorations and enabling the realization of complex electromagnetic functionalities. However, challenges such as maintaining numerical precision in highly intricate designs still remain, and future research will likely focus on accelerating simulations by leveraging physical principles and approximations while ensuring the preservation of accuracy.

The second strategy leverages AI and ML models to predict electromagnetic responses. AI-driven forward prediction models, such as CNNs and GNNs, offer significant speed advantages by approximating solutions once trained[354,369,379,421,493]. These models are inherently differentiable, which benefits gradient-based optimization techniques, thus enabling more efficient navigation of the design space. However, a major challenge lies in the accuracy of these AI models, particularly in multi-dimensional electromagnetic scenarios. Future research should focus on improving the precision of these AI models and developing strategies to mitigate prediction errors. One promising approach is uncertainty quantification, which could enhance the reliability and robustness of AI-driven models. Furthermore, hybrid models that combine AI predictions with traditional solvers could bridge the gap between speed and accuracy, making AI-based methods more applicable to practical metasurface design.

In conclusion, integrating fast solvers—whether through advanced numerical methods or AI-driven models—is critical for efficient metasurface design. These advancements not only reduce the time and computational resources required for simulations but also enable the exploration of more sophisticated and high-performance metasurface designs. Continued progress in these areas will pave the way for the development of innovative metasurface devices, unlocking new possibilities in applications of next-generation imaging.

Large-area metasurface design

In imaging applications, high-quality imaging systems typically require large optical elements to capture as much optical information as possible, thereby achieving a wide field of view and high resolution. Large-area metasurfaces, through the uniform design and precise control of subwavelength structures across the entire imaging plane, enable continuous and accurate wavefront shaping over the entire device[478,485,494,495]. Their ability to manipulate electromagnetic waves over extensive surfaces makes them ideal for applications such as high-resolution imaging, wide-field holography, and large-scale beam shaping. Recent advancements in fabrication technologies have significantly improved the scalability and uniformity of large-area metasurfaces, which is crucial for their integration into manufacturing sectors that demand high precision and consistency.

Despite these advancements, designing large-area metasurfaces remains a significant challenge[496–498]. On one hand, the design process must integrate detailed subwavelength features with the overall macroscopic optical performance, leading to an exponentially larger parameter space compared to small-area metasurfaces. This demands high-fidelity physical models that accurately simulate the interactions between individual meta-atoms and their collective effect on the wavefront. Additionally, the nonlinear coupling between local and global optical properties often results in complex optimization landscapes with numerous local minima, making it exceptionally difficult for conventional numerical methods to identify the global optimum. From a fabrication perspective, large-area implementation is also constrained by scalability. Electron-beam lithography, though precise, is costly and time-consuming. Alternatives such as nanoimprint and deep ultraviolet lithography offer higher throughput and lower cost, but still face issues related to defect tolerance and uniformity across wafer-scale areas[485,499,500].

To overcome these challenges, future advancements in large-area metasurface design for imaging are expected to center on the integration of intelligent optimization and multi-scale modeling techniques. The utilization of machine learning, deep learning, and topology optimization methods promises to automate and accelerate the global search for optimal design parameters, ensuring that both local structural features and overall system performance are harmoniously balanced. In parallel, incorporating fabrication constraints—such as pattern pitch limits, stitching tolerances, and aspect ratio requirements of scalable techniques like nanoimprint or UV-lithography—into the design process will be essential to ensure manufacturability and yield. Furthermore, the development of advanced multi-physics simulation frameworks capable of concurrently addressing electromagnetic interactions and structural nuances will help reduce computational complexity. These innovations are poised to overcome current design bottlenecks, ultimately leading to more robust, high-performance metasurface-based imaging systems with superior wavefront control and minimized aberrations.

Metasurface array design

Array-based metasurfaces have demonstrated remarkable potential in applications such as wide-field imaging, multi-channel sensing, and light field imaging. In contrast to single metasurfaces, arrayed architectures can

effectively expand the optical aperture on a macroscopic scale, enabling parallel functionalities. This capability provides a more favorable balance among resolution, field of view, and system flexibility. Several studies have highlighted these advantages: a 9 × 9 microlens array significantly improves scanning efficiency in fluorescence microscopy[501], directional metalens arrays enable wide-angle, three-dimensional LiDAR by eliminating the need for mechanical scanning[502], and monolithic integration of microlenses with optical detectors enhances near-infrared detection sensitivity[503]. In more complex applications—ranging from large-area floating displays[504] and near-eye three-dimensional imaging[201] to single-shot full-Stokes polarization detection and multiphoton quantum sources[132,505]—array-based metasurfaces similarly offer higher-dimensional degrees of freedom and increased functional integration.

However, as the size of these arrays increases, the design and optimization process becomes significantly more complex. Current metasurface array designs predominantly assume homogeneous elements to simplify modeling through periodic boundary conditions. However, as imaging applications advance, there is a growing need for heterogeneous arrays—where each metasurface element possesses a unique design to capture diverse optical information such as angular distributions. This heterogeneity introduces several challenges. Firstly, individual elements must be optimized to deliver high-precision optical responses over specific wavelengths and incident angles. At the same time, their non-identical responses lead to complex inter-element coupling, making it difficult to predict the overall system performance. Secondly, the design process must address an exponentially larger parameter space due to the independent optimization of each element, resulting in a highly nonlinear, multi-objective optimization problem that is prone to local minima. These challenges necessitate the development of new computational models and simulation tools that can handle multi-scale and multi-physics phenomena.

Looking ahead, future research on array-based metasurfaces is anticipated to concentrate on several key avenues. First, addressing the inherent complexity of large, heterogeneous arrays will necessitate high-dimensional cooperative optimization and accelerated algorithms. Such techniques are vital for effectively navigating the vast, nonlinear design space. Second, the integration of concurrent multifunctionality with adaptive control is imperative. Incorporating adaptive materials—such as phase-change substances or liquid crystals—can confer dynamic tuning capabilities, enabling individual elements to modulate their responses in real time and support functionalities like polarization or spectral imaging within a single metasurface plane. Finally, an application-driven, differentiated design paradigm will allow sub-arrays to specialize in discrete tasks (e.g., ultrawide-field microscopy, single-exposure polarization imaging, or quantum path encoding), thereby enhancing overall system performance. Collectively, these strategies are poised to fully exploit the potential of metasurface arrays in next-generation, multifunctional imaging systems.

Cascaded metasurface design

Cascaded metasurface design involves serially stacking multiple metasurface layers, with each layer engineered to perform a specific optical function[36,172,506–508]. This layered approach enables the decomposition of complex optical tasks—such as initial wavefront correction, dispersion compensation, and localized focusing—across different stages, thereby increasing the overall system's degrees of freedom and achieving broadband as well as multi-angular responses. By distributing the optical manipulation across several cascaded layers, the approach not only enhances optical efficiency but also alleviates the stringent fabrication tolerances required for single-layer designs. This makes cascaded metasurfaces particularly promising for advanced imaging, holographic displays, and optical sensing applications where compactness and multifunctionality are paramount.

However, the introduction of vertical stacking introduces complexities in the electromagnetic coupling between layers[199,509]. Each layer independently responds to phase and amplitude variations, and the superposition of these responses cannot be treated as a simple linear addition. Cross-layer interactions, therefore, can either reinforce or offset each other, complicating the overall system performance. Solely optimizing each layer independently risks ignoring these interlayer coupling effects, which often leads to suboptimal performance at the system level. Moreover, each layer's design parameters—such as the geometry, material properties, and thickness of its constituent meta-atoms—affect its individual optical response, while also interacting with adjacent layers through interference and diffraction phenomena. These interdependencies introduce highly nonlinear, multi-objective optimization problems that are not readily addressed by traditional single-layer design methods. Finally, practical issues such as interlayer alignment precision and material losses add additional layers of complexity, making it challenging to bridge the gap between theoretical models and experimental realizations.

Future research should specifically address the unique challenges posed by the layered structure of cascaded metasurfaces. One promising direction is the development of advanced simulation and analytical frameworks that accurately capture inter-layer interactions. This could involve extending rigorous methods—such as coupled-wave analysis, transfer matrix approaches, or finite-difference time-domain simulations—to fully account for the cumulative phase shifts and interference effects inherent in multi-layer systems. Additionally, novel design strategies are needed to incorporate inter-layer compensation techniques. For instance, integrating engineered spacer layers with tailored refractive properties or embedding calibration elements between metasurface layers could mitigate misalignment and phase accumulation errors. Furthermore, the incorporation of real-time feedback systems—such as in-situ optical monitoring combined with active alignment mechanisms (e.g., MEMS-based adjustments)—can provide dynamic compensation for fabrication variances and environmental fluctuations. These integrated, layer-specific innovations are expected to pave the way for next-generation cascaded metasurface designs with significantly enhanced performance and robustness in complex optical systems.

Dynamic tunable metasurface design

Dynamic tunable metasurface design is pivotal in imaging systems, particularly in scenarios where environmental conditions or imaging requirements vary over time[510–512]. By enabling real-time modulation of optical responses—such as adaptive wavefront correction, focal length adjustment, and variable field-of-view control—these systems can compensate for aberrations and optimize image quality under diverse conditions. This adaptability is crucial for advanced imaging applications, where high resolution and contrast must be maintained despite dynamic changes in illumination, scene depth, or object motion[510,513,514].

However, realizing tunability in metasurfaces requires more than simply embedding a drive mechanism[515–517]. From a design perspective, selecting suitable materials and control methods involves balancing various parameters, such as energy consumption, switching speed, and durability, while maintaining high transmission or reflection efficiencies. Moreover, dynamic tunability introduces significant challenges primarily due to the need for comprehensive multi-state modeling and robust multi-objective optimization. Designers must construct accurate, time-dependent optical models that capture the behavior of the metasurface across various dynamic states, accounting for nonlinear coupling effects during state transitions. Each state may target distinct optical functions—such as aberration correction or focal tuning—which must be balanced and integrated into a unified design. This requirement leads to a high-dimensional optimization problem, where the design space expands rapidly with additional degrees of freedom and conventional static design methods fall short. In addition to design complexity, manufacturing poses a practical bottleneck for tunable metasurfaces[19,518,519]. Current implementations often rely on electron-beam lithography, which is cost-prohibitive and lacks scalability. Emerging alternatives such as nanoimprint lithography offer improved throughput but still face challenges in overlay accuracy and material integration, particularly under dynamic actuation.

Future research should aim to develop integrated design frameworks that cohesively merge multi-state optical modeling with real-time control strategies. One promising direction is the creation of robust, multi-objective

optimization algorithms that incorporate sensitivity analysis and data-driven models to efficiently identify and fine-tune key design parameters across all dynamic states. Moreover, the development of simulation tools that integrate time-domain analysis with optical performance evaluation will be critical for predicting system responses during continuous tuning. Ultimately, incorporating adaptive feedback mechanisms to dynamically coordinate the design, simulation, and control processes is expected to enhance both the precision and responsiveness of dynamic tunable metasurface systems in complex imaging environments, while future manufacturing research should focus on scalable, high-yield fabrication strategies compatible with dynamic integration.

Hybrid optics and metasurface design

Metasurfaces have revealed new capabilities for fine-grained wavefront manipulation that traditional components alone cannot achieve[520]. However, the short-term limitations of metasurfaces—such as challenges with wide-band efficiency and large-area uniformity—mean that they are not yet suited to completely replace conventional optics. As a result, hybrid systems that combine macroscopic optical elements with metasurface layers provide a promising path forward, blending the proven strengths of classical devices with the subwavelength enhancements offered by metasurfaces[41,43]. The synergistic combination of these two approaches enables dynamic wavefront correction, multi-modal imaging, and enhanced contrast, ultimately elevating overall imaging performance and adaptability in challenging environments.

Nevertheless, simply adding a metasurface to a traditional lens or reflector does not automatically guarantee optimal system performance. At the system level, the coupling between the macroscopic geometry of the optical device and the micro-/nano-scale structures of the metasurface can introduce unexpected phase shifts, diffraction effects, or bandwidth distortions. If the metasurface is treated as a mere post-correction layer, without considering the interdependencies between the conventional component and the metasurface, issues, such as undesirable distortions or efficiency losses may arise. Furthermore, the overall imaging performance hinges on the simultaneous optimization of local metasurface functionalities and global optical behavior. This results in a high-dimensional, multi-objective, and nonlinear design problem that exceeds the capabilities of conventional optimization techniques.

Future research should focus on developing unified design frameworks that bridge the gap between geometric optics and full-wave electromagnetic analysis. A promising approach involves the creation of hybrid simulation tools that combine macroscopic ray-tracing with localized full-wave simulations, enabling precise prediction of system-level optical performance. Additionally, advanced multi-objective optimization algorithms—potentially augmented by data-driven methods—are essential for systematically balancing the conflicting requirements of resolution, aberration correction, and contrast. Moreover, exploring hierarchical and modular design strategies that decouple global imaging requirements from local metasurface functionalities could facilitate scalable and efficient system design. These design-centric innovations will form the foundation for next-generation, high-performance imaging systems that fully exploit the synergistic benefits of hybrid optics and metasurfaces.

Conclusion

This review has explored the remarkable potential of metasurfaces to transform next-generation optical imaging systems by providing subwavelength-scale electromagnetic control. Through the "From Performance to Structure" design paradigm, we have shown how essential 9 imaging specifications—such as achromatic imaging, expanded field of view imaging, depth of field extension imaging, resolution enhancement imaging, multidimensional data capture imaging, feature enhancement imaging, holographic field reconstruction imaging, functional intergration imaging and compact integration—can be translated into precise 6 electromagnetic requirements, including phase, amplitude, polarization, wavefront, orbital angular momentum, and spectral control. By mapping these performance requirements onto specialized metasurface microstructures, we highlighted how metasurfaces can enable unprecedented advancements in optical imaging while maintaining compactness and versatility.

A central theme of this review has been the integration of AI to streamline the design process. AI has played a crucial role in navigating vast design spaces and optimizing metasurface configurations with minimal trial-and-error. We have categorized three primary design approaches—physically-driven, meta-heuristic, and AI-driven—and analyzed six primary encoding and decoding strategies and eight common AI techniques. The AI-driven methodologies enable faster design cycles and more efficient solutions, accelerating the transition from theoretical models to practical, high-performance metasurface designs. This integration is especially critical in addressing the challenges of nonlinearity and complexity inherent in high-dimensional metasurface design.

Looking to the future, we identified nine key research directions—end-to-end metasurface design, multi-objective metasurface design, manufacturing-aware metasurface design, fast solver-aided metasurface design, large-area metasurface design, metasurface array design, cascaded metasurface design, dynamic tunable metasurface design, and hybrid optics and metasurface design. These emerging directions offer exciting prospects for scaling and enhancing metasurface performance across a wide range of imaging domains. The continued development of AI-driven design frameworks and advanced solvers will be pivotal in overcoming current limitations, including fabrication challenges, narrow operational bandwidths, and integration with conventional optical systems. In conclusion, the "From Performance to Structure" design paradigm, powered by AI, provides a robust framework for optimizing metasurface design and unlocking the full potential of these technologies in imaging applications. As AI continues to evolve, it will play an increasingly critical role in shaping the next generation of optical imaging systems, enabling highly functional, scalable, and efficient metasurface-based imaging devices that promise to revolutionize diverse fields.

Data availability

No datasets were generated or analyzed during the current study. A well-classified and continuously updated paper list related to this work can be found at https://github.com/Yunhui1998/metasurface-imaging-review.

Received: 23 March 2025; Accepted: 16 June 2025;
Published online: 21 October 2025

References

1. Peng, Y. et al. Metalens in improving imaging quality: advancements, challenges, and prospects for future display. *Laser Photonics Rev* **18**, 2300731 (2024).
2. Zou, X. et al. Advanced optical imaging based on metasurfaces. *Adv. Opt. Mater.* **12**, 2203149 (2024).
3. Mait, J. N., Euliss, G. W. & Athale, R. A. Computational imaging. *Adv. Opt. Photonics* **10**, 409–483 (2018).
4. Barbastathis, G., Ozcan, A. & Situ, G. On the use of deep learning for computational imaging. *Optica* **6**, 921–943 (2019).
5. Altmann, Y. et al. Quantum-inspired computational imaging. *Science* **361**, eaat2298 (2018).
6. Kuznetsov, A. I. et al. Roadmap for optical metasurfaces. *ACS Photonics* **11**, 816–865 (2024).
7. Xiong, B. et al. Breaking the limitation of polarization multiplexing in optical metasurfaces with engineered noise. *Science* **379**, 294–299 (2023).
8. Zhou, H. et al. Optical computing metasurfaces: applications and advances. *Nanophotonics* **13**, 419–441 (2024).
9. Shi, Y. et al. Ultra-thin, zoom capable, flexible metalenses with high focusing efficiency and large numerical aperture. *Nanophotonics* **13**, 1339–1349 (2024).
10. Reshef, O. et al. An optic to replace space and its application towards ultra-thin imaging systems. *Nat. Commun.* **12**, 3512 (2021).

11. Li, R. et al. Design of ultra-thin underwater acoustic metasurface for broadband low-frequency diffuse reflection by deep neural networks. *Sci. Rep.* **12**, 12037 (2022).
12. Cotrufo, M. et al. Reconfigurable image processing metasurfaces with phase-change materials. *Nat. Commun.* **15**, 4483 (2024).
13. Li, C. et al. Phase change materials-based bilayer metasurfaces for near-infrared photonic routing. *Adv. Funct. Mater.* **34**, 2310626 (2024).
14. Conrads, L. et al. Infrared beam-shaping on demand via tailored geometric phase metasurfaces employing the plasmonic phase-change material in3sbte2. *Nat. Commun.* **16**, 3698 (2025).
15. Popescu, C. C. et al. Electrically reconfigurable phase-change transmissive metasurface. *Adv. Mater.* **36**, 2400627 (2024).
16. Choi, S., Zuo, J., Das, N., Yao, Y. & Wang, C. Scalable nanoimprint manufacturing of functional multilayer metasurface devices. *Adv. Funct. Mater.* **34**, 2404852 (2024).
17. Gour, J. et al. Wafer-scale nanofabrication of sub-5 nm gaps in plasmonic metasurfaces. *Nanophotonics* **13**, 4191–4202 (2024).
18. Xu, K. et al. All-glass nanohole metalens by non-diffracting laser lithography. *Laser Photon. Rev.* **19**, 2402006 (2025).
19. Yang, W., Zhou, J., Tsai, D. P. & Xiao, S. Advanced manufacturing of dielectric meta-devices. *Photon. Insights* **3**, R04–R04 (2024).
20. Zhang, L., Mei, S., Huang, K. & Qiu, C.-W. Advances in full control of electromagnetic waves with metasurfaces. *Adv. Opt. Mater.* **4**, 818–833 (2016).
21. Bao, Y., Ni, J. & Qiu, C.-W. A minimalist single-layer metasurface for arbitrary and full control of vector vortex beams. *Adv. Mater.* **32**, 1905659 (2020).
22. Shaltout, A. M., Shalaev, V. M. & Brongersma, M. L. Spatiotemporal light control with active metasurfaces. *Science* **364**, eaat3100 (2019).
23. Yang, Y. et al. The road to commercializing optical metasurfaces: current challenges and future directions. *ACS Nano* **19**, 3008–3018 (2025).
24. Ueno, A., Hu, J. & An, S. Ai for optical metasurface. *npj Nanophotonics* **1**, 36 (2024).
25. Chen, M. K., Liu, X., Sun, Y. & Tsai, D. P. Artificial intelligence in meta-optics. *Chem. Rev.* **122**, 15356–15413 (2022).
26. Fu, Y. et al. Unleashing the potential: AI empowered advanced metasurface research. *Nanophotonics* **13**, 1239–1278 (2024).
27. Tezsezen, E., Yigci, D., Ahmadpour, A. & Tasoglu, S. AI-based metamaterial design. *ACS Appl. Mater. Interfaces.* **16**, 29547–29569 (2024).
28. Ma, W. et al. Deep learning for the design of photonic structures. *Nat. Photonics* **15**, 77–90 (2021).
29. Jiang, J., Chen, M. & Fan, J. A. Deep neural networks for the evaluation and design of photonic devices. *Nat. Rev. Mater.* **6**, 679–700 (2021).
30. Zang, W. et al. Chromatic dispersion manipulation based on metalenses. *Adv. Mater.* **32**, 1904935 (2020).
31. Aieta, F. et al. Aberration-free ultrathin flat lenses and axicons at telecom wavelengths based on plasmonic metasurfaces. *Nano Lett* **12**, 4932–4936 (2012).
32. Chen, W. T. et al. A broadband achromatic metalens for focusing and imaging in the visible. *Nat. Nanotechnol.* **13**, 220–226 (2018).
33. Wang, S. et al. Broadband achromatic optical metasurface devices. *Nat. Commun.* **8**, 187 (2017).
34. Khorasaninejad, M. et al. Achromatic metalens over 60 nm bandwidth in the visible and metalens with reverse chromatic dispersion. *Nano Lett* **17**, 1819–1824 (2017).
35. Avayu, O., Almeida, E., Prior, Y. & Ellenbogen, T. Composite functional metasurfaces for multispectral achromatic optics. *Nat. Commun.* **8**, 14992 (2017).
36. McClung, A., Mansouree, M. & Arbabi, A. At-will chromatic dispersion by prescribing light trajectories with cascaded metasurfaces. *Light Sci. Appl.* **9**, 93 (2020).
37. Ndao, A. et al. Octave bandwidth photonic fishnet-achromatic-metalens. *Nat. Commun.* **11**, 3205 (2020).
38. Chen, W. T., Zhu, A. Y., Sisler, J., Bharwani, Z. & Capasso, F. A broadband achromatic polarization-insensitive metalens consisting of anisotropic nanostructures. *Nat. Commun.* **10**, 355 (2019).
39. Heiden, J. T. & Jang, M. S. Design framework for polarization-insensitive multifunctional achromatic metalenses. *Nanophotonics* **11**, 583–591 (2022).
40. Wang, Y. et al. High-efficiency broadband achromatic metalens for near-IR biological imaging window. *Nat. Commun.* **12**, 5560 (2021).
41. Liu, M. et al. Achromatic and coma-corrected hybrid meta-optics for high-performance thermal imaging. *Nano Lett* **24**, 7609–7615 (2024).
42. Bayati, E. et al. Inverse designed extended depth of focus meta-optics for broadband imaging in the visible. *Nanophotonics* **11**, 2531–2540 (2022).
43. Huang, L., Whitehead, J., Colburn, S. & Majumdar, A. Design and analysis of extended depth of focus metalenses for achromatic computational imaging. *Photonics Res* **8**, 1613–1623 (2020).
44. Ou, K. et al. Broadband achromatic metalens in mid-wavelength infrared. *Laser Photon. Rev.* **15**, 2100020 (2021).
45. Hsu, W.-L. et al. High-resolution metalens imaging with sequential artificial intelligence models. *Nano Lett* **23**, 11614–11620 (2023).
46. Dong, Y. et al. Achromatic single metalens imaging via deep neural network. *ACS Photonics* **11**, 1645–1656 (2024).
47. Wang, F., Zhao, S., Wen, Y., Sun, J. & Zhou, J. High efficiency visible achromatic metalens design via deep learning. *Adv. Opt. Mater.* **11**, 2300394 (2023).
48. Wang, F. et al. Visible achromatic metalens design based on artificial neural network. *Adv. Opt. Mater.* **10**, 2101842 (2022).
49. Khorasaninejad, M. et al. Achromatic metasurface lens at telecommunication wavelengths. *Nano Lett* **15**, 5358–5362 (2015).
50. Chen, J., Huang, S.-X., Chan, K. F., Wu, G.-B. & Chan, C. H. 3d-printed aberration-free terahertz metalens for ultra-broadband achromatic super-resolution wide-angle imaging with high numerical aperture. *Nat. Commun.* **16**, 363 (2025).
51. You, X., Ako, R. T., Sriram, S. & Withayachumnankul, W. 3d terahertz confocal imaging with chromatic metasurface. *Laser Photonics Rev.* **19**, 2401011 (2025).
52. Xiao, X. et al. Large-scale achromatic flat lens by light frequency-domain coherence optimization. *Light Sci. Appl.* **11**, 323 (2022).
53. Presutti, F. & Monticone, F. Focusing on bandwidth: achromatic metalens limits. *Optica* **7**, 624–631 (2020).
54. Zhang, C. et al. Low-loss metasurface optics down to the deep ultraviolet region. *Light Sci. Appl.* **9**, 55 (2020).
55. He, H. et al. Meta-attention network based spectral reconstruction with snapshot near-infrared metasurface. *Adv. Mater.* **36**, 2313357 (2024).
56. Akselrod, G. M. et al. Large-area metasurface perfect absorbers from visible to near-infrared. *Adv. Mater.* **27**, 8028–8034 (2015).
57. Shalaginov, M. Y. et al. Single-element diffraction-limited fisheye metalens. *Nano Lett* **20**, 7429–7437 (2020).
58. Hao, C. et al. Single-layer aberration-compensated flat lens for robust wide-angle imaging. *Laser Photonics Rev* **14**, 2000017 (2020).
59. Martins, A. et al. On metalenses with arbitrarily wide field of view. *Acs Photonics* **7**, 2073–2079 (2020).
60. Lassalle, E. et al. Imaging properties of large field-of-view quadratic metalenses and their applications to fingerprint detection. *Acs Photonics* **8**, 1457–1468 (2021).
61. Wang, Y. et al. Compact meta-optics infrared camera based on a polarization-insensitive metalens with a large field of view. *Opt. Lett.* **48**, 4709–4712 (2023).
62. Wirth-Singh, A. et al. Wide field of view large aperture meta-doublet eyepiece. *Light Sci. Appl.* **14**, 17 (2025).

63. Arbabi, A. et al. Miniature optical planar camera based on a wide-angle metasurface doublet corrected for monochromatic aberrations. *Nat. Commun.* **7**, 13682 (2016).
64. Groever, B., Chen, W. T. & Capasso, F. Meta-lens doublet in the visible region. *Nano Lett* **17**, 4902–4907 (2017).
65. Xu, B. et al. Metalens-integrated compact imaging devices for wide-field microscopy. *Adv. Photonics* **2**, 066004–066004 (2020).
66. Chen, J. et al. Planar wide-angle-imaging camera enabled by metalens array. *Optica* **9**, 431–437 (2022).
67. Liu, J., Chu, J., Zhang, R., Liu, R. & Fu, J. Wide field of view and full stokes polarization imaging using metasurfaces inspired by the stomatopod eye. *Nanophotonics* **12**, 1137–1146 (2023).
68. Engelberg, J. et al. Near-IR wide-field-of-view huygens metalens for outdoor imaging applications. *Nanophotonics* **9**, 361–370 (2020).
69. Fan, C.-Y., Lin, C.-P. & Su, G.-D. J. Ultrawide-angle and high-efficiency metalens in hexagonal arrangement. *Sci. Rep.* **10**, 15677 (2020).
70. Liu, Y. et al. Ultra-wide fov meta-camera with transformer-neural-network color imaging methodology. *Adv. Photonics* **6**, 056001–056001 (2024).
71. Li, S. & Hsu, C. W. Thickness bound for nonlocal wide-field-of-view metalenses. *Light Sci. Appl.* **11**, 338 (2022).
72. Ansari, M. A. et al. Multifaceted control of focal points along an arbitrary 3d curved trajectory. *Light Sci. Appl.* **13**, 224 (2024).
73. Zhao, J. et al. Rapid cellular-resolution skin imaging with optical coherence tomography using all-glass multifocal metasurfaces. *ACS nano* **17**, 3442–3451 (2023).
74. Fan, Q. et al. Trilobite-inspired neural nanophotonic light-field camera with extreme depth-of-field. *Nat. Commun.* **13**, 2130 (2022).
75. Zhao, F. et al. Metalens-assisted system for underwater imaging. *Laser Photonics Rev* **15**, 2100097 (2021).
76. Tan, S., Yang, F., Boominathan, V., Veeraraghavan, A. & Naik, G. V. 3d imaging using extreme dispersion in optical metasurfaces. *ACS Photonics* **8**, 1421–1429 (2021).
77. Zheng, R. et al. Active multiband varifocal metalenses based on orbital angular momentum division multiplexing. *Nat. Commun.* **13**, 4292 (2022).
78. Zhang, Z., Yang, Q., Gong, M., Chen, M. & Long, Z. Metasurface lens with angular modulation for extended depth of focus imaging. *Opt. Lett.* **45**, 611–614 (2020).
79. Yin, B. & Wang, S. Research and design of a metasurface with an extended depth of focus in the near field. *Appl. Opt.* **62**, 7621–7627 (2023).
80. Zheng, Y. et al. Designing high-efficiency extended depth-of-focus metalens via topology-shape optimization. *Nanophotonics* **11**, 2967–2975 (2022).
81. Bayati, E. et al. Inverse designed metalenses with extended depth of focus. *ACS Photonics* **7**, 873–878 (2020).
82. Liu, X. et al. Underwater binocular meta-lens. *ACS Photonics* **10**, 2382–2389 (2023).
83. Colburn, S. & Majumdar, A. Single-shot three-dimensional imaging with a metasurface depth camera. *arXiv preprint arXiv:1910.12111* (2019).
84. Shen, Z. et al. Monocular metasurface camera for passive single-shot 4d imaging. *Nat. Commun.* **14**, 1035 (2023).
85. Hampson, K. M. et al. Adaptive optics for high-resolution imaging. *Nat. Rev. Methods Prim.* **1**, 68 (2021).
86. Basak, S. et al. Super-resolution optical fluctuation imaging. *Nat. Photonics* **19**, 229–237 (2025).
87. Khorasaninejad, M. et al. Metalenses at visible wavelengths: diffraction-limited focusing and subwavelength resolution imaging. *Science* **352**, 1190–1194 (2016).
88. Hajiahmadi, M. J., Faraji-Dana, R. & Skrivervik, A. K. Far field superlensing inside biological media through a nanorod lens using spatiotemporal information. *Sci. Rep.* **11**, 1953 (2021).
89. Yang, H. et al. Reflective metalens with sub-diffraction-limited and multifunctional focusing. *Sci. Rep.* **7**, 12632 (2017).
90. Chen, W. T. et al. Immersion meta-lenses at visible wavelengths for nanoscale imaging. *Nano Lett* **17**, 3188–3194 (2017).
91. Gao, H. et al. Super-resolution imaging with a bessel lens realized by a geometric metasurface. *Opt. Express* **25**, 13933–13943 (2017).
92. Zuo, R., Liu, W., Cheng, H., Chen, S. & Tian, J. Breaking the diffraction limit with radially polarized light based on dielectric metalenses. *Adv. Opt. Mater.* **6**, 1800795 (2018).
93. Chen, M.-H., Chou, W.-N., Su, V.-C., Kuan, C.-H. & Lin, H. Y. High-performance gallium nitride dielectric metalenses for imaging in the visible. *Sci. Rep.* **11**, 6500 (2021).
94. Paniagua-Dominguez, R. et al. A metalens with a near-unity numerical aperture. *Nano Lett* **18**, 2124–2132 (2018).
95. Hail, C. U., Poulikakos, D. & Eghlidi, H. High-efficiency, extreme-numerical-aperture metasurfaces based on partial control of the phase of light. *Adv. Opt. Mater.* **6**, 1800852 (2018).
96. Zhu, A. Y. et al. Compact aberration-corrected spectrometers in the visible using dispersion-tailored metasurfaces. *Adv. Opt. Mater.* **7**, 1801144 (2019).
97. Sawant, R. et al. Aberration-corrected large-scale hybrid metalenses. *Optica* **8**, 1405–1411 (2021).
98. Fang, N., Lee, H., Sun, C. & Zhang, X. Sub-diffraction-limited optical imaging with a silver superlens. *Science* **308**, 534–537 (2005).
99. Lu, D. & Liu, Z. Hyperlenses and metalenses for far-field super-resolution imaging. *Nat. Commun.* **3**, 1205 (2012).
100. Akbari-Chelaresi, H., Salami, P. & Yousefi, L. Far-field sub-wavelength imaging using high-order dielectric continuous metasurfaces. *Opt. Express* **30**, 39025–39039 (2022).
101. Li, W., Qi, J. & Alu, A. Single-pixel super-resolution with a space–time modulated computational metasurface imager. *Photonics Res* **12**, 2311–2322 (2024).
102. Holsteen, A. L., Lin, D., Kauvar, I., Wetzstein, G. & Brongersma, M. L. A light-field metasurface for high-resolution single-particle tracking. *Nano Lett* **19**, 2267–2271 (2019).
103. Conteduca, D. et al. Dielectric nanohole array metasurface for high-resolution near-field sensing and imaging. *Nat. Commun.* **12**, 3293 (2021).
104. Wang, J. et al. Quantitative phase imaging with a compact meta-microscope. *npj Nanophotonics* **1**, 4 (2024).
105. Zhou, Q. et al. Far-field phase-shifting structured light illumination enabled by polarization multiplexing metasurface for super-resolution imaging. *Nano Lett* **24**, 11036–11042 (2024).
106. Ye, X. et al. Chip-scale metalens microscope for wide-field and depth-of-field imaging. *Adv. Photonics* **4**, 046006–046006 (2022).
107. Tang, F. et al. Metasurface spectrometers beyond resolution-sensitivity constraints. *Sci. Adv.* **10**, eadr7155 (2024).
108. Fu, B. et al. Miniaturized high-efficiency snapshot polarimetric stereoscopic imaging. *Optica* **12**, 391–398 (2025).
109. Kim, G. et al. Metasurface-driven full-space structured light for three-dimensional imaging. *Nat. Commun.* **13**, 5920 (2022).
110. Jing, X. et al. Single-shot 3d imaging with point cloud projection based on metadevice. *Nat. Commun.* **13**, 7842 (2022).
111. Hao, H. et al. Single-shot 3d imaging meta-microscope. *Nano Lett* **24**, 13364–13373 (2024).
112. Lin, R. J. et al. Achromatic metalens array for full-colour light-field imaging. *Nat. Nanotechnol.* **14**, 227–231 (2019).
113. Chakravarthula, P. et al. Thin on-sensor nanophotonic array cameras. *ACM Trans. Graph.* **42**, 1–18 (2023).
114. Stewart, J. W., Akselrod, G. M., Smith, D. R. & Mikkelsen, M. H. Toward multispectral imaging with colloidal metasurface pixels. *Adv. Mater.* **29**, 1602971 (2017).
115. Faraji-Dana, M. et al. Hyperspectral imager with folded metasurface optics. *Acs Photonics* **6**, 2161–2167 (2019).

116. Yesilkoy, F. et al. Ultrasensitive hyperspectral imaging and biodetection enabled by dielectric metasurfaces. *Nat. Photonics* **13**, 390–396 (2019).
117. Zhao, Z. et al. Hyperspectral metachip-based 3d spatial map for cancer cell screening and quantification. *Adv. Mater.* **37**, 2412738 (2025).
118. Zhang, Z., Song, Q., Xiao, S. & Xu, K. Single-shot on-chip diffractive speckle spectrometer with high spectral channel density. *Laser Photonics Rev.* **19**, 2401987 (2025).
119. Diebold, A. V., Imani, M. F., Fromenteze, T., Marks, D. L. & Smith, D. R. Passive microwave spectral imaging with dynamic metasurface apertures. *Optica* **7**, 527–536 (2020).
120. McClung, A., Samudrala, S., Torfeh, M., Mansouree, M. & Arbabi, A. Snapshot spectral imaging with parallel metasystems. *Sci. Adv.* **6**, eabc7646 (2020).
121. Xiong, J. et al. Dynamic brain spectrum acquired by a real-time ultraspectral imaging chip with reconfigurable metasurfaces. *Optica* **9**, 461–468 (2022).
122. Makarenko, M. et al. Real-time hyperspectral imaging in hardware via trained metasurface encoders. In *Proc. IEEE/CVF Conference on Computer Vision and Pattern Recognition*, 12692–12702 (IEEE, 2022).
123. Yang, J. et al. Reconfigurable snapshot hyperspectral imaging sensor based on monochromatic pattern match of gradient geometry metasurface. *ACS Photonics* **11**, 3841–3851 (2024).
124. Cai, G. et al. Compact angle-resolved metasurface spectrometer. *Nat. Mater.* **23**, 71–78 (2024).
125. Zuo, J. et al. Metasurface-based mueller matrix microscope. *Adv. Funct. Mater.* **34**, 2405412 (2024).
126. Liu, Z. et al. Dual jones matrices empowered six phase channels modulation with single-layer monoatomic metasurfaces. *Laser Photonics Rev.* **19**, 2401526 (2025).
127. Arbabi, E., Kamali, S. M., Arbabi, A. & Faraon, A. Full-stokes imaging polarimetry using dielectric metasurfaces. *Acs Photonics* **5**, 3132–3140 (2018).
128. Rubin, N. A. et al. Matrix fourier optics enables a compact full-stokes polarization camera. *Science* **365**, eaax1839 (2019).
129. Zhang, C. et al. High efficiency all-dielectric pixelated metasurface for near-infrared full-stokes polarization detection. *Photonics Res* **9**, 583–589 (2021).
130. Bao, Y. et al. Observation of full-parameter jones matrix in bilayer metasurface. *Nat. Commun.* **13**, 7550 (2022).
131. Ren, Y. et al. Full-stokes polarimetry for visible light enabled by an all-dielectric metasurface. *Adv. Photonics Res.* **3**, 2100373 (2022).
132. Fan, Q. et al. Disordered metasurface enabled single-shot full-stokes polarization imaging leveraging weak dichroism. *Nat. Commun.* **14**, 7180 (2023).
133. Zuo, J. et al. Chip-integrated metasurface full-stokes polarimetric imaging sensor. *Light Sci. Appl.* **12**, 218 (2023).
134. Hu, Y. et al. Achromatic full stokes polarimetry metasurface for full-color polarization imaging in the visible range. *Nano Lett.* **24**, 13018–13026 (2024).
135. Zaidi, A. et al. Metasurface-enabled single-shot and complete mueller matrix imaging. *Nat. Photonics* **18**, 704–712 (2024).
136. Hua, X. et al. Ultra-compact snapshot spectral light-field imaging. *Nat. Commun.* **13**, 2732 (2022).
137. Fan, Y. et al. Dispersion-assisted high-dimensional photodetector. *Nature* **630**, 70–83 (2024).
138. Yan, R. et al. Enhancing detection capability of orbital angular momentum sorter. *Laser Photonics Rev.* **19**, 2401759 (2025).
139. Li, L. et al. Metasurface-based intelligent identification of total angular momentum spectra for beams. *ACS Photonics* **12**, 1418–1425 (2024).
140. Hao, Z. et al. Arbitrary acoustic orbital angular momentum detection using dual-layer metasurfaces. *Sci. China Phys. Mech. Astron.* **67**, 264311 (2024).
141. Zhang, S. et al. Broadband detection of multiple spin and orbital angular momenta via dielectric metasurface. *Laser Photonics Rev* **14**, 2000062 (2020).
142. Luo, Y. et al. Metasurface based symmetry transformation for single-shot angular momentum detection within a large mode space. *Front. Phys.* **11**, 1223136 (2023).
143. Divitt, S., Zhu, W., Zhang, C., Lezec, H. J. & Agrawal, A. Ultrafast optical pulse shaping using dielectric metasurfaces. *Science* **364**, 890–894 (2019).
144. Li, T. et al. Ultrafast metaphotonics. *Ultrafast Sci* **4**, 0074 (2024).
145. Maiuri, M., Schirato, A., Cerullo, G. & Della Valle, G. Ultrafast all-optical metasurfaces: challenges and new frontiers. *ACS Photonics* **11**, 2888–2905 (2024).
146. Pacheco-Peña, V., Fink, M. & Engheta, N. Temporal chirp, temporal lensing, and temporal routing via space-time interfaces. *Phys. Rev. B* **111**, L100306 (2025).
147. Geromel, R. et al. Compact metasurface-based optical pulse-shaping device. *Nano Lett* **23**, 3196–3201 (2023).
148. Zhou, J. et al. Optical edge detection based on high-efficiency dielectric metasurface. *Proc. Natl. Acad. Sci. USA* **116**, 11137–11140 (2019).
149. Zhou, Y., Zheng, H., Kravchenko, I. I. & Valentine, J. Flat optics for image differentiation. *Nat. Photonics* **14**, 316–323 (2020).
150. Swartz, B. T., Zheng, H., Forcherio, G. T. & Valentine, J. Broadband and large-aperture metasurface edge encoders for incoherent infrared radiation. *Sci. Adv.* **10**, eadk0024 (2024).
151. Bi, X. et al. Concurrent image differentiation and integration processings enabled by polarization-multiplexed metasurface. *Laser Photonics Rev.* **19**, 2400718 (2025).
152. Tanriover, I., Dereshgi, S. A. & Aydin, K. Metasurface enabled broadband all optical edge detection in visible frequencies. *Nat. Commun.* **14**, 6484 (2023).
153. Wang, S. et al. Metalens for accelerated optoelectronic edge detection under ambient illumination. *Nano Lett* **24**, 356–361 (2023).
154. Qu, G. et al. All-dielectric metasurface empowered optical-electronic hybrid neural networks. *Laser Photonics Rev* **16**, 2100732 (2022).
155. Weng, J. et al. Meta-neural-network for real-time and passive deep-learning-based object recognition. *Nat. Commun.* **11**, 6309 (2020).
156. Miyazaki, H. et al. Dual-band infrared metasurface thermal emitter for CO2 sensing. *Appl. Phys. Lett.* **105**, 121107 (2014).
157. Meng, J., Balendhran, S., Sabri, Y., Bhargava, S. K. & Crozier, K. B. Smart mid-infrared metasurface microspectrometer gas sensing system. *Microsyst. Nanoeng.* **10**, 74 (2024).
158. Tan, H., Meng, J. & Crozier, K. B. Multianalyte detection with metasurface-based midinfrared microspectrometer. *ACS Sens* **9**, 5839–5847 (2024).
159. Zhu, Y. et al. On-site quantitative detection of fentanyl in heroin by machine learning-enabled sers on super absorbing metasurfaces. *npj Nanophotonics* **2**, 7 (2025).
160. Li, L. et al. Intelligent metasurface imager and recognizer. *Light Sci. Appl.* **8**, 97 (2019).
161. Wang, H. P. et al. Noncontact electromagnetic wireless recognition for prosthesis based on intelligent metasurface. *Adv. Sci.* **9**, 2105056 (2022).
162. He, C. et al. Pluggable multitask diffractive neural networks based on cascaded metasurfaces. *Opto-Electron Adv* **7**, 230005 (2024).
163. Li, L. et al. Machine-learning reprogrammable metasurface imager. *Nat. Commun.* **10**, 1082 (2019).
164. Xu, D. et al. All-optical object identification and three-dimensional reconstruction based on optical computing metasurface. *Opto-Electron. Adv.* **6**, 230120 (2023).
165. Yang, S. et al. Realizing depth measurement and edge detection based on a single metasurface. *Nanophotonics* **12**, 3385–3393 (2023).

166. Li, Z. et al. Meta-optics achieves rgb-achromatic focusing for virtual reality. *Sci. Adv.* **7**, eabe4458 (2021).
167. Li, Z. et al. Inverse design enables large-scale high-performance meta-optics reshaping virtual reality. *Nat. Commun.* **13**, 2409 (2022).
168. Xiong, J., Hsiang, E.-L., He, Z., Zhan, T. & Wu, S.-T. Augmented reality and virtual reality displays: emerging technologies and future perspectives. *Light Sci. Appl.* **10**, 216 (2021).
169. Lee, G.-Y. et al. Metasurface eyepiece for augmented reality. *Nat. Commun.* **9**, 4562 (2018).
170. Li, Y. et al. Ultracompact multifunctional metalens visor for augmented reality displays. *PhotoniX* **3**, 29 (2022).
171. Gopakumar, M. et al. Full-colour 3d holographic augmented-reality displays with metasurface waveguides. *Nature* **629**, 791–797 (2024).
172. Georgi, P. et al. Optical secret sharing with cascaded metasurface holography. *Sci. Adv.* **7**, eabf9718 (2021).
173. Li, J. et al. Addressable metasurfaces for dynamic holography and optical information encryption. *Sci. Adv.* **4**, eaar6768 (2018).
174. Sun, S. et al. High-efficiency, broadband, and low-crosstalk 3d holography by multi-layer holographic-lens integrated metasurface. *APL Photonics* **9**, 086102 (2024).
175. Kim, I. et al. Pixelated bifunctional metasurface-driven dynamic vectorial holographic color prints for photonic security platform. *Nat. Commun.* **12**, 3614 (2021).
176. Kim, J. et al. Geometric and physical configurations of meta-atoms for advanced metasurface holography. *InfoMat* **3**, 739–754 (2021).
177. Yin, Y. et al. Multi-dimensional multiplexed metasurface holography by inverse design. *Adv. Mater.* **36**, 2312303 (2024).
178. Xiong, B. et al. Realizing colorful holographic mimicry by metasurfaces. *Adv. Mater.* **33**, 2005864 (2021).
179. Meng, W. et al. Ultranarrow-linewidth wavelength-vortex metasurface holography. *Sci. Adv.* **11**, eadt9159 (2025).
180. Wang, D. et al. Decimeter-depth and polarization addressable color 3d meta-holography. *Nat. Commun.* **15**, 8242 (2024).
181. Jue, J. et al. Three-photon direct laser writing of the qd–polymer metasurface for large field-of-view optical holography. *ACS Appl. Mater. Interfaces* **17**, 14520–14526 (2025).
182. Jiang, Q., Jin, G. & Cao, L. When metasurface meets hologram: principle and advances. *Adv. Opt. Photonics* **11**, 518–576 (2019).
183. Kim, J. et al. Tunable metasurfaces towards versatile metalenses and metaholograms: a review. *Adv. Photonics* **4**, 024001–024001 (2022).
184. Deng, Z.-L. & Li, G. Metasurface optical holography. *Mater. Today Phys.* **3**, 16–32 (2017).
185. Aththanayake, A., Lininger, A., Strangi, C., Griswold, M. A. & Strangi, G. Tunable holographic metasurfaces for augmented and virtual reality. *Nanophotonics* https://doi.org/10.1515/nanoph-2024-0734 (2025).
186. Ren, H. et al. Metasurface orbital angular momentum holography. *Nat. Commun.* **10**, 2986 (2019).
187. Wang, B. et al. Wavelength de-multiplexing metasurface hologram. *Sci. Rep.* **6**, 35657 (2016).
188. Yin, Y., Jiang, Q., Wang, H. & Huang, L. Color holographic display based on complex-amplitude metasurface. *Laser Photonics Rev.* **19**, 2400884 (2025).
189. Mu, Y., Zheng, M., Qi, J., Li, H. & Qiu, J. A large field-of-view metasurface for complex-amplitude hologram breaking numerical aperture limitation. *Nanophotonics* **9**, 4749–4759 (2020).
190. Deng, Z.-L. et al. Full-color complex-amplitude vectorial holograms based on multi-freedom metasurfaces. *Adv. Funct. Mater.* **30**, 1910610 (2020).
191. Yin, Y., Jiang, Q., Wang, H. & Huang, L. Color holographic display based on complex-amplitude metasurface. *Laser Photonics Rev* **19**, 2400884 (2025).
192. Li, L. et al. Electromagnetic reprogrammable coding-metasurface holograms. *Nat. Commun.* **8**, 197 (2017).
193. Qu, G. et al. Reprogrammable meta-hologram for optical encryption. *Nat. Commun.* **11**, 5484 (2020).
194. Zhang, J. C. et al. Programmable optical meta-holograms. *Nanophotonics* **13**, 1201–1217 (2024).
195. Li, Z., Shi, Y., Dai, C. & Li, Z. On-chip-driven multicolor 3d meta-display. *Laser Photonics Rev.* **18**, 2301240 (2024).
196. Rao, R., Shi, Y., Wang, Z., Wan, S. & Li, Z. On-chip cascaded metasurfaces for visible wavelength division multiplexing and color-routing meta-display. *Nano Lett.* **25**, 2452–2458 (2025).
197. Wan, W., Gao, J. & Yang, X. Full-color plasmonic metasurface holograms. *ACS Nano* **10**, 10671–10680 (2016).
198. Hu, Y. et al. 3d-integrated metasurfaces for full-colour holography. *Light Sci. Appl.* **8**, 86 (2019).
199. Sun, J. & Li, T. Cascaded metalenses boost applications in near-eye display. *Light Sci. Appl.* **14**, 58 (2025).
200. Liu, Z. et al. Metasurface-enabled augmented reality display: a review. *Adv. Photonics* **5**, 034001–034001 (2023).
201. Fan, Z.-B. et al. Integral imaging near-eye 3d display using a nanoimprint metalens array. *eLight* **4**, 3 (2024).
202. Boo, H. et al. Metasurface wavefront control for high-performance user-natural augmented reality waveguide glasses. *Sci. Rep.* **12**, 5832 (2022).
203. Chen, S., Liu, W., Li, Z., Cheng, H. & Tian, J. Metasurface-empowered optical multiplexing and multifunction. *Adv. Mater.* **32**, 1805912 (2020).
204. Zhou, Y. et al. Flexible metasurfaces for multifunctional interfaces. *ACS Nano* **18**, 2685–2707 (2024).
205. Tonkaev, P., Sinev, I. S., Rybin, M. V., Makarov, S. V. & Kivshar, Y. Multifunctional and transformative metaphotonics with emerging materials. *Chem. Rev.* **122**, 15414–15449 (2022).
206. Du, K. et al. Optical metasurfaces towards multifunctionality and tunability. *Nanophotonics* **11**, 1761–1781 (2022).
207. Xing, Z. et al. Monolithic spin-multiplexing metalens for dual-functional imaging. *Laser Photonics Rev.* **19**, 2401993 (2025).
208. Sulejman, S. B. et al. Metasurfaces for infrared multimodal microscopy: phase contrast and bright field. *ACS Photonics* **12**, 1494–1506 (2025).
209. Li, N., Zhang, J., Neshev, D. N. & Sukhorukov, A. A. Angle multifunctional dichroism in metasurfaces. *ACS Photonics* **12**, 1441–1447 (2025).
210. Liu, M. et al. Multifunctional metasurfaces enabled by simultaneous and independent control of phase and amplitude for orthogonal polarization states. *Light Sci. Appl.* **10**, 107 (2021).
211. Yu, S. et al. Dynamic nonlocal metasurface for multifunctional integration via phase-change materials. *Nanophotonics* **13**, 4317–4325 (2024).
212. Shabanpour, J., Beyraghi, S. & Cheldavi, A. Ultrafast reprogrammable multifunctional vanadium-dioxide-assisted metasurface for dynamic thz wavefront engineering. *Sci. Rep.* **10**, 8950 (2020).
213. Kwon, H., Arbabi, E., Kamali, S. M., Faraji-Dana, M. & Faraon, A. Single-shot quantitative phase gradient microscopy using a system of multifunctional metasurfaces. *Nat. Photonics* **14**, 109–114 (2020).
214. Intaravanne, Y. et al. Metasurface-enabled 3-in-1 microscopy. *ACS photonics* **10**, 544–551 (2023).
215. Dai, C., Liu, T., Wang, D. & Zhou, L. Multiplexing near-and far-field functionalities with high-efficiency bi-channel metasurfaces. *PhotoniX* **5**, 11 (2024).
216. Guo, S. et al. Multifunctional metasurface: Holography and spot cloud projection. *Adv. Opt. Mater.* **12**, 2401235 (2024).
217. Chen, M. K. et al. A meta-device for intelligent depth perception. *Adv. Mater.* **35**, 2107465 (2023).
218. Wang, Y. et al. Detection and anti-detection with microwave-infrared compatible camouflage using asymmetric composite metasurface. *Adv. Sci.* **11**, 2410364 (2024).

219. Ee, H.-S. & Agarwal, R. Tunable metasurface and flat optical zoom lens on a stretchable substrate. *Nano Lett* **16**, 2818–2823 (2016).
220. Li, F. et al. Flexible intelligent microwave metasurface with shape-guided adaptive programming. *Nat. Commun.* **16**, 3161 (2025).
221. Lan, F. et al. Real-time programmable metasurface for terahertz multifunctional wave front engineering. *Light Sci. Appl.* **12**, 191 (2023).
222. Shirmanesh, G. K., Sokhoyan, R., Wu, P. C. & Atwater, H. A. Electro-optically tunable multifunctional metasurfaces. *ACS Nano* **14**, 6912–6920 (2020).
223. Yang, G. et al. Nonlocal phase-change metaoptics for reconfigurable nonvolatile image processing. *Light Sci. Appl.* **14**, 1–10 (2025).
224. Abdollahramezani, S. et al. Reconfigurable multifunctional metasurfaces employing hybrid phase-change plasmonic architecture. *Nanophotonics* **11**, 3883–3893 (2022).
225. Ji, J. et al. On-chip multifunctional metasurfaces with full-parametric multiplexed jones matrix. *Nat. Commun.* **15**, 8271 (2024).
226. Yang, X., Wen, E., Bharadia, D. & Sievenpiper, D. F. Multifunctional metasurface: simultaneous beam steering, polarization conversion and phase offset. *IEEE Trans. Antennas Propagation* **72**, 4589–4593 (2024).
227. Dong, L. et al. Metasurface-enhanced multifunctional flag nanogenerator for efficient wind energy harvesting and environmental sensing. *Nano Energy* **124**, 109508 (2024).
228. Xu, X. et al. Multifunctional metamaterials for energy harvesting and vibration control. *Adv. Funct. Mater.* **32**, 2107896 (2022).
229. Armghan, A., Alsharari, M., Baqir, M. A., Saqlain, M. & Aliqab, K. A high-performance ultra-wideband metasurface absorber and thermal emitter for solar energy harvesting and thermal applications. *Phys. Chem. Chem. Phys.* **26**, 25469–25479 (2024).
230. Zhang, J., Shao, L., Li, Z., Zhang, C. & Zhu, W. Graphene-based optically transparent metasurface capable of dual-polarized modulation for electromagnetic stealth. *ACS Appl. Mater. Interfaces* **14**, 31075–31084 (2022).
231. Chu, H. et al. A hybrid invisibility cloak based on integration of transparent metasurfaces and zero-index materials. *Light Sci. Appl.* **7**, 50 (2018).
232. Zhang, Z. et al. Multifunctional ultrathin metasurface with a low radar cross section and variable infrared emissivity. *ACS Appl. Mater. Interfaces* **16**, 21109–21117 (2024).
233. Joo, W.-J. et al. Metasurface-driven oled displays beyond 10,000 pixels per inch. *Science* **370**, 459–463 (2020).
234. Cao, G. et al. Infrared metasurface-enabled compact polarization nanodevices. *Mater. Today* **50**, 499–515 (2021).
235. Wen, S. et al. Metasurface array for single-shot spectroscopic ellipsometry. *Light Sci. Appl.* **13**, 88 (2024).
236. Bao, Y. & Li, B. Single-shot simultaneous intensity, phase, and polarization imaging with metasurface. *Natl. Sci. Rev.* **12**, nwae418 (2025).
237. Pahlevaninezhad, H. et al. Nano-optic endoscope for high-resolution optical coherence tomography in vivo. *Nat. Photonics* **12**, 540–547 (2018).
238. Luo, X. et al. Metasurface-enabled on-chip multiplexed diffractive neural networks in the visible. *Light Sci. Appl.* **11**, 158 (2022).
239. Colburn, S., Zhan, A. & Majumdar, A. Metasurface optics for full-color computational imaging. *Sci. Adv.* **4**, eaar2114 (2018).
240. Seo, J. et al. Deep-learning-driven end-to-end metalens imaging. *Adv. Photonics* **6**, 066002–066002 (2024).
241. Chi, H. et al. Neural network-assisted end-to-end design for full light field control of meta-optics. *Adv. Mater* **37**, 2419621 (2025).
242. Nolen, J. R., Overvig, A. C., Cotrufo, M. & Alù, A. Local control of polarization and geometric phase in thermal metasurfaces. *Nat. Nanotechnol* **19**, 1627–1634 (2024).
243. Li, Z. et al. Controlling propagation and coupling of waveguide modes using phase-gradient metasurfaces. *Nat. Nanotechnol.* **12**, 675–683 (2017).
244. Arbabi, A., Horie, Y., Bagheri, M. & Faraon, A. Dielectric metasurfaces for complete control of phase and polarization with subwavelength spatial resolution and high transmission. *Nat. Nanotechnol.* **10**, 937–943 (2015).
245. Wang, Q. et al. Optically reconfigurable metasurfaces and photonic devices based on phase change materials. *Nat. Photonics* **10**, 60–65 (2016).
246. Yao, J., Lin, R., Chen, M. K. & Tsai, D. P. Integrated-resonant metadevices: a review. *Adv. Photonics* **5**, 024001–024001 (2023).
247. Santiago-Cruz, T. et al. Resonant metasurfaces for generating complex quantum states. *Science* **377**, 991–995 (2022).
248. Zhang, X., Liu, Y., Han, J., Kivshar, Y. & Song, Q. Chiral emission from resonant metasurfaces. *Science* **377**, 1215–1218 (2022).
249. High, A. A. et al. Visible-frequency hyperbolic metasurface. *Nature* **522**, 192–196 (2015).
250. Chen, H.-T., Taylor, A. J. & Yu, N. A review of metasurfaces: physics and applications. *Rep. Prog. Phys.* **79**, 076401 (2016).
251. So, S., Mun, J., Park, J. & Rho, J. Revisiting the design strategies for metasurfaces: fundamental physics, optimization, and beyond. *Adv. Mater.* **35**, 2206399 (2023).
252. Berry, M. V. Quantal phase factors accompanying adiabatic changes. *Proc. R. Soc. Lond. A. Math. Phys. Sci.* **392**, 45–57 (1984).
253. Guo, Y. et al. Classical and generalized geometric phase in electromagnetic metasurfaces. *Photonics Insights* **1**, R03–R03 (2022).
254. Yijia, S. et al. Achromatic metalens based on coordinative modulation of propagation phase and geometric phase. *Opto-Electron. Eng.* **47**, 200237–1 (2020).
255. Maguid, E. et al. Multifunctional interleaved geometric-phase dielectric metasurfaces. *Light Sci. Appl.* **6**, e17027 (2017).
256. Min, C. et al. Plasmonic nano-slits assisted polarization selective detour phase meta-hologram. *Laser Photonics Rev.* **10**, 978–985 (2016).
257. Deng, Z.-L. et al. Facile metagrating holograms with broadband and extreme angle tolerance. *Light Sci. Appl.* **7**, 78 (2018).
258. Feldman, N., Goeloe, K. M., den Boef, A. J., Amitonova, L. V. & Koenderink, A. F. Nanometer interlaced displacement metrology using diffractive pancharatnam-berry and detour phase metasurfaces. *ACS Photonics* **11**, 5229–5238 (2024).
259. Zhao, Z., Wang, Z., Shi, Y., Wan, S. & Li, Z. Multidimensional-encrypted meta-optics storage empowered by diffraction-order decoupling. *Adv. Mater* **37**, 2419322 (2025).
260. El-Helou, A. J. et al. Optical metasurfaces for the next-generation biosensing and bioimaging. *Laser Photonics Rev.* **19**, 2401715 (2025).
261. Yu, N. et al. Light propagation with phase discontinuities: generalized laws of reflection and refraction. *Science* **334**, 333–337 (2011).
262. Balthasar Mueller, J., Rubin, N. A., Devlin, R. C., Groever, B. & Capasso, F. Metasurface polarization optics: independent phase control of arbitrary orthogonal states of polarization. *Phys. Rev. Lett.* **118**, 113901 (2017).
263. Wang, C., Xu, H.-X., Liu, T. & Zhang, F. Hybrid-phase assisted amplitude and phase control using full-space metasurface. *Adv. Opt. Mater.* **12**, 2302153 (2024).
264. Yuan, Y. et al. A fully phase-modulated metasurface as an energy-controllable circular polarization router. *Adv. Sci.* **7**, 2001437 (2020).
265. Zhou, H. et al. Multi-fold phase metasurface holography based on frequency and hybrid decoupling polarizations. *Adv. Opt. Mater* **13**, 2402303 (2025).

266. Gu, Z. et al. Dual-band complex-amplitude metasurface empowered high security cryptography with ultra-massive encodable patterns. *Nanophotonics* **13**, 3915–3924 (2024).
267. Dai, J. Y., Zhao, J., Cheng, Q. & Cui, T. J. Independent control of harmonic amplitudes and phases via a time-domain digital coding metasurface. *Light Sci. Appl.* **7**, 90 (2018).
268. Yang, Y. et al. Full-polarization 3d metasurface cloak with preserved amplitude and phase. *Adv. Mater.* **28**, 6866–6871 (2016).
269. Li, L. & Wu, W. Phase-modulation metasurface-based visible broadband absorbers with polarization sensitivity or independence. *Adv. Opt. Mater* **13**, 2402643 (2025).
270. Kim, S., Jang, H., Han, J., Lee, J. & Jun, Y. C. Ultranarrowband chiral absorbers in the visible region based on brillouin zone folding metasurfaces. *Nano Lett.* **25**, 2841–2849 (2025).
271. Jha, P. K., Ni, X., Wu, C., Wang, Y. & Zhang, X. Metasurface-enabled remote quantum interference. *Phys. Rev. Lett.* **115**, 025501 (2015).
272. Wang, K. et al. Quantum metasurface for multiphoton interference and state reconstruction. *Science* **361**, 1104–1108 (2018).
273. Babicheva, V. E. & Evlyukhin, A. B. Metasurfaces with electric quadrupole and magnetic dipole resonant coupling. *ACS Photonics* **5**, 2022–2033 (2018).
274. Yuan, J. et al. Pump-wavelength selective all-optical terahertz metasurface with independent amplitude and frequency modulations. *Nano Lett* **24**, 15414–15420 (2024).
275. Li, X. M. et al. Full-space trifunctional metasurface with independent control of amplitude and phase for circularly polarized waves. *Nanophotonics* **13**, 4471–4481 (2024).
276. Duan, K. et al. Prephase-based reconfigurable joint amplitude-phase control metasurface for multifunctional scattering manipulation. *Adv. Opt. Mater* **13**, 2402664 (2024).
277. Zou, X. et al. Imaging based on metalenses. *PhotoniX* **1**, 1–24 (2020).
278. Li, T. et al. Revolutionary meta-imaging: from superlens to metalens. *Photonics Insights* **2**, R01–R01 (2023).
279. Zhang, Y. et al. Crosstalk-free achromatic full stokes imaging polarimetry metasurface enabled by polarization-dependent phase optimization. *Opto-Electron. Adv.* **5**, 220058–1 (2022).
280. Zheng, C. et al. Full-stokes metasurface polarimetry requiring only a single measurement. *Photonics Res* **12**, 514–521 (2024).
281. Liang, Y. et al. Full-stokes polarization perfect absorption with diatomic metasurfaces. *Nano Lett* **21**, 1090–1095 (2021).
282. Wu, L., Tao, J. & Zheng, G. Controlling phase of arbitrary polarizations using both the geometric phase and the propagation phase. *Phys. Rev. B* **97**, 245426 (2018).
283. Jisha, C. P., Nolte, S. & Alberucci, A. Geometric phase in optics: from wavefront manipulation to waveguiding. *Laser Photonics Rev* **15**, 2100003 (2021).
284. Lin, B.-Q. et al. Multiple-band linear-polarization conversion and circular polarization in reflection mode using a symmetric anisotropic metasurface. *Phys. Rev. Appl.* **9**, 024038 (2018).
285. Nicholls, L. H. et al. Ultrafast synthesis and switching of light polarization in nonlinear anisotropic metamaterials. *Nat. Photonics* **11**, 628–633 (2017).
286. Li, S. et al. Metasurface polarization optics: phase manipulation for arbitrary polarization conversion condition. *Phys. Rev. Lett.* **134**, 023803 (2025).
287. Yang, J. et al. Simultaneous conversion of polarization and frequency via time-division-multiplexing metasurfaces. *Adv. Opt. Mater.* **9**, 2101043 (2021).
288. Shi, Z. et al. Continuous angle-tunable birefringence with freeform metasurfaces for arbitrary polarization conversion. *Sci. Adv.* **6**, eaba3367 (2020).
289. Cotrufo, M., Singh, S., Arora, A., Majewski, A. & Alù, A. Polarization imaging and edge detection with image-processing metasurfaces. *Optica* **10**, 1331–1338 (2023).
290. Kim, H. et al. Optical metasurfaces for biomedical imaging and sensing. *ACS Nano* **19**, 3085–3114 (2025).
291. Xue, S. et al. Chip-integrated millimeter-wave imaging system via a low-profile and polarization-multiplexed holographic tensor metasurface. *Adv. Opt. Mater* **13**, 2500062 (2025).
292. Xu, Y., Takida, Y., Suzuki, T. & Minamide, H. Terahertz-wave polarization space-division multiplexing meta-devices based on spin-decoupled phase control. *Adv. Sci.* **12**, 2412688 (2025).
293. Wang, Z. et al. On-chip wavefront shaping with dielectric metasurface. *Nat. Commun.* **10**, 3547 (2019).
294. Huang, S.-H. et al. Microcavity-assisted multi-resonant metasurfaces enabling versatile wavefront engineering. *Nat. Commun.* **15**, 9658 (2024).
295. Cohen, N. et al. Enhancing the performance of the light field microscope using wavefront coding. *Opt. express* **22**, 24817–24839 (2014).
296. Mohammadi Estakhri, N. & Alu, A. Wave-front transformation with gradient metasurfaces. *Phys. Rev. X* **6**, 041008 (2016).
297. Zang, J. W. et al. Nonreciprocal wavefront engineering with time-modulated gradient metasurfaces. *Phys. Rev. Appl.* **11**, 054054 (2019).
298. Yi, H., Qu, S.-W., Ng, K.-B., Wong, C. K. & Chan, C. H. Terahertz wavefront control on both sides of the cascaded metasurfaces. *IEEE Trans. Antennas Propag* **66**, 209–216 (2017).
299. Cai, X. et al. Dynamically controlling terahertz wavefronts with cascaded metasurfaces. *Adv. Photonics* **3**, 036003–036003 (2021).
300. Hu, S., Wang, C., Du, S., Han, Z. & Gu, C. Dynamic and polarization-independent wavefront control based on hybrid topological metasurfaces. *Nano Lett* **24**, 2041–2047 (2024).
301. Kamali, S. M., Arbabi, E., Arbabi, A. & Faraon, A. A review of dielectric optical metasurfaces for wavefront control. *Nanophotonics* **7**, 1041–1068 (2018).
302. Go, G.-H. et al. Meta Shack–Hartmann wavefront sensor with large sampling density and large angular field of view: phase imaging of complex objects. *Light Sci. Appl.* **13**, 187 (2024).
303. Song, J.-H., van de Groep, J., Kim, S. J. & Brongersma, M. L. Non-local metasurfaces for spectrally decoupled wavefront manipulation and eye tracking. *Nat. Nanotechnol.* **16**, 1224–1230 (2021).
304. Jin, Z. et al. Phyllotaxis-inspired nanosieves with multiplexed orbital angular momentum. *ELight* **1**, 1–11 (2021).
305. Kong, L.-J., Zhang, F., Cheng, S. & Zhang, X. 3d orbital angular momentum multiplexing holography with metasurfaces: encryption and dynamic display of 3d multi-targets. *Laser Photonics Rev.* **19**, 2401608 (2025).
306. Guo, Y. et al. Merging geometric phase and plasmon retardation phase in continuously shaped metasurfaces for arbitrary orbital angular momentum generation. *Acs Photonics* **3**, 2022–2029 (2016).
307. Galvez, E. et al. Geometric phase associated with mode transformations<? format?> of optical beams bearing orbital angular momentum. *Phys. Rev. Lett.* **90**, 203901 (2003).
308. Chen, M. L., Jiang, L. J. & Sha, W. E. Orbital angular momentum generation and detection by geometric-phase based metasurfaces. *Appl. Sci.* **8**, 362 (2018).
309. Jiang, X., Li, Y., Liang, B., Cheng, J.-C. & Zhang, L. Convert acoustic resonances to orbital angular momentum. *Phys. Rev. Lett.* **117**, 034301 (2016).
310. Ho, T.-L. & Diener, R. B. Fermion superfluids of nonzero orbital angular momentum near resonance. *Phys. Rev. Lett.* **94**, 090402 (2005).
311. Lin, C.-H., Huang, S.-H., Lin, T.-H. & Wu, P. C. Metasurface-empowered snapshot hyperspectral imaging with convex/deep (code) small-data learning theory. *Nat. Commun.* **14**, 6979 (2023).
312. He, G. et al. Multiplexed manipulation of orbital angular momentum and wavelength in metasurfaces based on arbitrary complex-amplitude control. *Light Sci. Appl.* **13**, 98 (2024).

313. Hong, J. et al. Absorptive metasurface color filters based on hyperbolic metamaterials for a cmos image sensor. *Opt. Express* **29**, 3643–3658 (2021).
314. Han, X., Fan, Z., Liu, Z., Li, C. & Guo, L. J. Inverse design of metasurface optical filters using deep neural network with high degrees of freedom. *InfoMat* **3**, 432–442 (2021).
315. Zhang, X. et al. Twofold optical display and encryption of binary and grayscale images with a wavelength-multiplexed metasurface. *Nanophotonics* **12**, 3747–3756 (2023).
316. Liu, Y., Shi, Y., Wang, Z. & Li, Z. On-chip integrated metasystem with inverse-design wavelength demultiplexing for augmented reality. *ACS Photonics* **10**, 1268–1274 (2023).
317. Dong, S. et al. Wavelength multiplexing infrared metasurfaces for protein recognition and trace detection. *Nanophotonics* **12**, 3963–3976 (2023).
318. Chen, C. et al. Spectral tomographic imaging with aplanatic metalens. *Light Sci. Appl.* **8**, 99 (2019).
319. Sun, S. et al. Gradient-index meta-surfaces as a bridge linking propagating waves and surface waves. *Nat. Mater.* **11**, 426–431 (2012).
320. Huang, L. et al. Dispersionless phase discontinuities for controlling light propagation. *Nano Lett* **12**, 5750–5755 (2012).
321. Zhou, Z. et al. Efficient silicon metasurfaces for visible light. *Acs Photonics* **4**, 544–551 (2017).
322. Dong, H.-W. et al. Inverse design of phononic meta-structured materials. *Mater. Today* **80**, 824–855 (2024).
323. Li, Z., Pestourie, R., Lin, Z., Johnson, S. G. & Capasso, F. Empowering metasurfaces with inverse design: principles and applications. *Acs Photonics* **9**, 2178–2192 (2022).
324. Kim, J. et al. Inverse design of nanophotonic devices enabled by optimization algorithms and deep learning: recent achievements and future prospects. *Nanophotonics* **14**, 121–151 (2025).
325. Elsawy, M. M., Lanteri, S., Duvigneau, R., Fan, J. A. & Genevet, P. Numerical optimization methods for metasurfaces. *Laser Photonics Rev* **14**, 1900445 (2020).
326. Campbell, S. D. et al. Review of numerical optimization techniques for meta-device design. *Opt. Mater. Express* **9**, 1842–1863 (2019).
327. Mansouree, M., McClung, A., Samudrala, S. & Arbabi, A. Large-scale parametrized metasurface design using adjoint optimization. *Acs Photonics* **8**, 455–463 (2021).
328. Xiao, T. P. et al. Diffractive spectral-splitting optical element designed by adjoint-based electromagnetic optimization and fabricated by femtosecond 3d direct laser writing. *ACS Photonics* **3**, 886–894 (2016).
329. Mansouree, M. et al. Multifunctional 2.5 d metastructures enabled by adjoint optimization. *Optica* **7**, 77–84 (2020).
330. Khoram, E., Yu, Z. & Hassani Gangaraj, S. A. Adjoint-optimized large dielectric metasurface for enhanced purcell factor and directional photon emission. *ACS omega* **9**, 24356–24361 (2024).
331. Zhou, M. et al. Inverse design of metasurfaces based on coupled-mode theory and adjoint optimization. *Acs Photonics* **8**, 2265–2273 (2021).
332. Kang, C., Seo, D., Boriskina, S. V. & Chung, H. Adjoint method in machine learning: a pathway to efficient inverse design of photonic devices. *Mater. Des.* **239**, 112737 (2024).
333. Zhang, D., Liu, Z., Yang, X. & Xiao, J. J. Inverse design of multifunctional metasurface based on multipole decomposition and the adjoint method. *ACS Photonics* **9**, 3899–3905 (2022).
334. Cai, H. et al. Inverse design of metasurfaces with non-local interactions. *npj Comput. Mater.* **6**, 116 (2020).
335. Hsu, W.-L. et al. Simplest but efficient design of a color router optimized by genetic algorithms. *ACS Photonics* **12**, 1402–1408 (2025).
336. Fan, Y. et al. Phase-controlled metasurface design via optimized genetic algorithm. *Nanophotonics* **9**, 3931–3939 (2020).
337. Liu, C., Maier, S. A. & Li, G. Genetic-algorithm-aided meta-atom multiplication for improved absorption and coloration in nanophotonics. *ACS Photonics* **7**, 1716–1722 (2020).
338. Zhu, D. Z., Whiting, E. B., Campbell, S. D., Burckel, D. B. & Werner, D. H. Optimal high efficiency 3d plasmonic metasurface elements revealed by lazy ants. *ACS Photonics* **6**, 2741–2748 (2019).
339. Zhang, J. et al. Design of pixel terahertz metamaterial absorber sensor based on an improved ant colony algorithm. *IEEE Sensors J.* **24**, 40801–40810 (2024).
340. Nam, J. et al. Flexible metasurface for microwave-infrared compatible camouflage via particle swarm optimization algorithm. *Small* **19**, 2302848 (2023).
341. Lalbakhsh, A., Afzal, M. U. & Esselle, K. P. Multiobjective particle swarm optimization to design a time-delay equalizer metasurface for an electromagnetic band-gap resonator antenna. *IEEE Antennas Wirel. Propag. Lett.* **16**, 912–915 (2016).
342. Yang, H. et al. Polarization-independent dispersive complex-amplitude modulation via anisotropic metasurfaces. *Laser Photonics Rev.* **19**, 2401398 (2025).
343. Jiao, P. et al. Artificial intelligence-guided inverse design of deployable thermo-metamaterial implants. *ACS Appl. Mater. Interfaces* **17**, 2991–3001 (2025).
344. Wu, B. et al. Integrated electromagnetic sensing system based on a deep-neural-network-intervened genetic algorithm. *Photonics Res.* **13**, 387–394 (2025).
345. Zhu, R. et al. Overcome chromatism of metasurface via greedy algorithm empowered by self-organizing map neural network. *Opt. Express* **28**, 35724–35733 (2020).
346. Park, T., Mondal, S. & Cai, W. Interfacing nanophotonics with deep neural networks: AI for photonic design and photonic implementation of AI. *Laser Photonics Rev.* **19**, 2401520 (2025).
347. Dong, Y. et al. Advanced deep learning approaches in metasurface modeling and design: a review. *Progress Quantum Electron* **99**, 100554 (2025).
348. Zhu, C., Bamidele, E. A., Shen, X., Zhu, G. & Li, B. Machine learning aided design and optimization of thermal metamaterials. *Chem. Rev.* **124**, 4258–4331 (2024).
349. Wiecha, P. R. et al. Evolutionary multi-objective optimization of colour pixels based on dielectric nanoantennas. *Nat. Nanotechnol.* **12**, 163–169 (2017).
350. Jin, Z. et al. Complex inverse design of meta-optics by segmented hierarchical evolutionary algorithm. *ACS nano* **13**, 821–829 (2019).
351. Chen, W. et al. Empowering nanophotonic applications via artificial intelligence: pathways, progress, and prospects. *Nanophotonics* **14**, 429–447 (2025).
352. Wang, Q., Makarenko, M., Burguete Lopez, A., Getman, F. & Fratalocchi, A. Advancing statistical learning and artificial intelligence in nanophotonics inverse design. *Nanophotonics* **11**, 2483–2505 (2022).
353. Qian, C., Kaminer, I. & Chen, H. A guidance to intelligent metamaterials and metamaterials intelligence. *Nat. Commun.* **16**, 1154 (2025).
354. Ahmed, W. W. et al. Machine learning assisted plasmonic metascreen for enhanced broadband absorption in ultra-thin silicon films. *Light Sci. Appl.* **14**, 42 (2025).
355. Huang, L. et al. Broadband thermal imaging using meta-optics. *Nat. Commun.* **15**, 1662 (2024).
356. An, S. et al. A deep learning approach for objective-driven all-dielectric metasurface design. *Acs Photonics* **6**, 3196–3207 (2019).
357. Zhang, J. et al. Physics-driven machine-learning approach incorporating temporal coupled mode theory for intelligent design of metasurfaces. *IEEE Trans. Microw. Theory Tech.* **71**, 2875–2887 (2023).
358. Qiu, T. et al. Deep learning: a rapid and efficient route to automatic metasurface design. *Adv. Sci.* **6**, 1900128 (2019).

359. Jiang, J. & Fan, J. A. Simulator-based training of generative neural networks for the inverse design of metasurfaces. *Nanophotonics* **9**, 1059–1069 (2020).
360. Zeng, Y., Cao, H. & Jin, X. Anchor-controlled generative adversarial network for high-fidelity electromagnetic and structurally diverse metasurface design. *Nanophotonics* https://doi.org/10.1515/nanoph-2025-0210 (2025).
361. Yeung, C. et al. Global inverse design across multiple photonic structure classes using generative deep learning. *Adv. Opt. Mater.* **9**, 2100548 (2021).
362. Yeung, C., Pham, B., Tsai, R., Fountaine, K. T. & Raman, A. P. Deepadjoint: an all-in-one photonic inverse design framework integrating data-driven machine learning with optimization algorithms. *ACS Photonics* **10**, 884–891 (2022).
363. Wu, O., Qian, C., Fan, Z., Zhu, X. & Chen, H. General characterization of intelligent metasurfaces with graph coupling network. *Laser Photonics Rev.* **19**, 2400979 (2024).
364. Kwon, D.-H. Design of single-layer dense metasurfaces on irregular grids using discrete dipole approximation. *IEEE Trans. Antennas Propag* **70**, 10592–10603 (2022).
365. Zhang, J. et al. Harnessing the missing spectral correlation for metasurface inverse design. *Adv. Sci.* **11**, 2308807 (2024).
366. Zhu, E. et al. Frequency transfer and inverse design for metasurface under multi-physics coupling by euler latent dynamic and data-analytical regularizations. *Nat. Commun.* **16**, 2251 (2025).
367. Lu, C. et al. Design and optimization of the low-frequency metasurface shield for wireless power transfer system. *IEEE Trans. Transport. Electrification* **8**, 723–733 (2021).
368. Malkiel, I. et al. Plasmonic nanostructure design and characterization via deep learning. *Light Sci. Appl.* **7**, 60 (2018).
369. Khatib, O., Ren, S., Malof, J. & Padilla, W. J. Learning the physics of all-dielectric metamaterials with deep lorentz neural networks. *Adv. Opt. Mater.* **10**, 2200097 (2022).
370. An, S. et al. Deep convolutional neural networks to predict mutual coupling effects in metasurfaces. *Adv. Opt. Mater.* **10**, 2102113 (2022).
371. Xu, L. et al. Enhanced light–matter interactions in dielectric nanostructures via machine-learning approach. *Adv. Photonics* **2**, 026003–026003 (2020).
372. An, S. et al. Deep neural network enabled active metasurface embedded design. *Nanophotonics* **11**, 4149–4158 (2022).
373. Chen, W. et al. All-dielectric sers metasurface with strong coupling quasi-bic energized by transformer-based deep learning. *Adv. Opt. Mater.* **12**, 2301697 (2024).
374. Gao, Y. et al. Meta-attention deep learning for smart development of metasurface sensors. *Adv. Sci.* **11**, 2405750 (2024).
375. Liu, Y., Geng, Q., Zhan, W. & Geng, Z. A cascaded deep neural network for design and verification of surface lattice resonance metasurfaces biosensors. *Eng. Appl. Artif. Intell.* **144**, 110172 (2025).
376. Chen, J., Duan, H. & Huang, G. Transformer-based inverse-design model for optimal multilayer microperforated panels. *Phys. Rev. Appl.* **23**, 024044 (2025).
377. Kong, W., Chen, J., Huang, Z. & Kuang, D. Bidirectional cascaded deep neural networks with a pretrained autoencoder for dielectric metasurfaces. *Photonics Res* **9**, 1607–1615 (2021).
378. Xi, J. et al. Deep-learning assisted polarization holograms. *Adv. Opt. Mater.* **12**, 2202663 (2024).
379. Kanmaz, T. B., Ozturk, E., Demir, H. V. & Gunduz-Demir, C. Deep-learning-enabled electromagnetic near-field prediction and inverse design of metasurfaces. *Optica* **10**, 1373–1382 (2023).
380. Jenkins, R. P., Campbell, S. D. & Werner, D. H. Establishing exhaustive metasurface robustness against fabrication uncertainties through deep learning. *Nanophotonics* **10**, 4497–4509 (2021).
381. Jia, Y., Fan, Z., Qian, C., del Hougne, P. & Chen, H. Dynamic inverse design of broadband metasurfaces with synthetical neural networks. *Laser Photonics Rev.* **18**, 2400063 (2024).
382. Deng, W., Xu, Z., Wang, J. & Lv, J. Long short-term memory neural network for directly inverse design of nanofin metasurface. *Opt. Lett.* **47**, 3239–3242 (2022).
383. Tang, Y. et al. Physics-informed recurrent neural network for time dynamics in optical resonances. *Nat. Comput. Sci.* **2**, 169–178 (2022).
384. Wang, P. et al. Space-time-coding digital metasurface element design based on state recognition and mapping methods with CNN-LSTM-DNN. *IEEE Trans. Antennas Propag.* **72**, 4962–4975 (2024).
385. Yan, T. et al. All-optical graph representation learning using integrated diffractive photonic computing units. *Sci. Adv.* **8**, eabn7630 (2022).
386. Wu, L., Cui, P., Pei, J., Zhao, L. & Guo, X. Graph neural networks: foundation, frontiers and applications. In *Proc. 28th ACM SIGKDD conference on knowledge discovery and data mining*, 4840–4841 (ACM, 2022).
387. Wu, O., Qian, C., Fan, Z., Zhu, X. & Chen, H. General characterization of intelligent metasurfaces with graph coupling network. *Laser Photonics Rev* **19**, 2400979 (2025).
388. Khoram, E., Wu, Z., Qu, Y., Zhou, M. & Yu, Z. Graph neural networks for metasurface modeling. *ACS Photonics* **10**, 892–899 (2022).
389. Bao, Q., Zhang, D., Liu, X., Ma, T. & Xiao, J.-J. Gat-net: inverse design of multifunctional metasurface based on graph attention network. *Opt. Laser Technol.* **183**, 112273 (2025).
390. Liu, Z., Zhu, D., Rodrigues, S. P., Lee, K.-T. & Cai, W. Generative model for the inverse design of metasurfaces. *Nano Lett* **18**, 6570–6576 (2018).
391. Kudyshev, Z. A., Kildishev, A. V., Shalaev, V. M. & Boltasseva, A. Machine-learning-assisted metasurface design for high-efficiency thermal emitter optimization. *Appl. Phys. Rev.* **7**, 021407 (2020).
392. Jiang, J. et al. Free-form diffractive metagrating design based on generative adversarial networks. *ACS Nano* **13**, 8872–8878 (2019).
393. Wen, F., Jiang, J. & Fan, J. A. Robust freeform metasurface design based on progressively growing generative networks. *Acs Photonics* **7**, 2098–2104 (2020).
394. Zandehshahvar, M. et al. Metric learning: harnessing the power of machine learning in nanophotonics. *Acs Photonics* **10**, 900–909 (2023).
395. Ding, W., Chen, J. & Wu, R.-X. A generative meta-atom model for metasurface-based absorber designs. *Adv. Opt. Mater.* **11**, 2201959 (2023).
396. Ma, W., Cheng, F., Xu, Y., Wen, Q. & Liu, Y. Probabilistic representation and inverse design of metamaterials based on a deep generative model with semi-supervised learning strategy. *Adv. Mater.* **31**, 1901111 (2019).
397. An, S. et al. Multifunctional metasurface design with a generative adversarial network. *Adv. Opt. Mater.* **9**, 2001433 (2021).
398. S, R. P., Jain, A., kumar, R. & Mitra, A. Ai-enabled inverse design and molecular identification using phase change metamaterial absorber. *Adv. Opt. Mater.* **n/a**, 2402407 (2024).
399. You, G. et al. Flow-based electromagnetic information recovery for inaccessible area and low-resolution detection. *Laser Photonics Rev.* **19**, 2401199 (2024).
400. Liu, C., Yu, W. M., Ma, Q., Li, L. & Cui, T. J. Intelligent coding metasurface holograms by physics-assisted unsupervised generative adversarial network. *Photonics Res* **9**, B159–B167 (2021).
401. Ju, H., Juan, R., Gomez, R., Nakamura, K. & Li, G. Transferring policy of deep reinforcement learning from simulation to reality for robotics. *Nat. Mach. Intell.* **4**, 1077–1087 (2022).

402. Kaufmann, E. et al. Champion-level drone racing using deep reinforcement learning. *Nature* **620**, 982–987 (2023).
403. Jin, Y., Liu, X., Shao, Y., Wang, H. & Yang, W. High-speed quadrupedal locomotion by imitation-relaxation reinforcement learning. *Nat. Mach. Intell.* **4**, 1198–1208 (2022).
404. Vinyals, O. et al. Grandmaster level in starcraft ii using multi-agent reinforcement learning. *Nature* **575**, 350–354 (2019).
405. Mnih, V. et al. Human-level control through deep reinforcement learning. *Nature* **518**, 529–533 (2015).
406. Silver, D. et al. Mastering the game of go without human knowledge. *Nature* **550**, 354–359 (2017).
407. Cao, Z. et al. Continuous improvement of self-driving cars using dynamic confidence-aware reinforcement learning. *Nat. Mach. Intell.* **5**, 145–158 (2023).
408. Feng, S. et al. Dense reinforcement learning for safety validation of autonomous vehicles. *Nature* **615**, 620–627 (2023).
409. Kiran, B. R. et al. Deep reinforcement learning for autonomous driving: A survey. *IEEE Trans. Intell. Transp. Syst.* **23**, 4909–4926 (2021).
410. Park, C. et al. Sample-efficient inverse design of freeform nanophotonic devices with physics-informed reinforcement learning. *Nanophotonics* **13**, 1483–1492 (2024).
411. Hooten, S., Beausoleil, R. G. & Van Vaerenbergh, T. Inverse design of grating couplers using the policy gradient method from reinforcement learning. *Nanophotonics* **10**, 3843–3856 (2021).
412. Sajedian, I., Badloe, T. & Rho, J. Optimisation of colour generation from dielectric nanostructures using reinforcement learning. *Opt. Express* **27**, 5874–5883 (2019).
413. Sajedian, I., Lee, H. & Rho, J. Double-deep q-learning to increase the efficiency of metasurface holograms. *Sci. Rep.* **9**, 10899 (2019).
414. Jiang, A., Osamu, Y. & Chen, L. Multilayer optical thin film design with deep q learning. *Sci. Rep.* **10**, 12780 (2020).
415. Seo, D., Nam, D. W., Park, J., Park, C. Y. & Jang, M. S. Structural optimization of a one-dimensional freeform metagrating deflector via deep reinforcement learning. *Acs Photonics* **9**, 452–458 (2021).
416. Zhao, Y., Li, L., Lanteri, S. & Viquerat, J. Dynamic metasurface control using deep reinforcement learning. *Math. Comput. Simul.* **197**, 377–395 (2022).
417. Yi, C., Chen, Z., Gao, Y. & Du, Q. Designing high efficiency asymmetric polarization converter for blue light: a deep reinforcement learning approach. *Opt. Express* **30**, 10032–10049 (2022).
418. Liu, C. et al. A programmable diffractive deep neural network based on a digital-coding metasurface array. *Nat. Electron.* **5**, 113–122 (2022).
419. Shao, G. et al. Reliable, efficient, and scalable photonic inverse design empowered by physics-inspired deep learning. *Nanophotonics* **14**, 2799–2810 (2025).
420. Ha, Y. et al. Physics-data-driven intelligent optimization for large-aperture metalenses. *Opto-Electron. Adv.* **6**, 230133–1 (2023).
421. Chen, M. et al. High speed simulation and freeform optimization of nanophotonic devices with physics-augmented deep learning. *ACS Photonics* **9**, 3110–3123 (2022).
422. Medvedev, V., Erdmann, A. & Rosskopf, A. Physics-informed deep learning for 3d modeling of light diffraction from optical metasurfaces. *Opt. Express* **33**, 1371–1384 (2025).
423. Davoodi, F. Active physics-informed deep learning: surrogate modeling for nonplanar wavefront excitation of topological nanophotonic devices. *Nano Lett.* **25**, 768–775 (2025).
424. Su, J. L. et al. Multi-dimensional multiplexed metasurface for multifunctional near-field modulation by physics-driven intelligent design. *Adv. Sci.* **12**, 2503899 (2025).
425. Jing, G. et al. Neural network-based surrogate model for inverse design of metasurfaces. *Photonics Res* **10**, 1462–1471 (2022).
426. Ma, W. et al. Pushing the limits of functionality-multiplexing capability in metasurface design based on statistical machine learning. *Adv. Mater.* **34**, 2110022 (2022).
427. Jiang, J. & Fan, J. A. Global optimization of dielectric metasurfaces using a physics-driven neural network. *Nano Lett* **19**, 5366–5372 (2019).
428. Ji, W. et al. Recent advances in metasurface design and quantum optics applications with machine learning, physics-informed neural networks, and topology optimization methods. *Light Sci. Appl.* **12**, 169 (2023).
429. Deng, Y., Ren, S., Fan, K., Malof, J. M. & Padilla, W. J. Neural-adjoint method for the inverse design of all-dielectric metasurfaces. *Opt. Express* **29**, 7526–7534 (2021).
430. Garg, P. et al. Inverse-designed dispersive time-varying nanostructures. *Adv. Opt. Mater* **13**, 2402444 (2025).
431. Ahmed, S. F. et al. Deep learning modelling techniques: current progress, applications, advantages, and challenges. *Artif. Intell. Rev.* **56**, 13521–13617 (2023).
432. Xu, Y. et al. Spectral transfer-learning-based metasurface design assisted by complex-valued deep neural network. *Adv. Photonics Nexus* **3**, 026002–026002 (2024).
433. Peng, R., Ren, S., Malof, J. & Padilla, W. J. Transfer learning for metamaterial design and simulation. *Nanophotonics* **13**, 2323–2334 (2024).
434. Fan, Z. et al. Transfer-learning-assisted inverse metasurface design for 30% data savings. *Phys. Rev. Appl.* **18**, 024022 (2022).
435. Lookman, T., Balachandran, P. V., Xue, D. & Yuan, R. Active learning in materials science with emphasis on adaptive sampling using uncertainties for targeted design. *npj Comput. Mater.* **5**, 21 (2019).
436. Zhuang, F. et al. A comprehensive survey on transfer learning. *Proc. IEEE* **109**, 43–76 (2020).
437. Theodoris, C. V. et al. Transfer learning enables predictions in network biology. *Nature* **618**, 616–624 (2023).
438. Zhu, R. et al. Phase-to-pattern inverse design paradigm for fast realization of functional metasurfaces via transfer learning. *Nat. Commun.* **12**, 2974 (2021).
439. Zhang, J. et al. Heterogeneous transfer-learning-enabled diverse metasurface design. *Adv. Opt. Mater.* **10**, 2200748 (2022).
440. Zhu, L., Lv, C., Hua, W., Huang, D. & Liu, Y. Ptlor-net: physical transfer learning based optical response prediction network of metasurfaces. *ACS Photonics* **12**, 2624–2636 (2025).
441. Wang, S. et al. Transfer learning empowered multiple-indicator optimization design for terahertz quasi-bound state in the continuum biosensors. *Adv. Sci*. 2504855 (2025).
442. Jiang, X.-Q. et al. High accuracy inverse design of reconfigurable metasurfaces with transmission-reflection-integrated achromatic functionalities. *Nanophotonics* **14**, 921–934 (2025).
443. Gao, M. et al. Consistency-based semi-supervised active learning: towards minimizing labeling cost. In *European Conference on Computer Vision*, 510–526 (Springer, 2020).
444. Ren, P. et al. A survey of deep active learning. *ACM Comput. Surv.* **54**, 1–40 (2021).
445. Kim, Y.-B. et al. W-band frequency selective digital metasurface using active learning-based binary optimization. *Nanophotonics* **14**, 1597–1606 (2025).
446. Kim, Y. et al. Deep learning framework for material design space exploration using active transfer learning and data augmentation. *npj Comput. Mater.* **7**, 140 (2021).
447. Pestourie, R., Mroueh, Y., Nguyen, T. V., Das, P. & Johnson, S. G. Active learning of deep surrogates for pdes: application to metasurface design. *npj Comput. Mater.* **6**, 164 (2020).
448. Xu, F. et al. Explainable AI: A brief survey on history, research areas, approaches and challenges. In *Natural language processing and Chinese computing*: *8th CCF international conference, NLPCC*

2019, dunhuang, China, October 9–14, 2019, proceedings, *part II 8*, 563–574 (Springer, 2019).
449. Dwivedi, R. et al. Explainable AI (xai): core ideas, techniques, and solutions. *ACM Comput. Surv.* **55**, 1–33 (2023).
450. Yeung, C. et al. Elucidating the behavior of nanophotonic structures through explainable machine learning algorithms. *Acs Photonics* **7**, 2309–2318 (2020).
451. Razi, A., Safdar, A. & Irfan, R. Enhancing tandem solar cell's efficiency through convolutional neural network-based optimization of metasurfaces. *Mater. Des.* **236**, 112475 (2023).
452. Yeung, C. et al. Enhancing adjoint optimization-based photonic inverse design with explainable machine learning. *Acs Photonics* **9**, 1577–1585 (2022).
453. Li, J. et al. On-demand design of metasurfaces through multineural network fusion. *ACS Appl. Mater. Interfaces* **16**, 49673–49686 (2024).
454. Zhang, J., Qian, C., Chen, J., Wu, B. & Chen, H. Uncertainty qualification for metasurface design with amendatory bayesian network. *Laser Photonics Rev* **17**, 2200807 (2023).
455. Yeung, C. et al. Multiplexed supercell metasurface design and optimization with tandem residual networks. *Nanophotonics* **10**, 1133–1143 (2021).
456. Fröch, J. E. et al. Beating spectral bandwidth limits for large aperture broadband nano-optics. *Nat. Commun.* **16**, 3025 (2025).
457. Park, Y. et al. End-to-end optimization of metalens for broadband and wide-angle imaging. *Adv. Opt. Mater* **13**, 2402853 (2025).
458. Lee, D., Chen, W., Wang, L., Chan, Y.-C. & Chen, W. Data-driven design for metamaterials and multiscale systems: a review. *Adv. Mater.* **36**, 2305254 (2024).
459. Tang, Y. et al. Generative deep learning model for inverse design of integrated nanophotonic devices. *Laser Photonics Rev* **14**, 2000287 (2020).
460. Zandehshahvar, M. et al. Manifold learning for knowledge discovery and intelligent inverse design of photonic nanostructures: breaking the geometric complexity. *Acs Photonics* **9**, 714–721 (2022).
461. Li, W., Qi, J. & Sihvola, A. Meta-imaging: from non-computational to computational. *Adv. Opt. Mater.* **8**, 2001000 (2020).
462. Hu, X. et al. Metasurface-based computational imaging: a review. *Adv. Photonics* **6**, 014002–014002 (2024).
463. Wang, Z., Peng, Y., Fang, L. & Gao, L. Computational optical imaging: on the convergence of physical and digital layers. *Optica* **12**, 113–130 (2025).
464. Arya, G. et al. End-to-end optimization of metasurfaces for imaging with compressed sensing. *ACS Photonics* **11**, 2077–2087 (2024).
465. Wei, W. et al. End-to-end design of metasurface-based complex-amplitude holograms by physics-driven deep neural networks. *Nanophotonics* **11**, 2921–2929 (2022).
466. Lin, Z. et al. End-to-end metasurface inverse design for single-shot multi-channel imaging. *Opt. express* **30**, 28358–28370 (2022).
467. Fisher, S., Arya, G., Majumdar, A., Lin, Z. & Johnson, S. G. End-to-end metasurface design for temperature imaging via broadband planck-radiation regression. *Adv. Opt. Mater*. 2402498 (2025).
468. Tseng, E. et al. Neural nano-optics for high-quality thin lens imaging. *Nat. Commun.* **12**, 6493 (2021).
469. Xia, H. et al. Joint optimization of coded aperture metasurface and residual self-attention network for snapshot full-stokes imaging. *Opt. Express* **32**, 29609–29619 (2024).
470. Zhu, R. et al. Direct field-to-pattern monolithic design of holographic metasurface via residual encoder-decoder convolutional neural network. *Opto-Electron. Adv.* **6**, 220148–1 (2023).
471. Liao, X. et al. Multi-objective optimization of chiral metasurface for sensing based on a distributed algorithm. *IEEE Photonics J.* **16**, 1–6 (2023).
472. Zeng, Y., Qing, X. & Chia, M. Y.-W. A wideband circularly polarized antenna with a non-uniform metasurface designed via multi-objective bayesian optimization. *IEEE Antennas Wireless Propagat. Lett.* **23**, 1739–1743 (2024).
473. Zhang, Z. et al. Addressing high-performance data sparsity in metasurface inverse design using multi-objective optimization and diffusion probabilistic models. *Opt. Express* **32**, 40869–40885 (2024).
474. Chen, S., Li, Z., Liu, W., Cheng, H. & Tian, J. From single-dimensional to multidimensional manipulation of optical waves with metasurfaces. *Adv. Mater.* **31**, 1802458 (2019).
475. Bao, Y., Jiang, Q., Kang, Y., Zhu, X. & Fang, Z. Enhanced optical performance of multifocal metalens with conic shapes. *Light Sci. Appl.* **6**, e17071 (2017).
476. Zhang, X. et al. Multifocal plane display based on dual polarity stereoscopic metasurface. *Adv. Funct. Mater.* **32**, 2209460 (2022).
477. Cao, G. et al. Two hundred nanometer thin multifocal graphene oxide metalens for varying magnification broadband imaging. *ACS Nano* **18**, 35550–35558 (2024).
478. Zhou, Y., Mao, C., Gershnabel, E., Chen, M. & Fan, J. A. Large-area, high-numerical-aperture, freeform metasurfaces. *Laser Photonics Rev* **18**, 2300988 (2024).
479. Xu, M. et al. Emerging long-range order from a freeform disordered metasurface. *Adv. Mater.* **34**, 2108709 (2022).
480. Sell, D., Yang, J., Doshay, S., Yang, R. & Fan, J. A. Large-angle, multifunctional metagratings based on freeform multimode geometries. *Nano Lett* **17**, 3752–3757 (2017).
481. Ueno, A. et al. Dual-band optical collimator based on deep-learning designed, fabrication-friendly metasurfaces. *Nanophotonics* **12**, 3491–3499 (2023).
482. Huang, H., Zhang, X., Gan, F. & Ni, X. Fabrication-friendly random meta-atom generation for phase-shifting metasurfaces. *IEEE Photonics J* **14**, 1–4 (2022).
483. Pitilakis, A. et al. A multi-functional reconfigurable metasurface: electromagnetic design accounting for fabrication aspects. *IEEE Trans. Antennas Propag* **69**, 1440–1454 (2020).
484. Zhang, X. et al. Metasurface-based broadband hologram with high tolerance to fabrication errors. *Sci. Rep.* **6**, 19856 (2016).
485. Choi, M. et al. Realization of high-performance optical metasurfaces over a large area: a review from a design perspective. *npj Nanophotonics* **1**, 31 (2024).
486. Skarda, J. et al. Low-overhead distribution strategy for simulation and optimization of large-area metasurfaces. *npj Comput. Mater.* **8**, 78 (2022).
487. Kim, C. & Lee, B. Torcwa: Gpu-accelerated fourier modal method and gradient-based optimization for metasurface design. *Comput. Phys. Commun.* **282**, 108552 (2023).
488. Yoon, G. & Rho, J. Maxim: metasurfaces-oriented electromagnetic wave simulation software with intuitive graphical user interfaces. *Comput. Phys. Commun.* **264**, 107846 (2021).
489. Darve, E. The fast multipole method: numerical implementation. *J. Comput. Phys.* **160**, 195–240 (2000).
490. White, C. A., Johnson, B. G., Gill, P. M. & Head-Gordon, M. The continuous fast multipole method. *Chem. Phys. Lett.* **230**, 8–16 (1994).
491. Wooldridge, J. M. Applications of generalized method of moments estimation. *J. Econ. Perspect.* **15**, 87–100 (2001).
492. Hall, A. R. Generalized method of moments. *Companion Theoretical Econometrics* 230–255 (2003).
493. Nadell, C. C., Huang, B., Malof, J. M. & Padilla, W. J. Deep learning for accelerated all-dielectric metasurface design. *Opt. Express* **27**, 27523–27535 (2019).
494. Park, J.-S. et al. All-glass 100 mm diameter visible metalens for imaging the cosmos. *ACS Nano* **18**, 3187–3198 (2024).
495. Park, J.-S. et al. All-glass, large metalens at visible wavelength using deep-ultraviolet projection lithography. *Nano Lett* **19**, 8673–8682 (2019).

496. Pestourie, R., Yao, W., Kanté, B. & Johnson, S. G. Efficient inverse design of large-area metasurfaces for incoherent light. *Acs Photonics* **10**, 854–860 (2022).
497. She, A., Zhang, S., Shian, S., Clarke, D. R. & Capasso, F. Large area metalenses: design, characterization, and mass manufacturing. *Opt. Express* **26**, 1573–1585 (2018).
498. Pestourie, R. et al. Inverse design of large-area metasurfaces. *Opt. Express* **26**, 33732–33747 (2018).
499. Moon, S.-W. et al. Wafer-scale manufacturing of near-infrared metalenses. *Laser Photonics Rev* **18**, 2300929 (2024).
500. Jung, D. E. et al. Full wafer scale manufacturing of directly printed TiO2 metalenses at visible wavelengths with outstanding focusing efficiencies. *Adv. Mater* **37**, 2500327 (2025).
501. Suresh, S. A. et al. All-dielectric meta-microlens-array confocal fluorescence microscopy. *Laser Photonics Rev.* **n/a**, 2401314 (2024).
502. Majorel, C. et al. Bio-inspired flat optics for directional 3d light detection and ranging. *npj Nanophotonics* **1**, 18 (2024).
503. Luo, Z. et al. Optomechanical infrared detector monolithically integrated with micro-metalens array. *ACS Photonics* **11**, 4597–4605 (2024).
504. Kim, J. et al. Large-area floating display with wafer-scale manufactured metalens arrays. *Laser Photonics Rev.* **19**, 2401425 (2025).
505. Li, L. et al. Metalens-array–based high-dimensional and multiphoton quantum source. *Science* **368**, 1487–1490 (2020).
506. Wu, X. et al. Wavelength-insensitive snapshot stokes polarimetric imaging based on cascaded metasurfaces. *Adv. Photonics* **7**, 016008–016008 (2025).
507. Li, X. et al. Cascaded metasurfaces enabling adaptive aberration corrections for focus scanning. *Opto-Electron. Adv.* **7**, 240085–1 (2024).
508. Ji, J. et al. High-dimensional poincaré beams generated through cascaded metasurfaces for high-security optical encryption. *PhotoniX* **5**, 13 (2024).
509. He, G. et al. Twisted metasurfaces for on-demand focusing localization. *Adv. Opt. Mater.* **13**, 2401933 (2025).
510. Wang, Z. et al. Two-dimensional materials for tunable and nonlinear metaoptics. *Adv. Photonics* **6**, 034001–034001 (2024).
511. Tian, J. & Cao, W. Reconfigurable flexible metasurfaces: from fundamentals towards biomedical applications. *PhotoniX* **5**, 2 (2024).
512. Cui, T. J., Qi, M. Q., Wan, X., Zhao, J. & Cheng, Q. Coding metamaterials, digital metamaterials and programmable metamaterials. *Light Sci. Appl.* **3**, e218 (2014).
513. Arbabi, E. et al. Mems-tunable dielectric metasurface lens. *Nat. Commun.* **9**, 812 (2018).
514. Meng, C., Thrane, P. C., Wang, C., Ding, F. & Bozhevolnyi, S. I. Mems-tunable topological bilayer metasurfaces for reconfigurable dual-state phase control. *Optica* **11**, 1556–1566 (2024).
515. Lu, Y. J. et al. A high-efficiency and versatile reconfigurable intelligent surface design paradigm with novel topological representation. *Engineering* **48**, 163–173 (2025).
516. Jiang, G. et al. Abnormal beam steering with kirigami reconfigurable metasurfaces. *Nat. Commun.* **16**, 1660 (2025).
517. Wu, H. et al. A programmable metasurface antenna that approaches the wireless information mapping limit. *Nat. Electron* **8**, 179–191 (2025).
518. Leng, B., Zhang, Y., Tsai, D. P. & Xiao, S. Meta-device: advanced manufacturing. *Light Adv. Manuf.* **5**, 117–132 (2025).
519. Brongersma, M. L. et al. The second optical metasurface revolution: moving from science to technology. *Nat. Rev. Electrical Eng.* **2**, 125–143 (2025).
520. Zhang, Q. et al. Diffractive optical elements 75 years on: from micro-optics to metasurfaces. *Photonics Insights* **2**, R09 (2023).
521. Jia, Y. et al. In situ customized illusion enabled by global metasurface reconstruction. *Adv. Funct. Mater.* **32**, 2109331 (2022).

Acknowledgements

This work is supported in part by Shenzhen Science and Technology Program under Grant JCYJ20241202123921029; in part by Natural Science Foundation of China under Grant 62131011 and in part by the Major Key Project of PCL under Grant PCL2023A10-3.

Author contributions

The review proposal was initiated by Y.Z., with contributions from X.J., H.C., Z.L. and H.Z. The primary responsibility for the thesis's main body lies with Y.Z., while X.J. and H.C. serve as the primary supervisors. H.Z.'s role encompasses the organization and analysis of the literature indicators, and Z.L. assists in revising the initial draft of the thesis.

Competing interests

The authors declare no competing interests.

Additional information

Correspondence and requests for materials should be addressed to Xin Jin.